Small Microseismic Surface Acquisition System: Case Studies

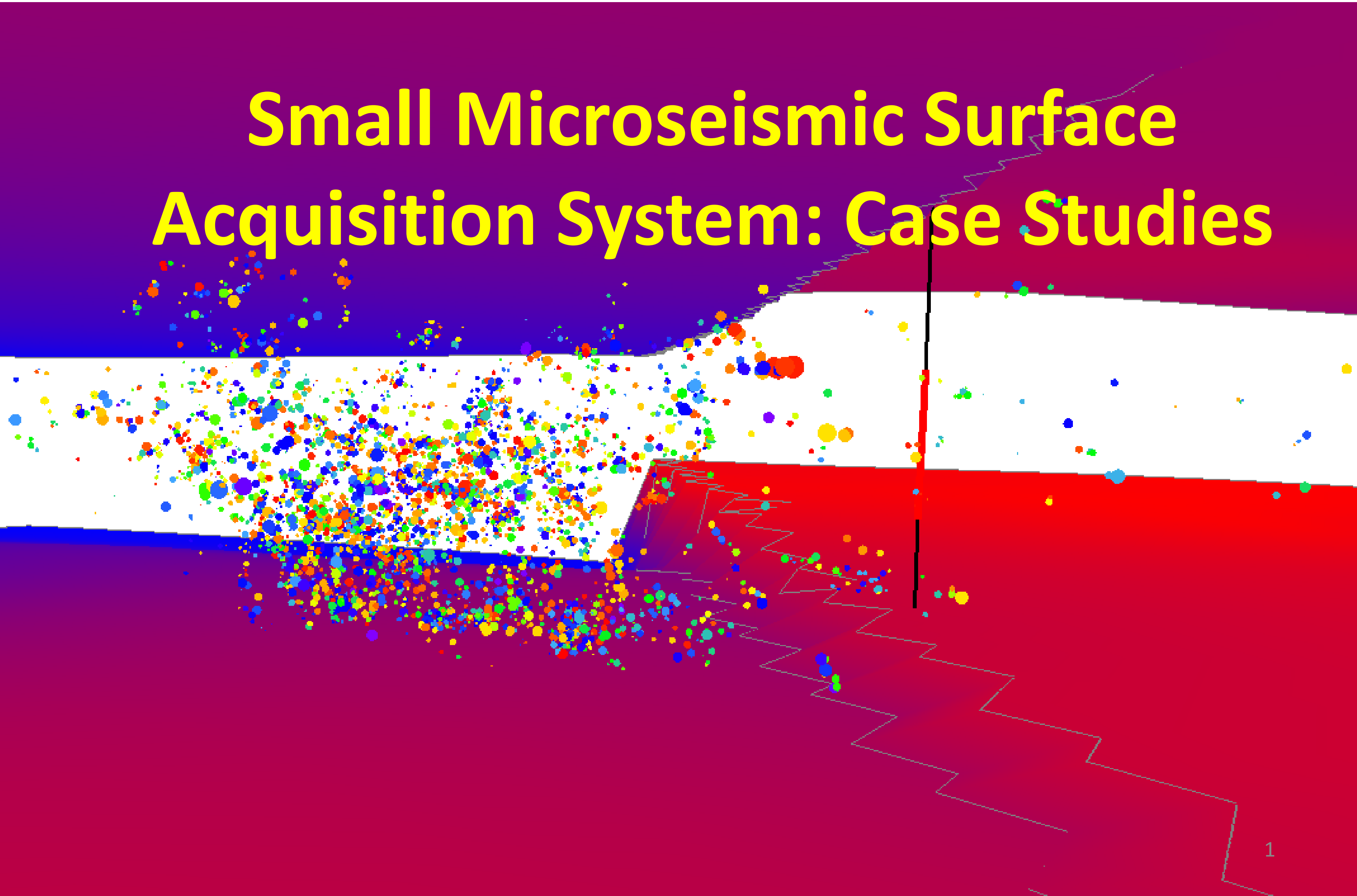

New aspects covered

- Long-duration surface microseismic monitoring of fluid injection
- Surface microseismic monitoring of multistage hydraulic fracturing with subsequent long-duration passive monitoring for the estimation of perforation productivity
- Estimation of drainage area for oilfield
- Oilfield block structure mapping
- Complex interpretation pre-existing fracture (CSP) and results of MicroseismicCSP long-duration microseismic monitoring

Outline

Brief description of the MicroseismicCSP Technology

-Mathematical statement and publications;

-MicroseismicCSP Technology roadmap;

- Computational aspects of the kinematic and dynamic MicroseismicCSP solution;

- MicroseismicCSP acquisition schemes and their specifics

Case Studies

Conclusions

Brief description of the MicroseismicCSP Technology

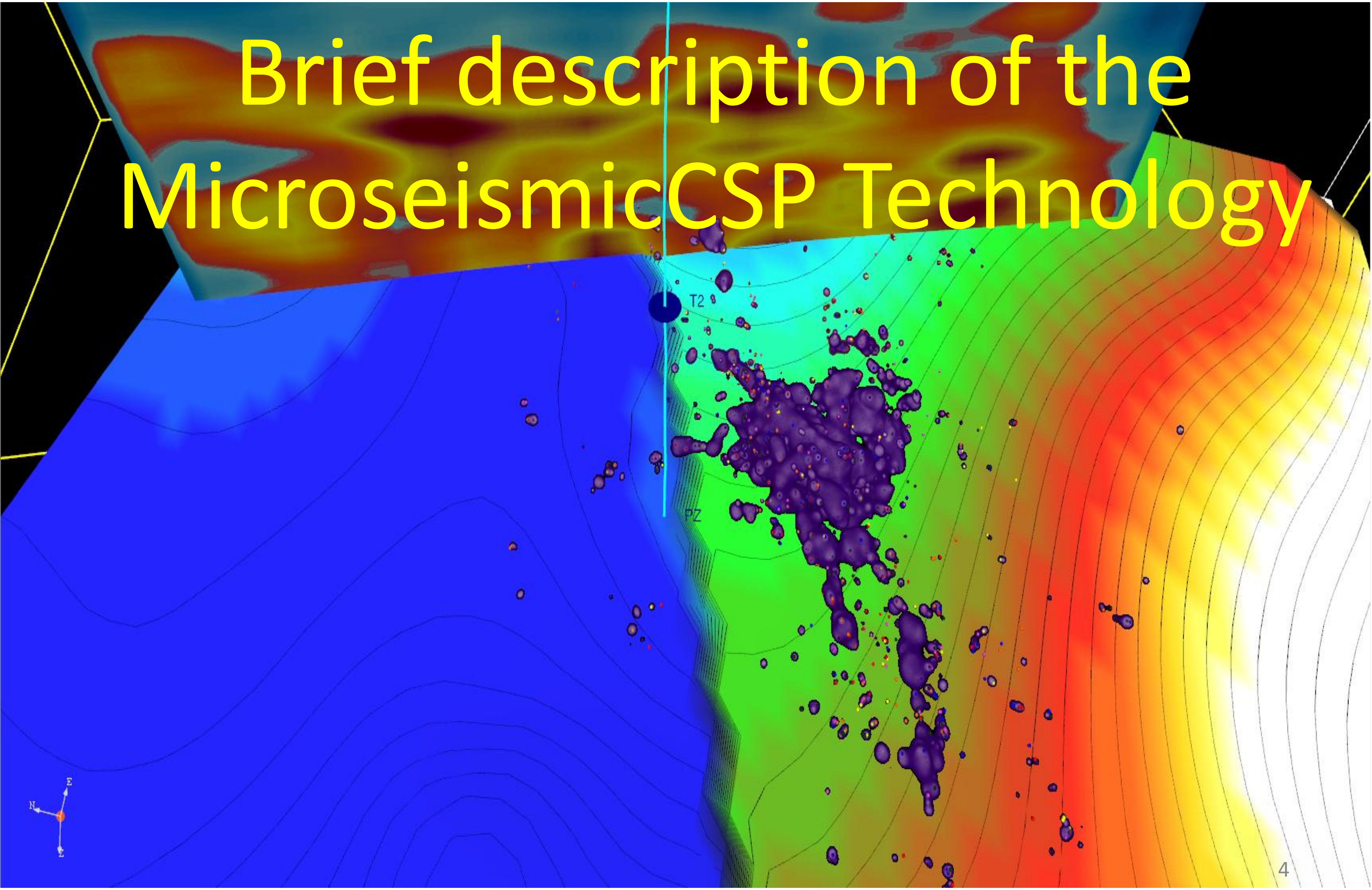

What the MicroseismicCSP Technology is based on?

- Mathematical results for dynamic inverse source problem - Seismic Moment Tensor Inverse Problem (Erokhin G. etc. 1987, Anikonov Y. etc. 1997)
- Parallel Supercomputing Processing (Erokhin G. etc. 2002)
- Small Surface Microseismic Acquisition System (Erokhin G. etc. 2007, 2008)

Our key publications:

- Erokhin, G.N., and P.B. Bortnikov, **1987**, Inverse problem of determination of the earthquake source seismic moment tensor: Geology and Geophysics, **4**, 115-123
- Anikonov, U.E., B.A., Bubnov and G.N. Erokhin, **1997,** Inverse and Ill-Posed Sources Problems, VSP, ISBN 90-6764-273-8.
- Erokhin G.N. , V.P. Kutov, N.L. Podkolodny, S.A. Fedorov, A.F. Kushnir and L.M. Haikin. Computational aspects of seismic monitoring technology of weak earthquakes and explosions on the basis of the solution of a seismic moment tensor inverse problem. // Inverse Problems and Information Technologies. - Khanty-Mansyisk, **2002.** Vol. 1, №2, pp.41-67.
- Erokhin, G.N., S.M. Mynagashev, P.B. Bortnikov, A.P. Kuzmenko, and M.V.Roshkov , Control method of development of hydrocarbons deposits using microseismic emission:RU No. 2309434, Published **2007**.27.10., bulletin 30.
- Erokhin, G.N., S.M. Mynagashev, P.B. Bortnikov, A.P. Kuzmenko, and S.V. Rodin, 2008, The technique of hydrocarbons deposit hydraulic fracturing monitoring: RU No. 2319177, Published **2008.**10.09., bulletin 7.

Mathematical Statement of Seismic Moment Tensor Inverse Problem (SMTIP).

The core of technology is digital processing of data of microseismic surface monitoring of subsurface events which is based on mathematical algorithms for inversion of determining the right-hand side of the Lame's differential equation system (G.N. Erokhin, P.B. Bortnikov 1987; Anikonov Yu.E. etc. 1997; G.N.Erokhin etc. 2002):

$$\frac{\partial \sigma_{ij}}{\partial x_j} - \rho \frac{\partial^2 u_i}{\partial t^2} = \frac{\partial}{\partial x_j} \sigma^0{}_{ij}(x,t) \qquad (1)$$

Here $i, j = 1,2,3,\ x, y \in R^3;\ \ t \in R^1;\ \ \rho$ - the medium density, σ_{ij} - the stress tensor related to the displacement vector $u(x,t) = (u_1, u_2, u_3)$ in the form of

$$\sigma_{ij} = \mu\left(\frac{\partial u_i}{\partial x_j} + \frac{\partial u_j}{\partial x_i}\right) + \lambda \delta_{ij} \frac{\partial u_k}{\partial x_k} \qquad (2)$$

where λ, μ - are the Lame constants and the repetition of indices mean summation and $\sigma^0{}_{ij(x,t)}$ - the stress tensor of the crack which is of the form

$$\sigma^0{}_{ij} = M_{ij}(t)\delta(x-y) \qquad (3),$$

where $i, j = 1,2,3\ y \in R^3$, $\delta(x)$ - is Dirak function of order zero, $M_{ij}(t)$ - symmetric tensor of second order. $M_{ij}(t)$ is called the seismic moment tensor. The tensor $M_{ij}(t)$ has dimension of units of energy measurement $(g \cdot cm^2 \cdot s^{-1})$. The distribution dimension $\delta(x)$ - $1/sm^3$. The vector y describes the coordinates of the earthquake source.

Let the parameter t_0 characterize the time of process beginning in the source $(M_{ij}(t) \equiv 0, t < t_0)$. Let us also suppose that λ, μ and ρ - are the known constants.

Mathematical Statement of Seismic Moment Tensor Inverse Problem (continued).

The inverse problem is in the determination of the parameters t_0, y and the symmetrical tensor $M_{ij}(t)$ from the data of the form

$$v_k(t) = u(x_k, t) + \varepsilon_k(t), \qquad k \geq 4. \tag{4}$$

Here $x_k \in R^3$, ε_k - is the noise of normal distribution, the zero mean value and some known covariance matrix $G_\varepsilon(x_k, x_{k'})$.

Determination of the parameters t_0, y - is the essence of the **kinematic inversion.** The kinematic inversion allows us to determine spatial location of microseismic emission sources and the time of the process beginning The algorithm of determining the kinematic parameters of sources is described in the patent (G.N. Erokhin et al. 2008).

Determination of the tensor components $M_{ij}(t)$ - is the essence of **dynamic inversion**.
To solve both the kinematic inverse problem and its dynamic part, the high level software system using super computer parallel computing has been developed.

MicroseismicCSP as ill-posed inverse problem. Regularized solution.

The results of the kinematic stage of the inverse problem solution are **four parameters**: three coordinates of the events and its beginning time. **Estimation of the velocity is carried out too**. It is supposed that initial value of the velocity is known.

Determination of the beginning time of events is based on automatic cross-correlation data.

The results of the dynamic stage of the inverse problem solution are **six functions** $M_{ij}(t)$

Determination of the events coordinates is based on the minimization the functional (Anikonov etc., 1997, Erokhin etc., 2007, 2008)):

$$J(\eta) = (w - F(\eta))^T V(w - F(\eta)) + (\eta - \eta_0)^T G(\eta - \eta_0) + Sh(\eta) \qquad (5)$$

Here $w = (w_{1,}, \ldots, w_N)$ is the vector of measurements $\eta = (\eta_1, \ldots, \eta_n)$ is the vector of the desired parameters; $F(\eta)$ is the vector of functions for the solution determined from equation (1) with the same dimension as one for the data $w; (\cdot)^T$ denotes the line vector; V is a positively determined symmetric matrix which can completely coincide with G_ε^{-1}, and $Sh(\eta)$ is some external penalty functional; G is some positively defined symmetric $n \times n$ - matrix of the regularity coefficients, η_0 is the vector of a priori values of the stabilizing functional. It should be noted that if we know the covariance matrix of the parameters $G_\eta = \langle \eta \eta' \rangle$, then we may take $G = G_\eta^{-1}$.

The method of minimization

The minimum of functional (5) is determined by the method which is the combination of the Marquardt technique and the regularized quasi-Newtonian method which uses only the first derivatives. The controlled iterative step is given as follows:

$$\eta^{k+1} = \eta^k + \alpha_k p^k \tag{6}$$

$$p^k = -A^{-1}(\eta^k, \zeta^k) Y(\eta^k, \zeta^k). \tag{7}$$

Here α_k is the step of the parameter regulation, $1 \le k \le k_{\max}$,

$$Y = \left(\frac{\partial F}{\partial \eta}\right)^T V\left(F - w\right) + G(\eta - \eta_0) + \frac{\partial\ Sh}{\partial\ \eta}, \tag{8}$$

$$A = \left(\frac{\partial F}{\partial \eta}\right)^T V\left(\frac{\partial F}{\partial \eta}\right) + \Lambda + \frac{\partial^2 Sh}{\partial^2 \eta}. \tag{9}$$

The vector ζ denotes the combination of all the free parameters of functional (5) and iterative processes (6)-(9) being adjusted at each step with respect to k:

$$\zeta^{k+1} = \zeta^k + \Delta\zeta\ (\eta^1, \ldots, \eta^k).$$

Control solution. Creating the optimal algorithm for the inverse problem.

$$J(\eta) = \left(w + \nu_\varepsilon - F(\eta)\right)^T V\left(w + \nu_\varepsilon - F(\eta)\right) + (\eta - \eta_o)^T G(\eta - \eta_o) + \mathrm{Sh}(\eta)$$

ε – relative error of arrival time

δ – relative error of solution

$$\nu_\varepsilon \sim N(0, \varepsilon^2) \quad G = \begin{pmatrix} \alpha_r & 0 & 0 \\ 0 & \alpha_r & 0 \\ 0 & 0 & a_z \end{pmatrix}$$

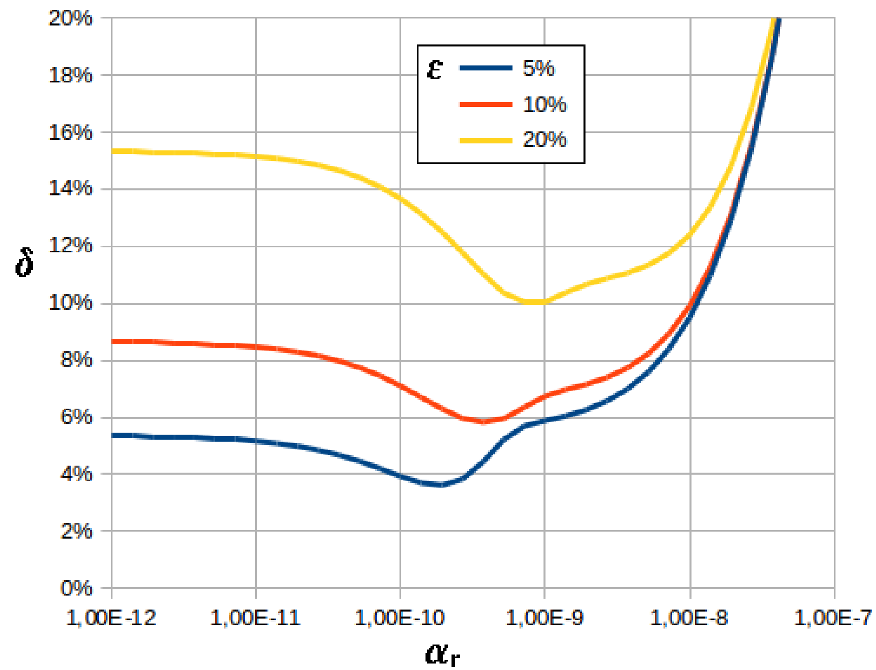

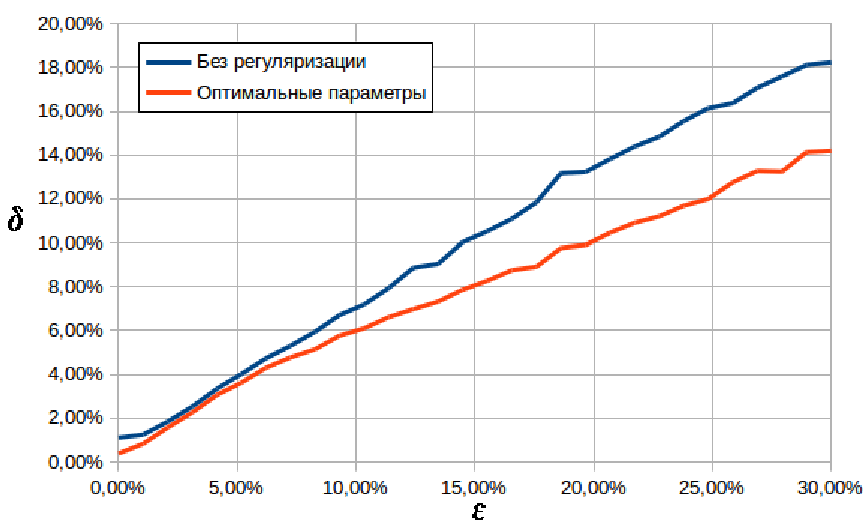

Control of solution accuracy during data processing

Key of control is to follow the roadmap of the optimal inverse problem solutions, which has four steps:

I. Mathematical simulation of seismic wave propagation for the fixed event and for the specific sensor array;

II. The perturbation of simulated data by noise with pre-fixed variance (usually 25-30%);

III. Search the optimal algorithm of inverse problem for preset noise, event parameters and sensor array in the fixed stability interval (*so called correctness of domain for the inverse operator - ill-posed problems theory*);

IV. Apply the optimal algorithm to real microseismic data

Small Surface Microseismic Acquisition System

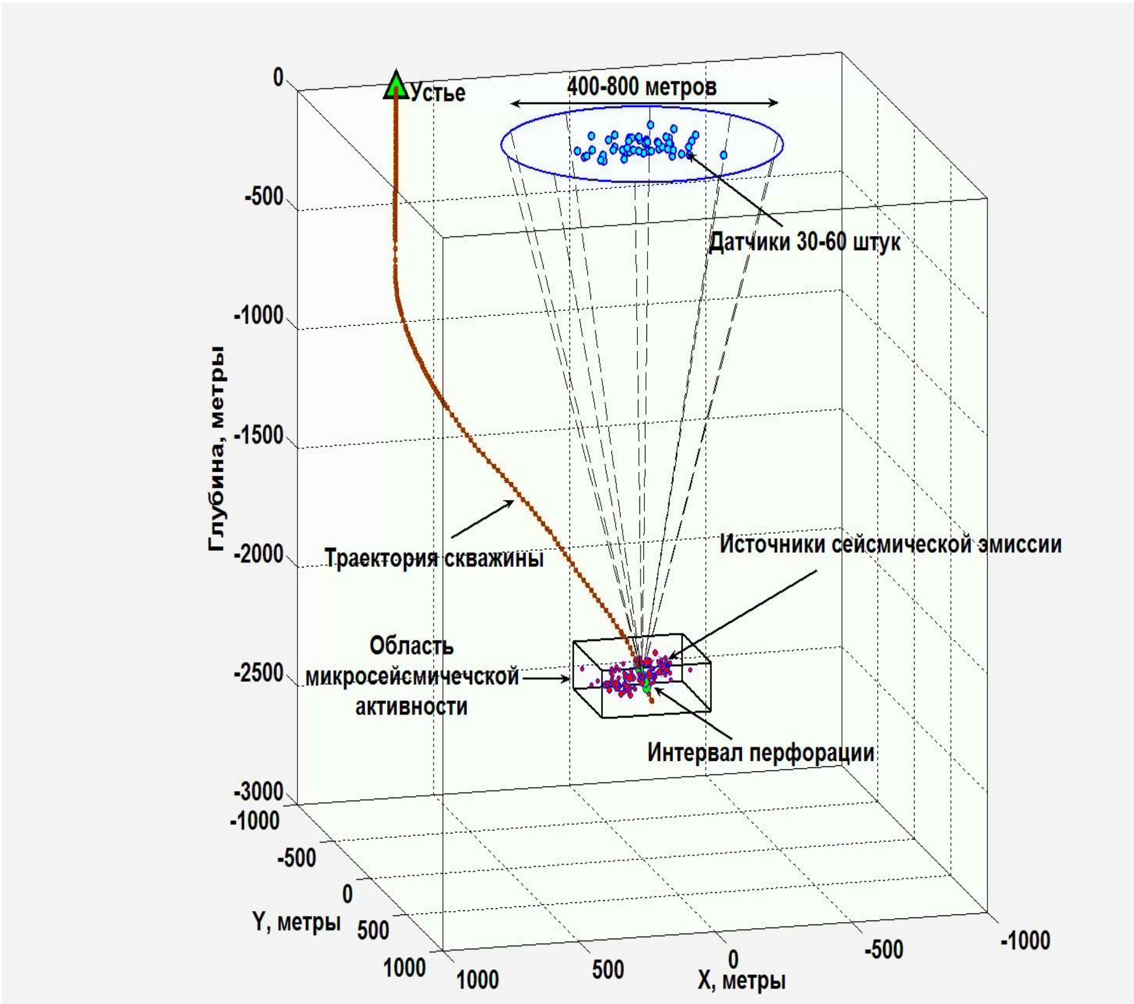

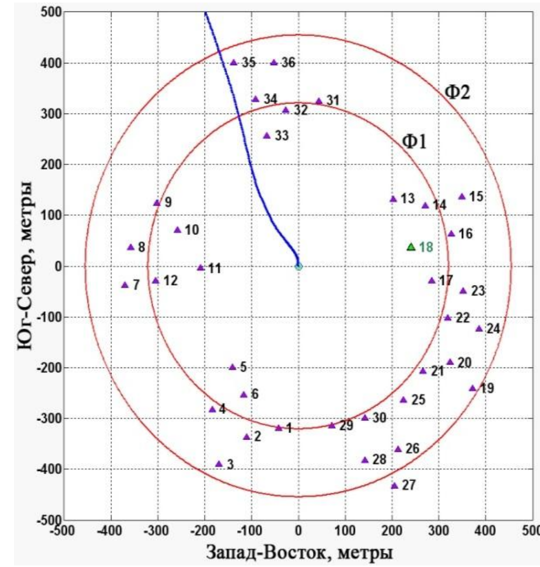

Acquisition scheme. The blue curve shows the wellbore path.
Triangles - the location of the sensors with the numbers

The vertical geophones GS-11D or similar are located on 1-3 m depth. Aperture diameter is about 800 m. The number of sensors equals 30-60 units (Figure 1). Coordinates of each sensor in the aperture are calculated with high precision on the basis of GPS. Data sampling is not more than 2 ms. Optimum depths for monitoring in this case are in the range of 2-4 km. **Assumption that event time duration is not more that 50 ms.**

Figure 1. Scheme of Small Surface Microseismic Acquisition System.

Kinematic and Dynamic parts of the MicroseismicCSP

The results of Kinematic stage of the inverse problem solution **are four parameters** : three coordinates of the event and its beginning time.

The results of Dynamic stage of the inverse problem solution are **six components** of Seismic Moment Tensor, which **depend on time.**

Determination of the components is based on the minimization the functional (5) based on the minimization method in equations (6)-(9). (Erokhin G. and P. Bortnikov, 1987, Anikonov Y.etc., 1997, Erokhin G. etc., 2002)).

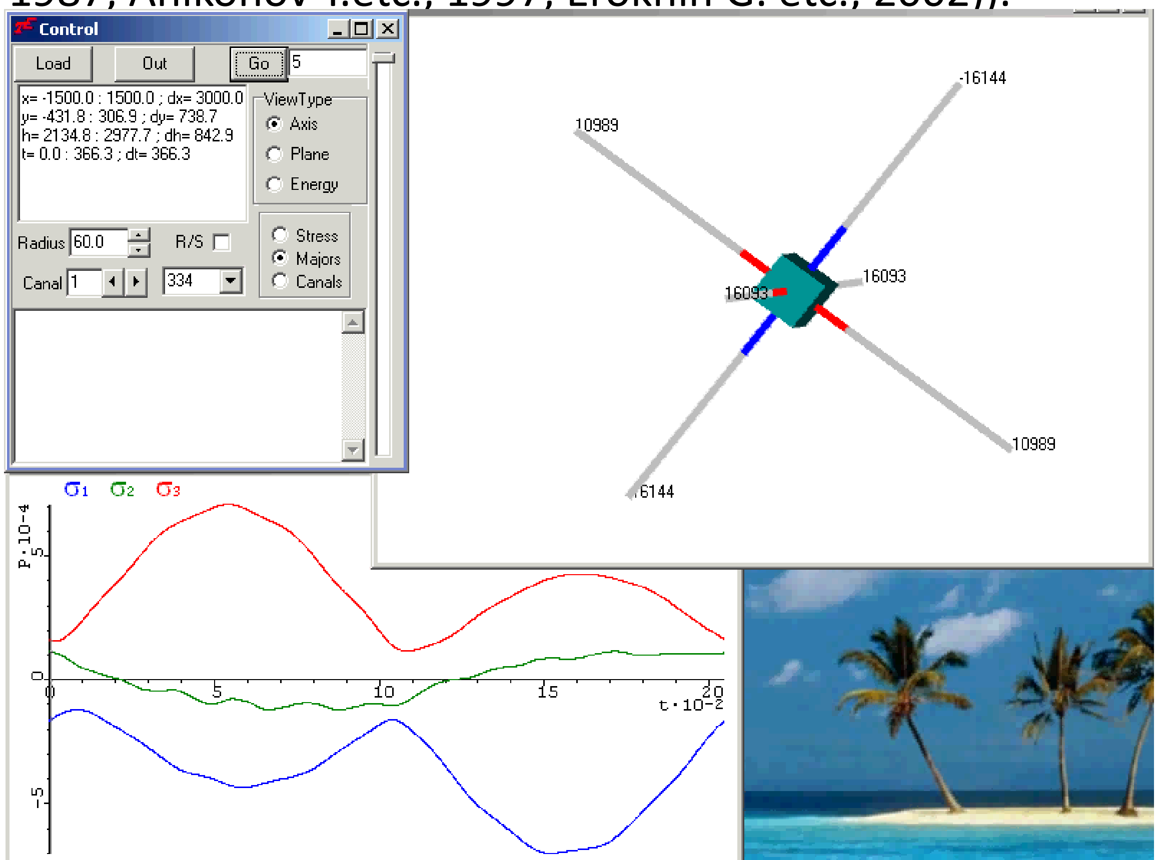

3D visualization of Seismic Moment Tensor **in principal stress axes** during time event

Microseismic event distribution with 3D visualization of seismic moment tensor on principal stress axes

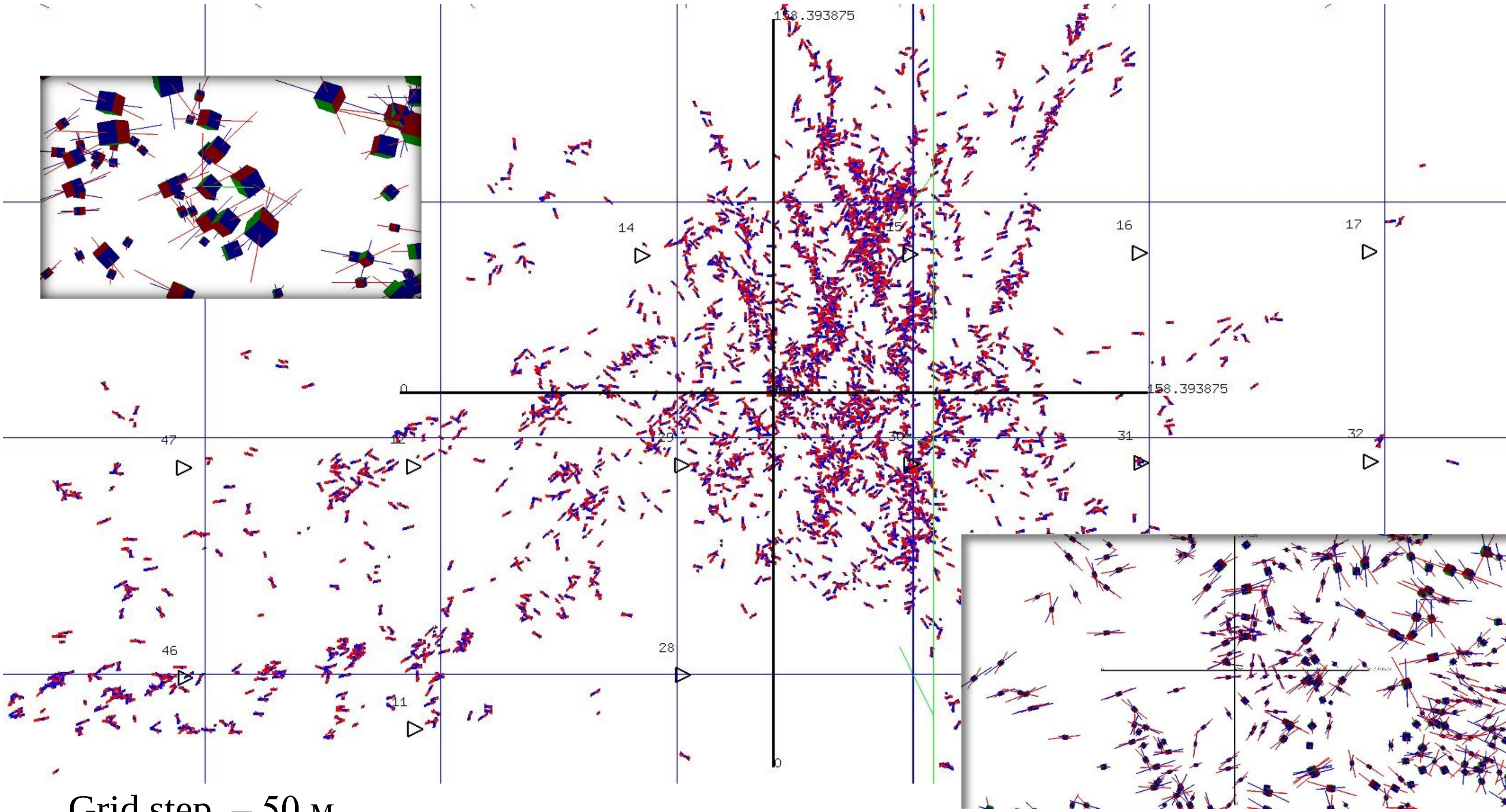

Grid step – 50 м

Microseismic events distribution with 3D visualization of seismic moment tensor in components DC-CLVD-ISO

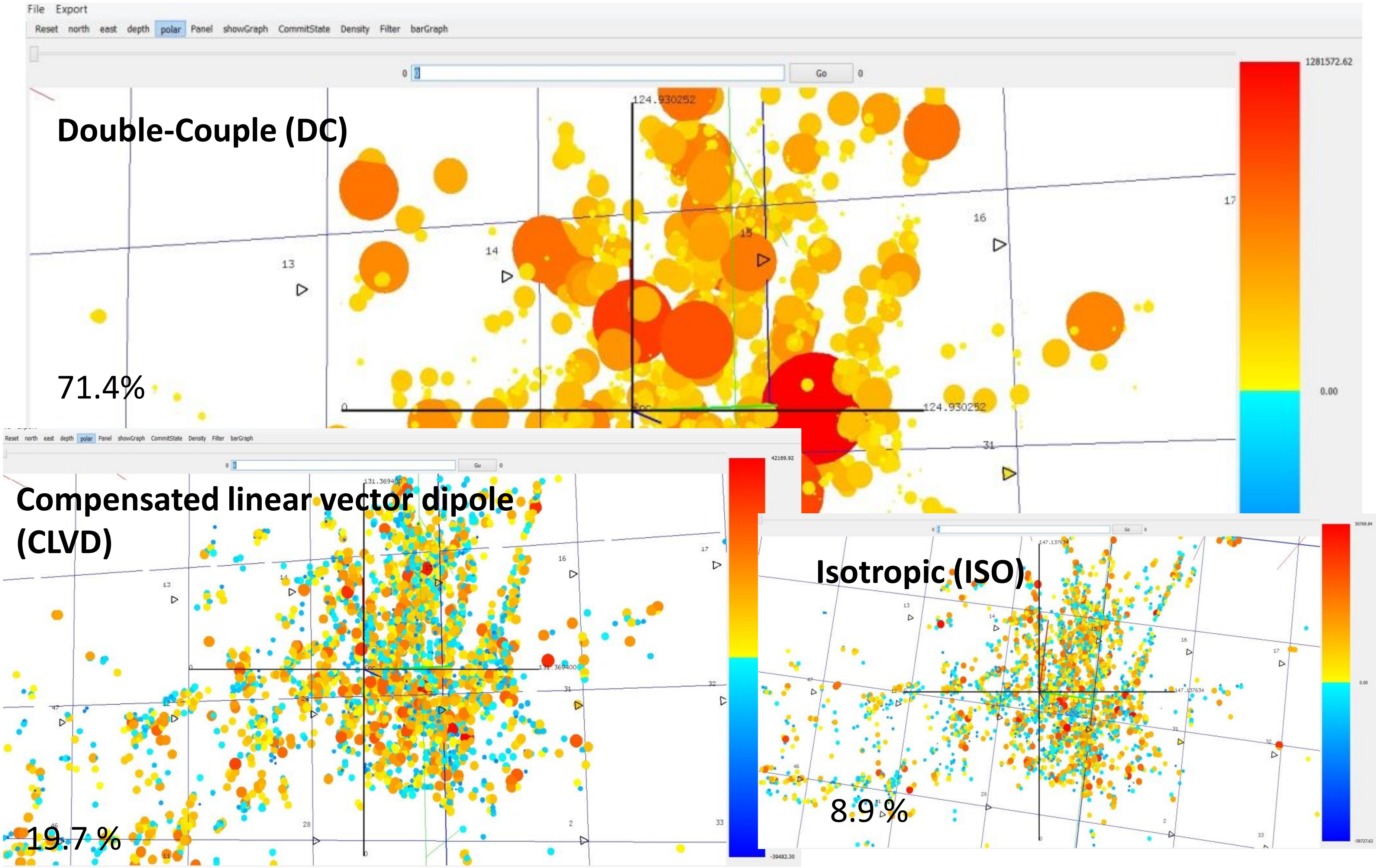

MicroseismicCSP Technology roadmap

Stages of MicroseismicCSP Technology include:

- Array design and installation of acquisition system
- Registration of the noise and perforation shots (calibration)
- Registration on surface microseismic data due to microseismic events
- Preliminary data processing
- Solution of the kinematic and dynamic parts of MicroseismicCSP
- Interpretation of the results

Control of determination coordinates accuracy using perforation

Autonomous node «RefTek 130.1» (6 registrars)

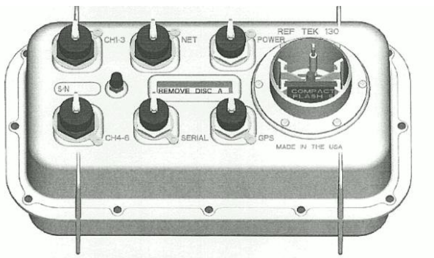

SGD 48/96

Recording equipment

Sensor GS- 11D

Sensor GS-20DX

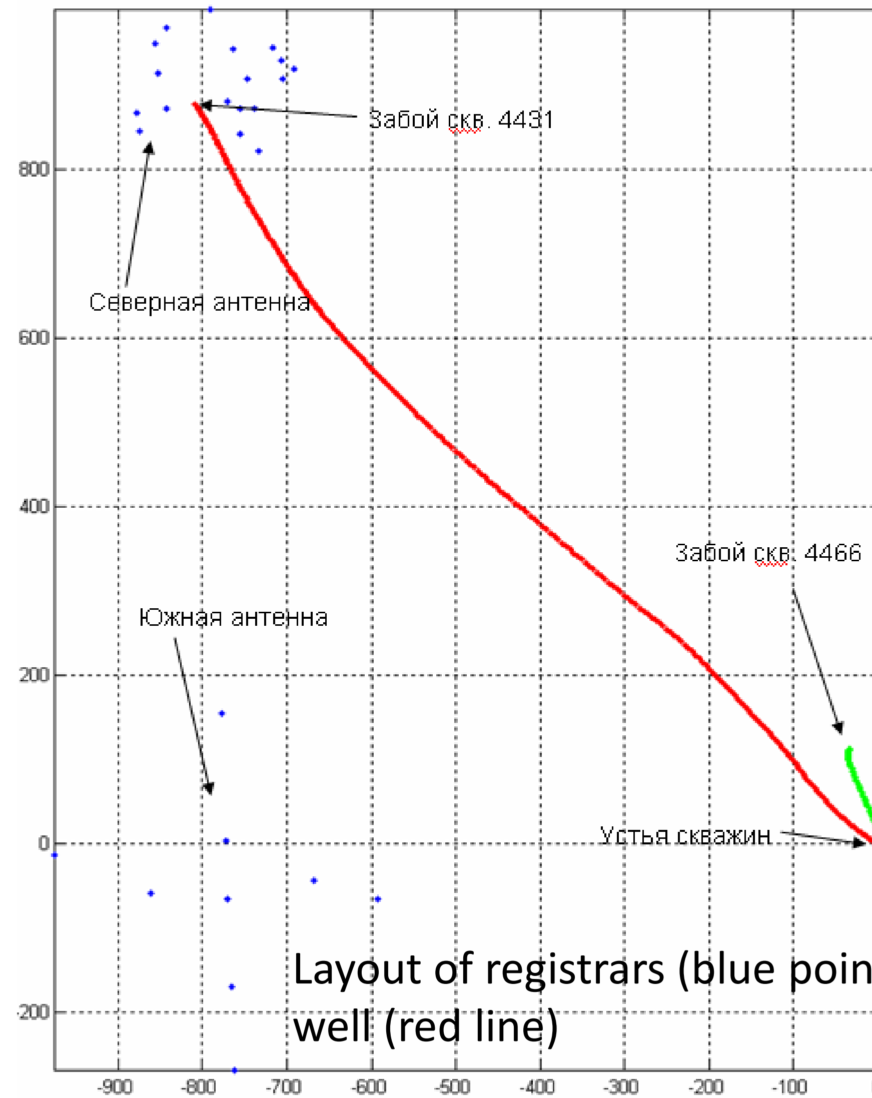

Layout of registrars (blue points) well (red line)

Malobalikskoe oilfield. Well cluster #604, well#4431, The depth is 2760 meters, RefTek, 2006, Ugra.

Perforation. Well #4431, West Siberia

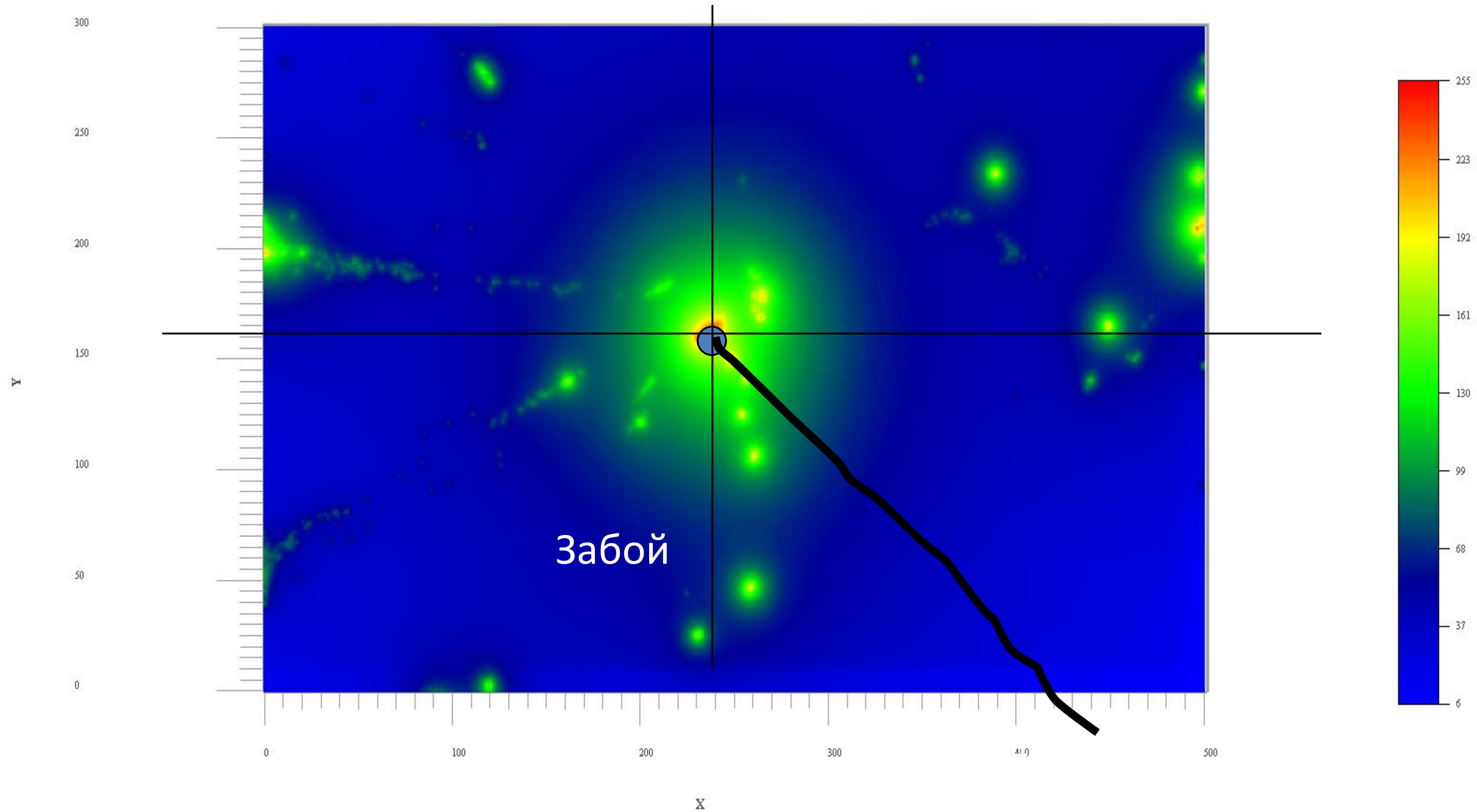

Image of seismic emission for perforation in horizontal plane. Accuracy is 10 meters or better. Malobalikskoe oilfield. Well cluster #604, well#4431. The depth is 2760 meters. 2006, Ugra.

Perforation. Well #3591, Kazakhstan

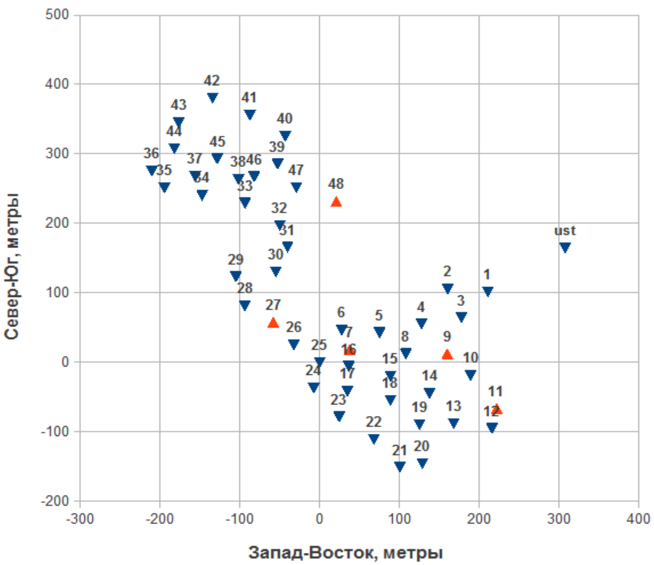

Geometry of the surface receiver array, well #3591.

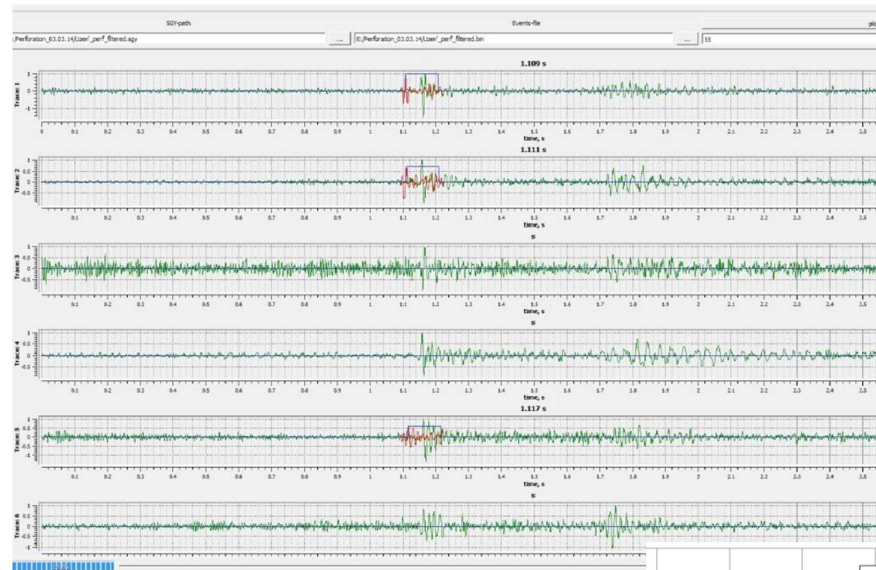

Perforation after filtering. Automated picking the arrivals based on cross-correlation

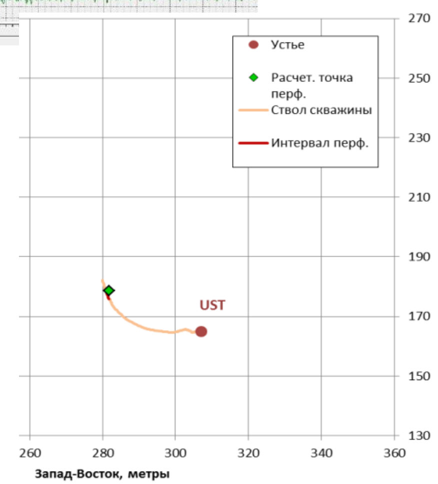

Perforation. Result of processing

Main difference the MicroseismicCSP kinematic inversion from another surface microseismic monitoring approaches consists of the using the massive cross-correlation piking of arrivals and usage the optimization algorithm for simultaneous estimation the coordinates of the event and the effective velocity for each event.

Oilfield Uzen, well #3591, depth 1253-1258 m, SGD-48, Kazakhstan, 2012

Preliminary data processing.
Hydraulic fracturing, well #3591, Kazakhstan

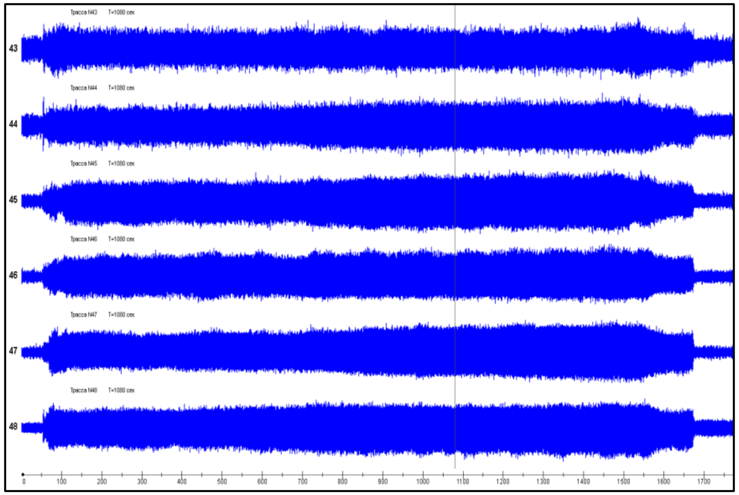

Traces during hydraulic fracturing

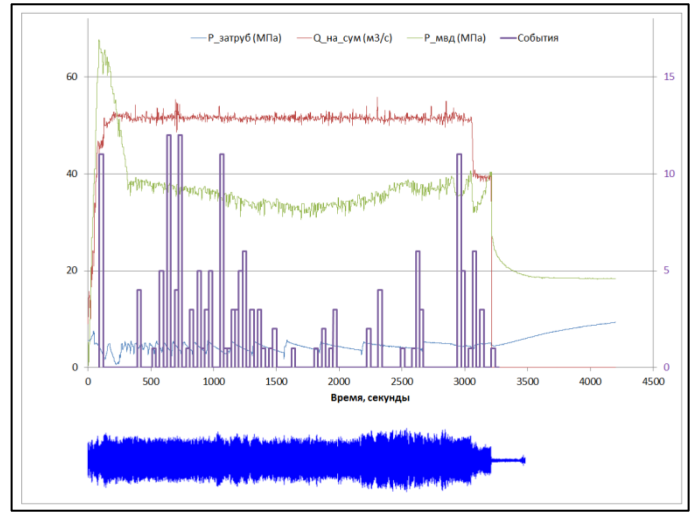

Events during hydraulic fracturing

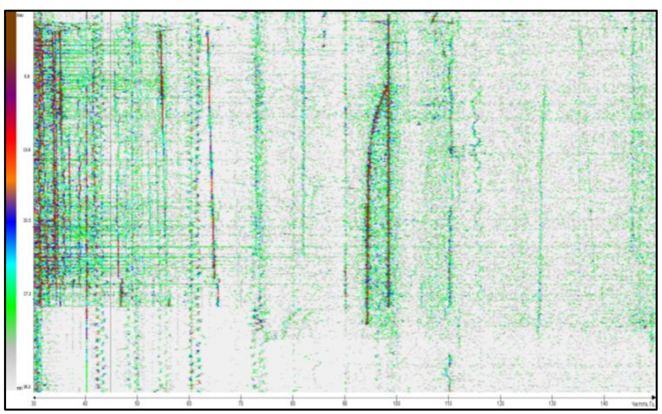

Hydraulic fracturing. Time-frequency map

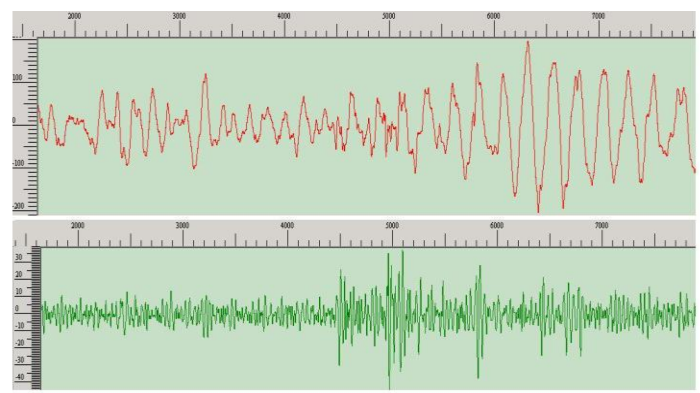

Filtering

Preliminary data processing.
Estimation of the signal level and Seismic Moment
for: (i)perforation, (ii)fracking and (iii) induced microseismic events due to oil inflow

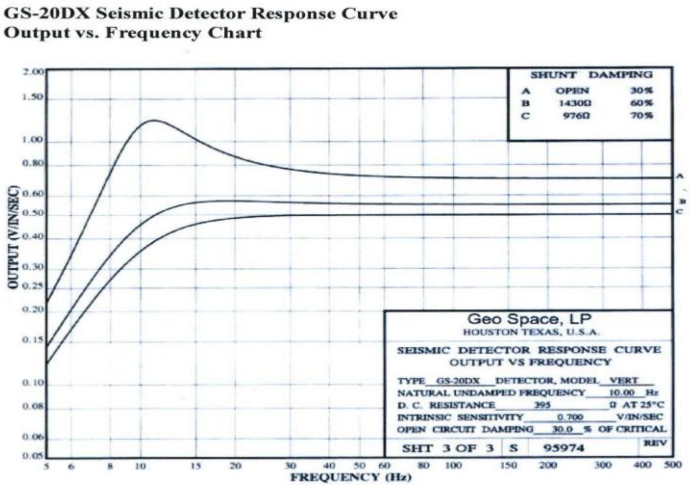

Technical characteristic of sensor GS-20DX

Signal level:

Perforation: 1566.5 nm/sec

(Sig= 37530, K=512)

Shot– 1,1 kg, Perforation depth – 1253-1266 (4 shots)

SGD SHF96:

IVS = 56 V/m/sec

$Sig \in [-2^{23}; 2^{23}]$

W = 598.4 nV

$K \in$ [1;4096]

Fracking: 654.5 nm/sec

(Sig = 1960 , K= 32)

Passive monitoring : 174 nm/sec

(Sig = 2085, K=128)

$$S = \frac{Sig * W}{IVS * K}$$

IVS – intrinsic voltage sensitivity [V/m/sec]

W – bit weight [nV]

S – signal [m/sec]

Sig – digital signal

K – gain constant

SGD SHF48:

IVS = 28 V/m/sec

$Sig \in [-2^{23}; 2^{23}]$

W = 598.4 nV

$K \in$ [1;4096]

Seismic Moment Magnitude:

Perforation: -1.6

Fracking: -1.9

Passive monitoring: -2.3

The Schemes Examples and MicroseismicCSP Features of Acquisition Systems

Features:

- **Small size of aperture (0,2 sq. km)**
- **High density of sensors: 200 sen./sq. km.**
- **Data sampling under 1 ms.**
- **Possibility of long duration observation (more 2 weeks).**

“Srediy Nazim” oilfield

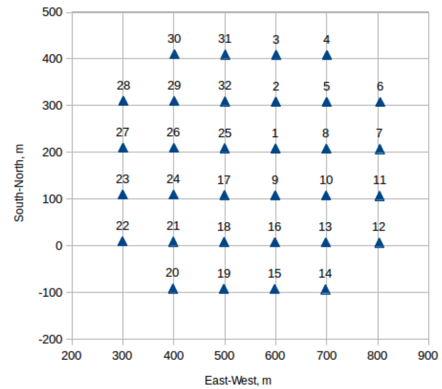

“Oimasha” oilfield

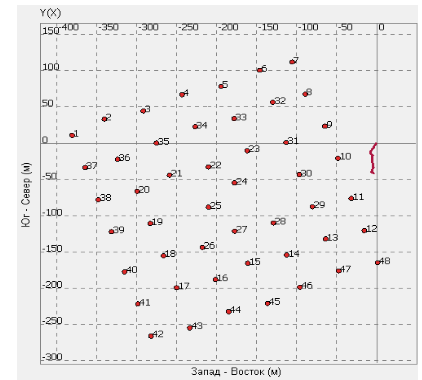

“Nazim” oilfield

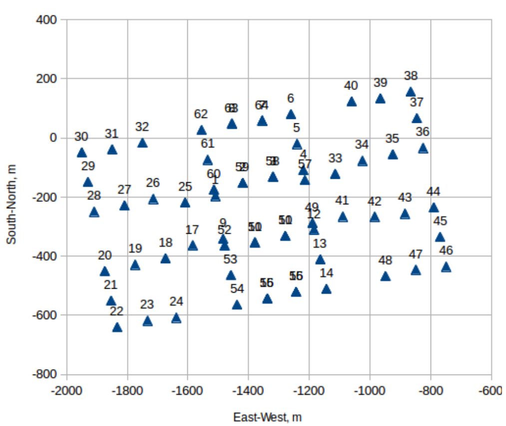

“Uzen” oilfield

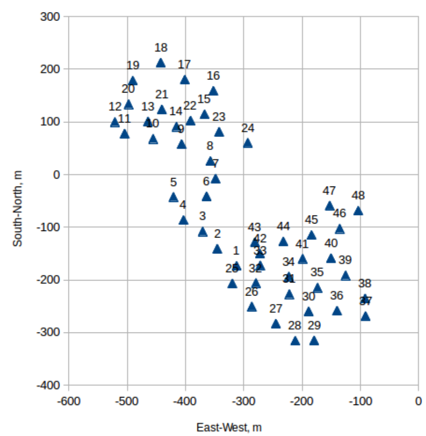

“Ashiagar” oilfield

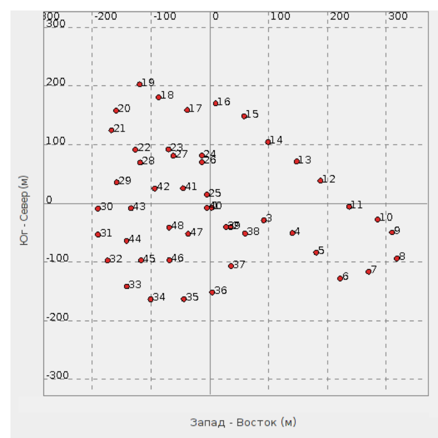

“Alatube” oilfield

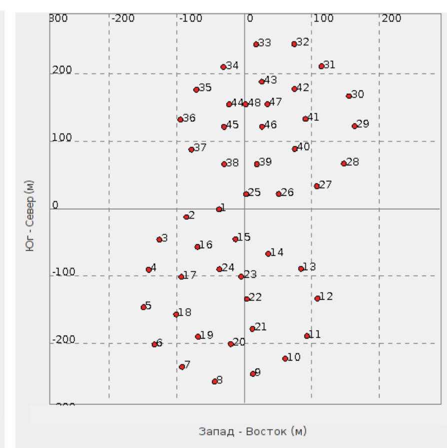

MicroseismicCSP Software

- Data Acquisition

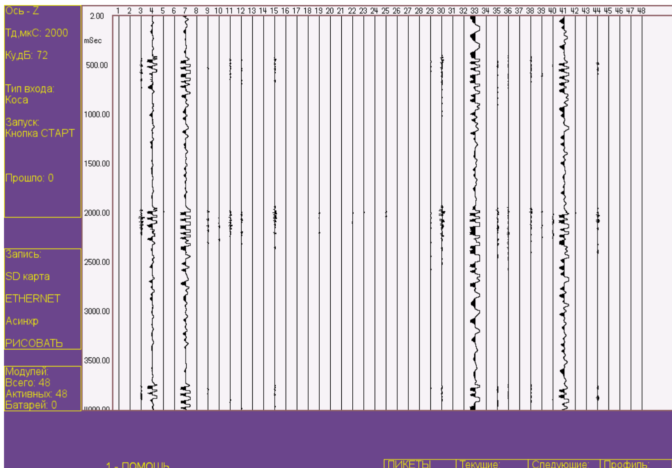

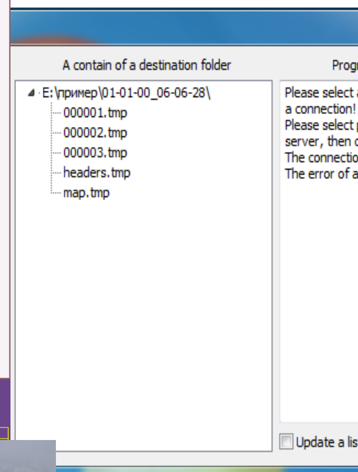

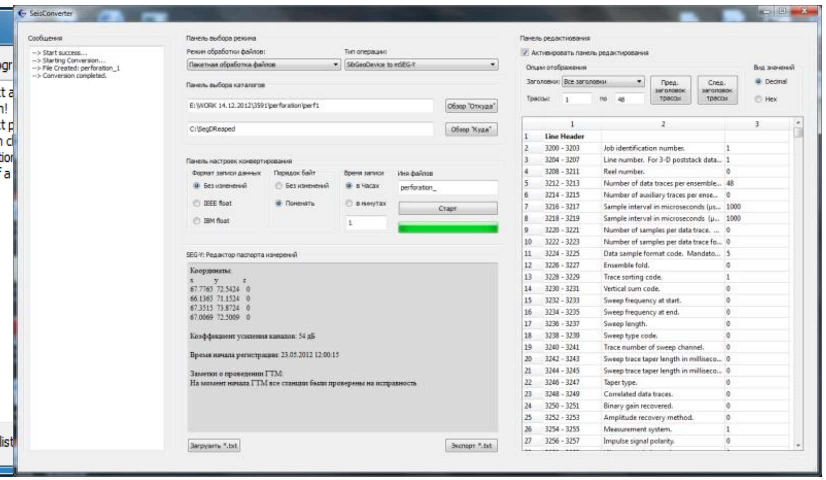

Database

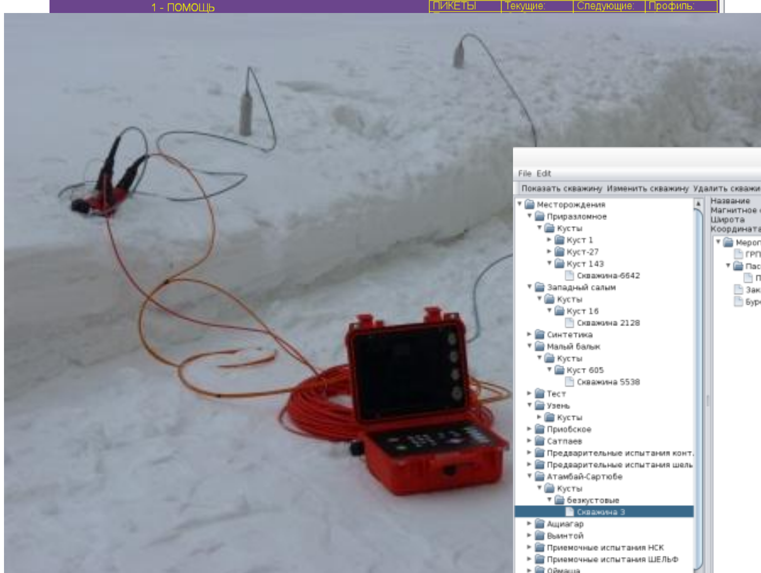

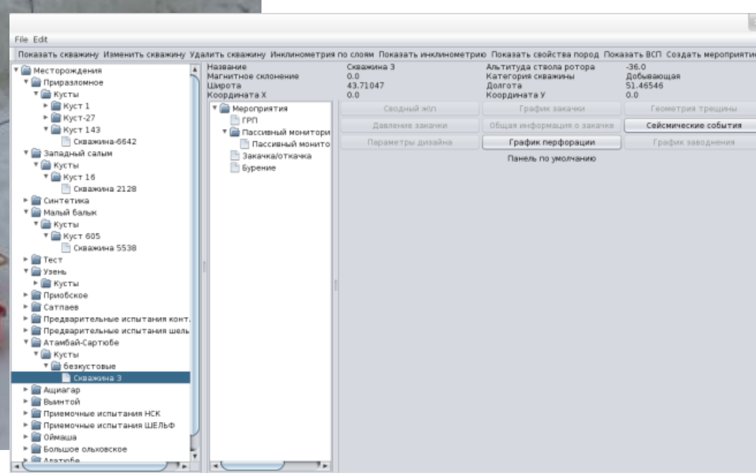

SGD 48D

MicroseismicCSP Software

- Supercomputer Processing

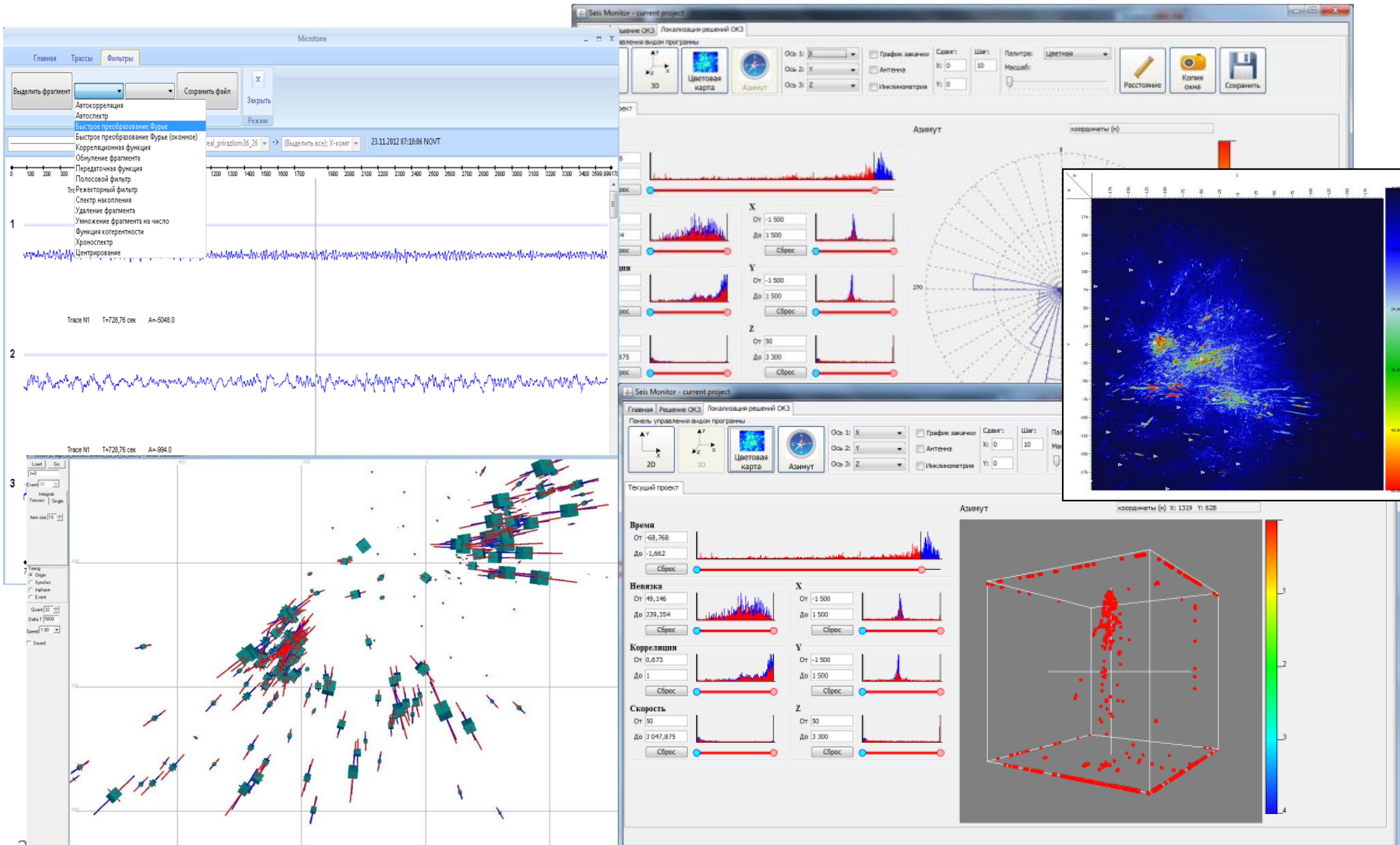

MicroseismicCSP Software

- 3D Visualization

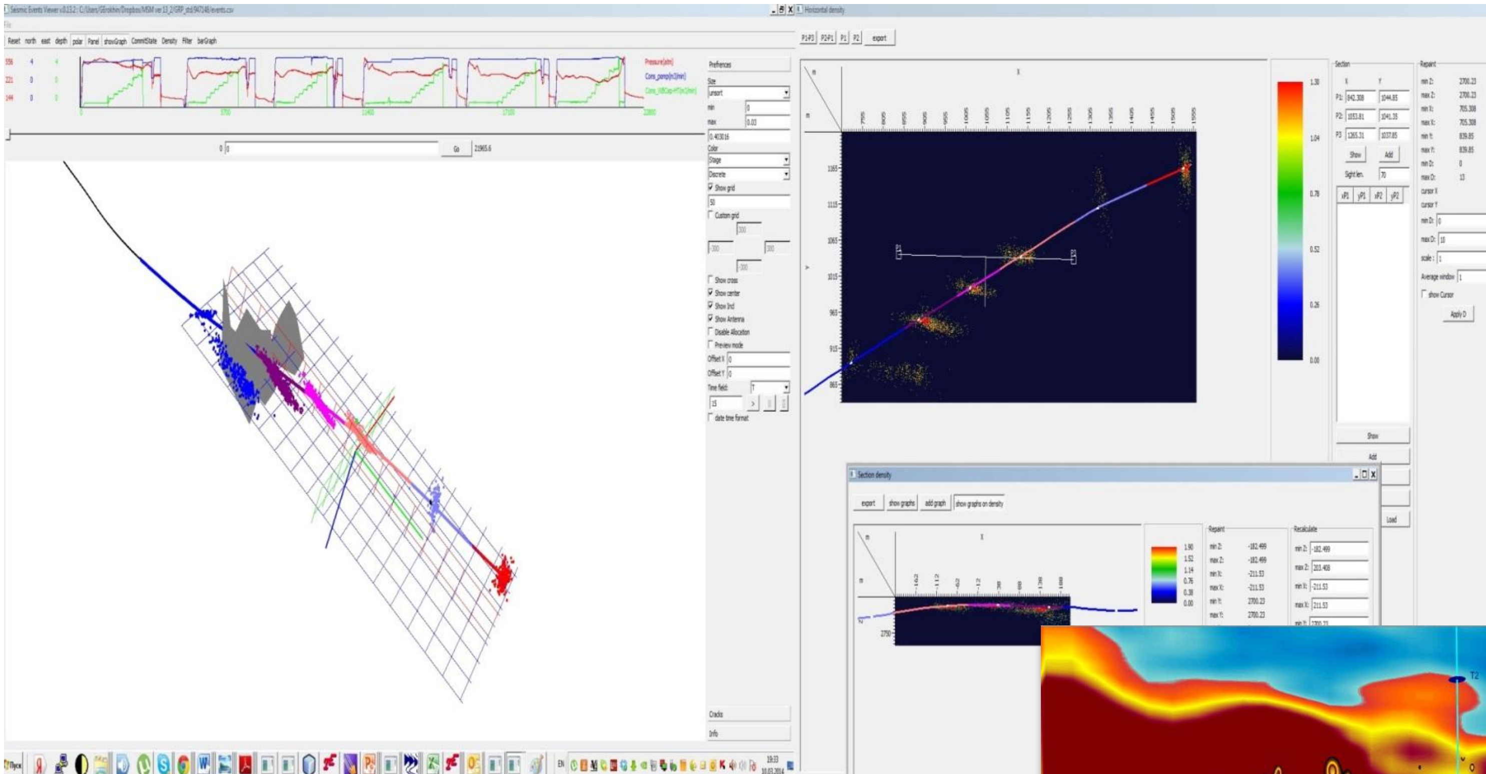

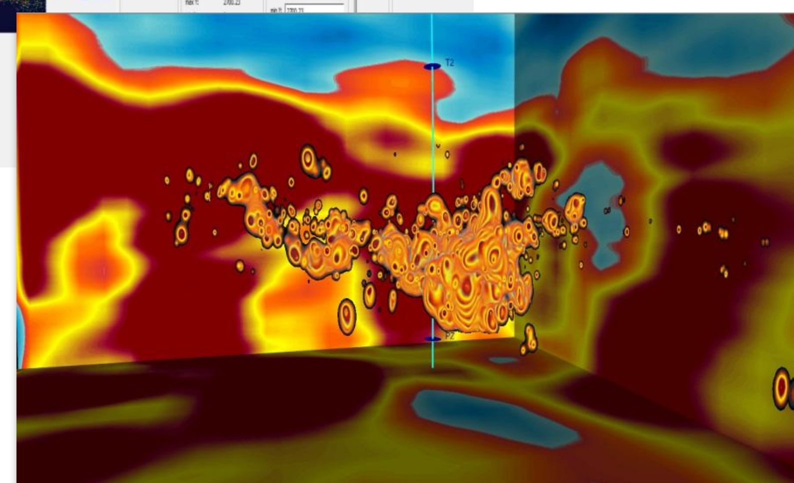

MicroseismicCSP Software

- Interpretation

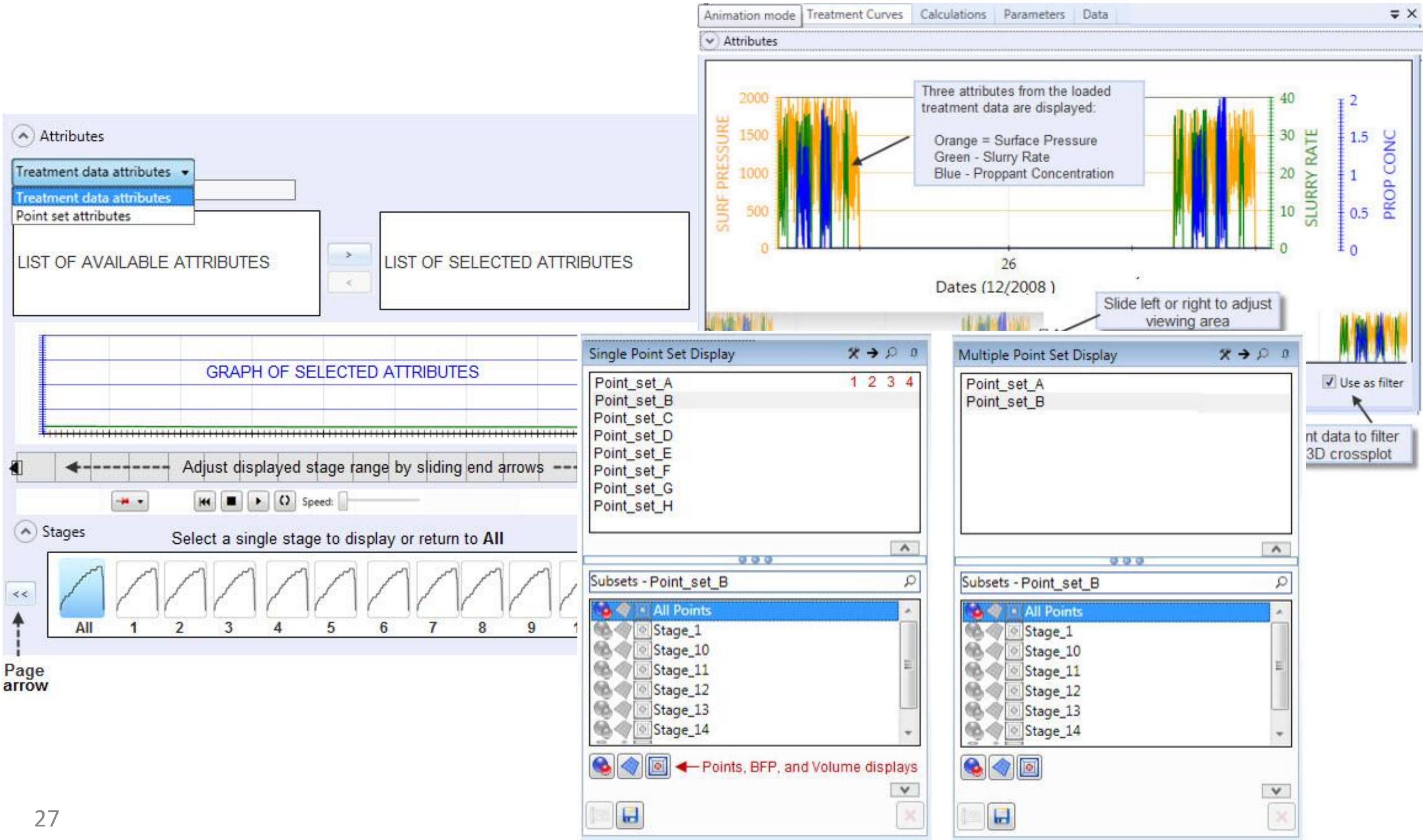

Case Studies

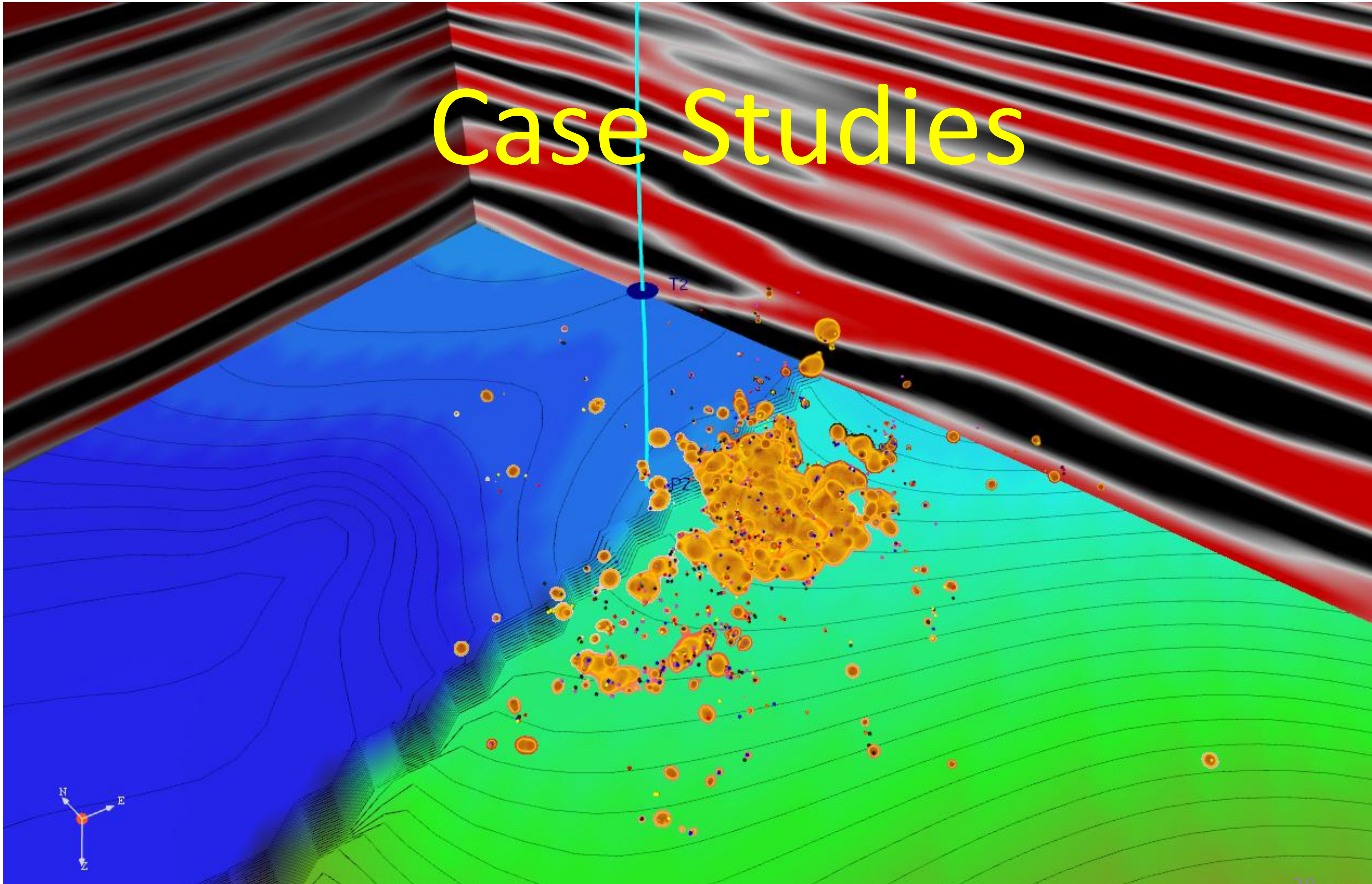

List of the problems, solved by MicroseismicCSP Technology

- **Monitoring of hydraulic fracturing**
- **Control of waterflooding**
- **Estimation of port productivity after multistage hydraulic fracturing**
- **Estimation of area of oil sources of deposits (drainage area)**
- **Oilfield fault-block structure mapping**

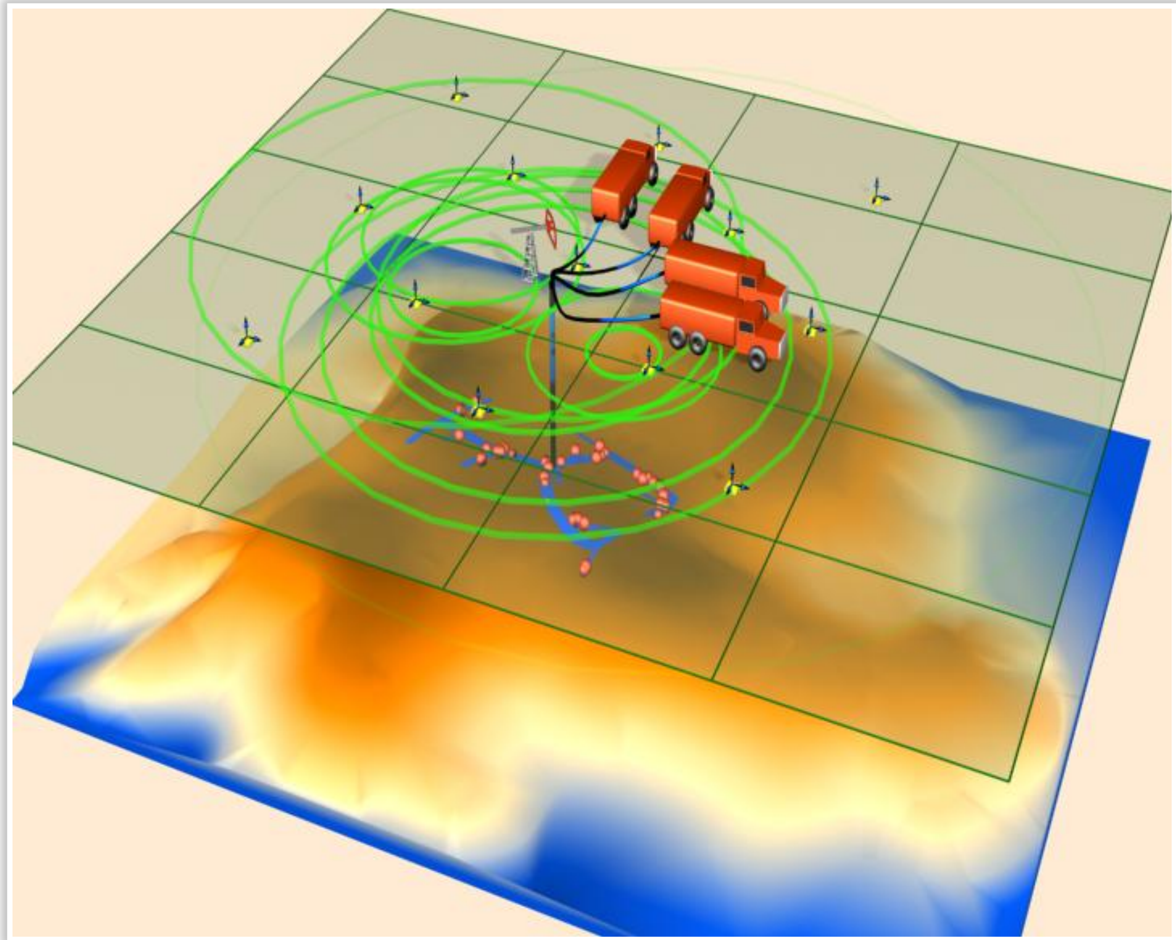

Case study #1: Monitoring of hydraulic fracturing

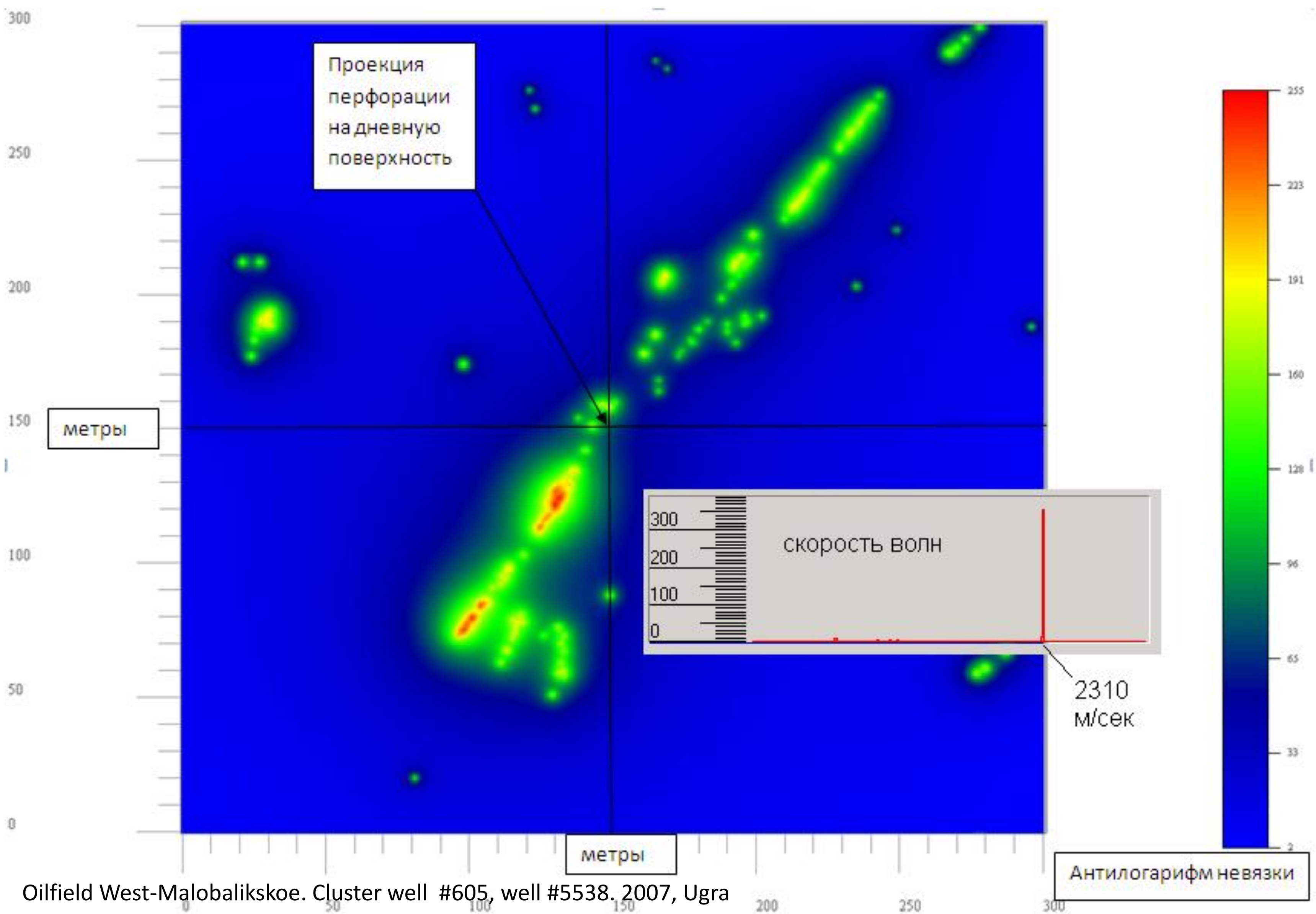

Oilfield West-Malobalikskoe. Cluster well #605, well #5538. 2007, Ugra

Case study #1: Source Mechanisms. Directions of the principal axes of stress at fracturing

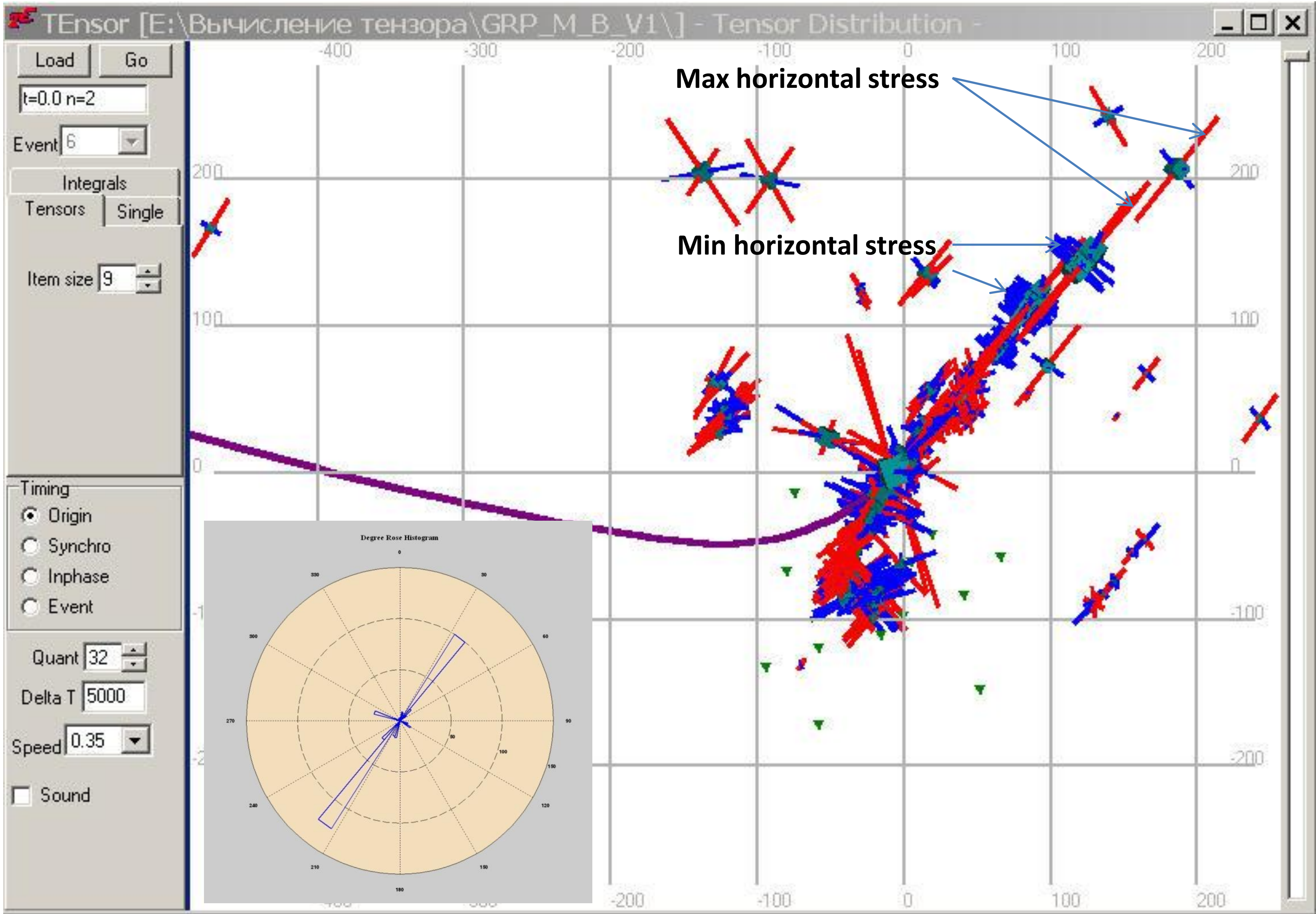

Oilfield West-Malobalikskoe. Cluster well #605, well #5538. 2007, Ugra

Case study #2: Example of unilateral crack.

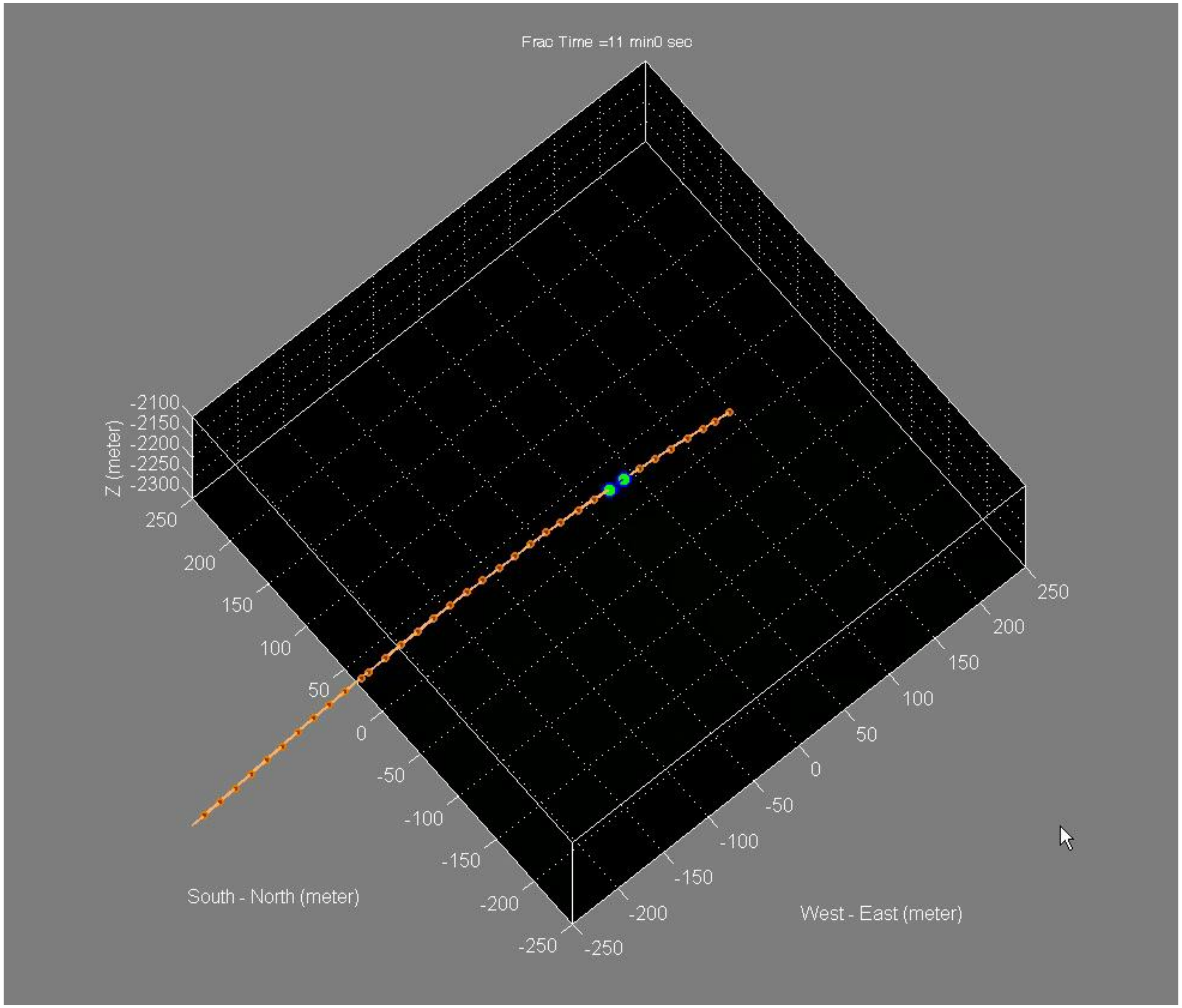

Oilfield Ugno-Khilinchuskoe, well 2011, Komi, 2011

Case study #3: Experimental confirmation of reliability of results of MicroseismicCSP Technology by practice. Case of big crack during fracturing.

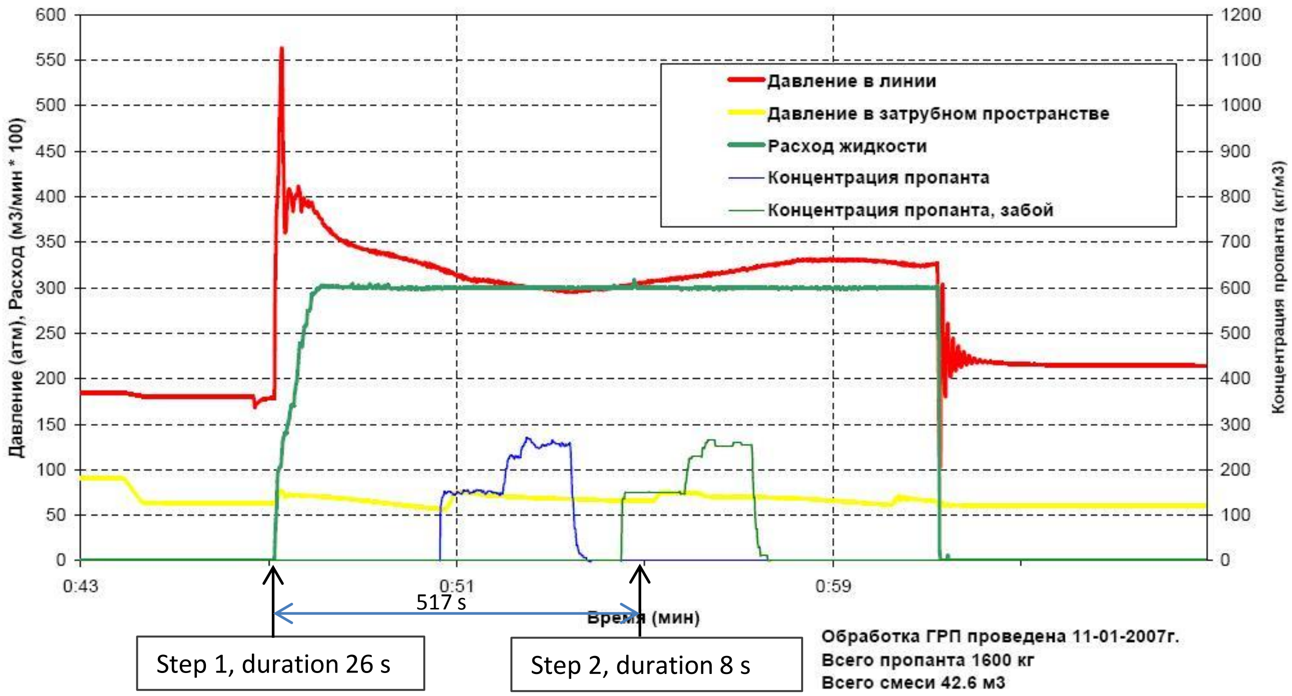

Mini-fracturing. Galianovskay oilfield, UGRA, 2007, well cluster #1, well #39, depth 2538 m, Crack length 510 m, Tight oil (Bashenovsky suite), RefTek

Case study #3: MicroseismicCSP mapping of microseismic events for Step 1& Step 2 in quasi-real time

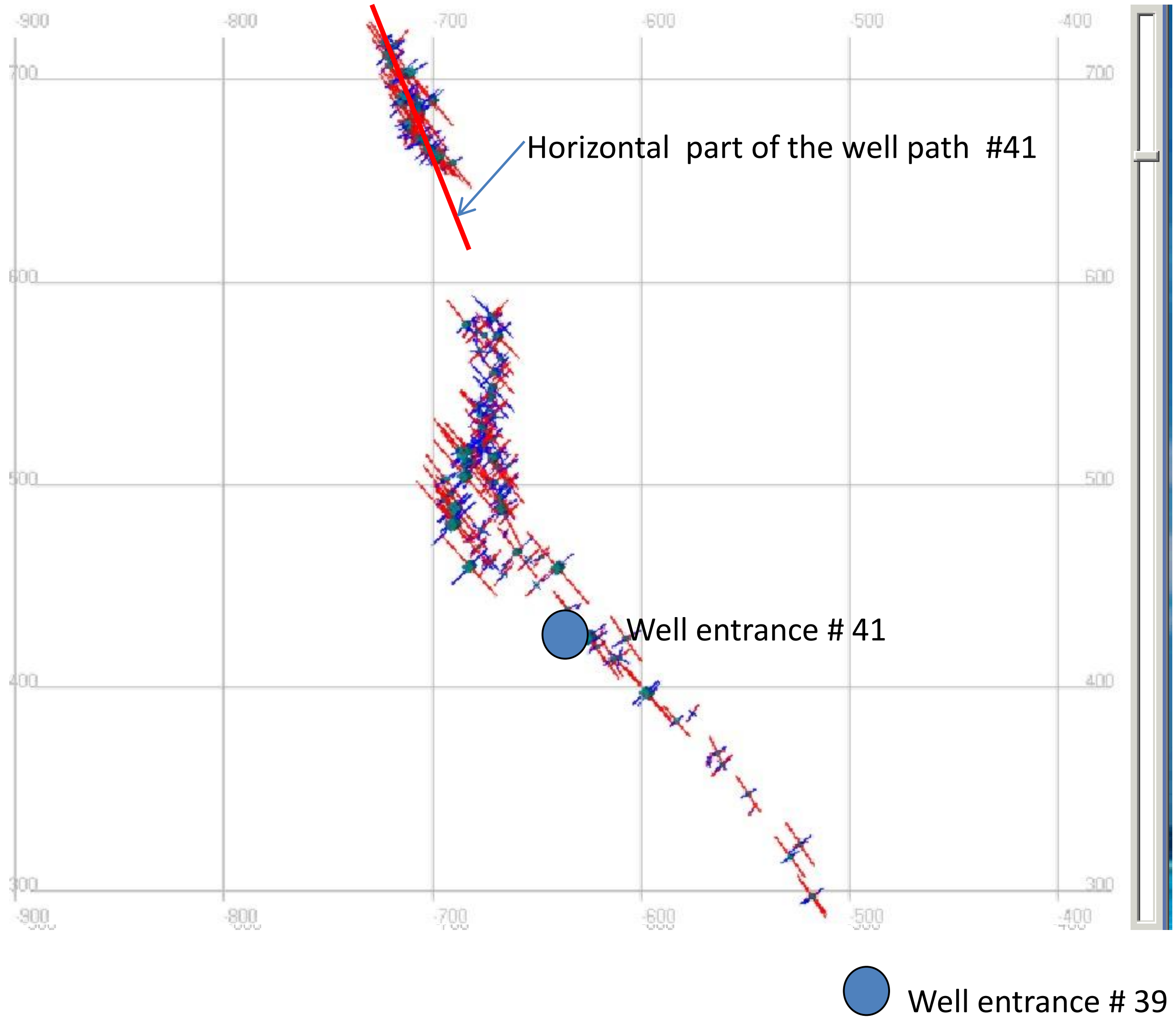

The oil influence of well #41 fell down from 60 tons per day to 40 tons per day **at the next day after fracturing** in well #39

Case study #4: Mapping of filtration water channels during hydraulic fracturing in oilfield

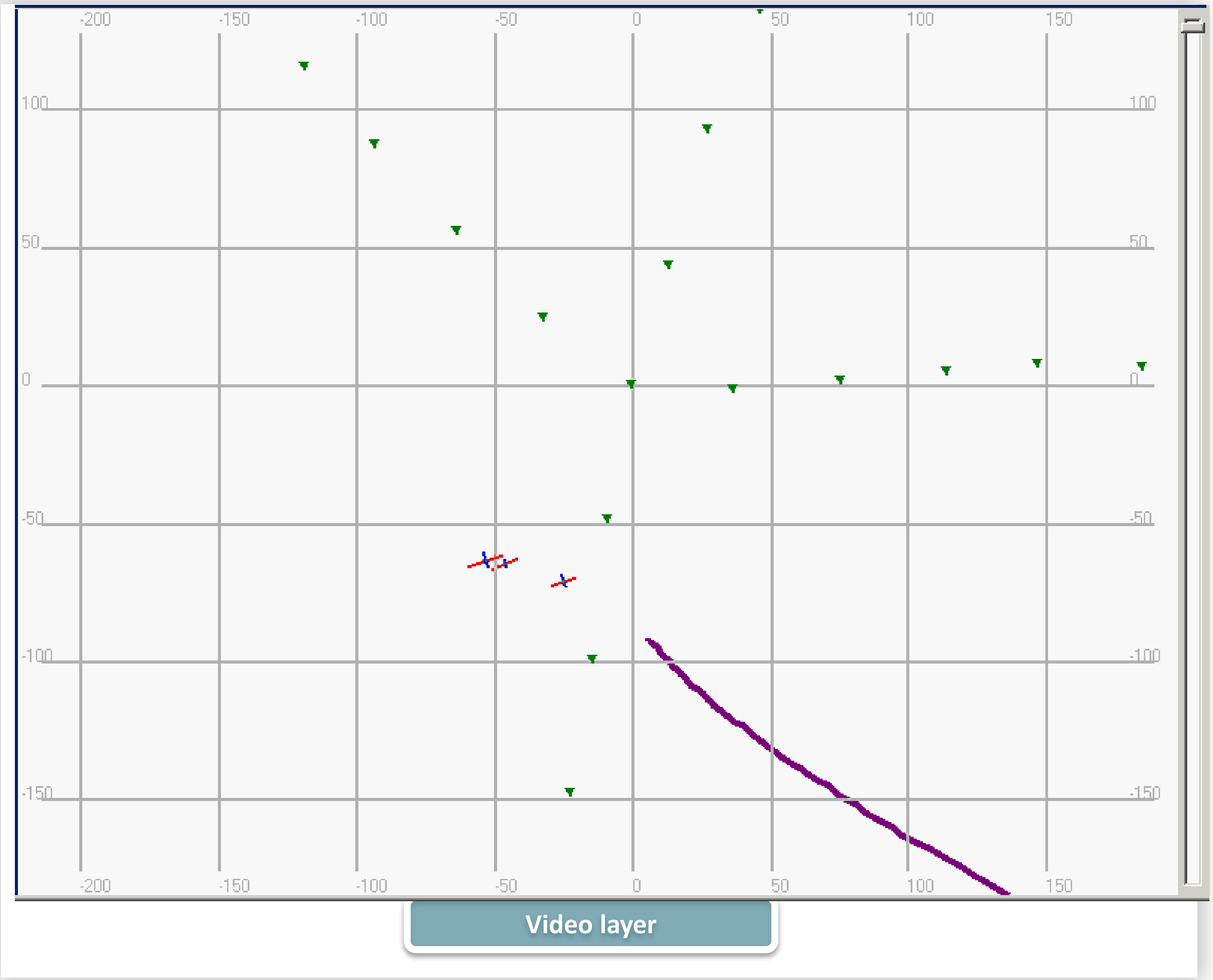

Oilfield Prirazlomnoe. Cluster well #143, well 6642, depth 2640, Ugra, 2005

Case study #5: Multistage Fracturing

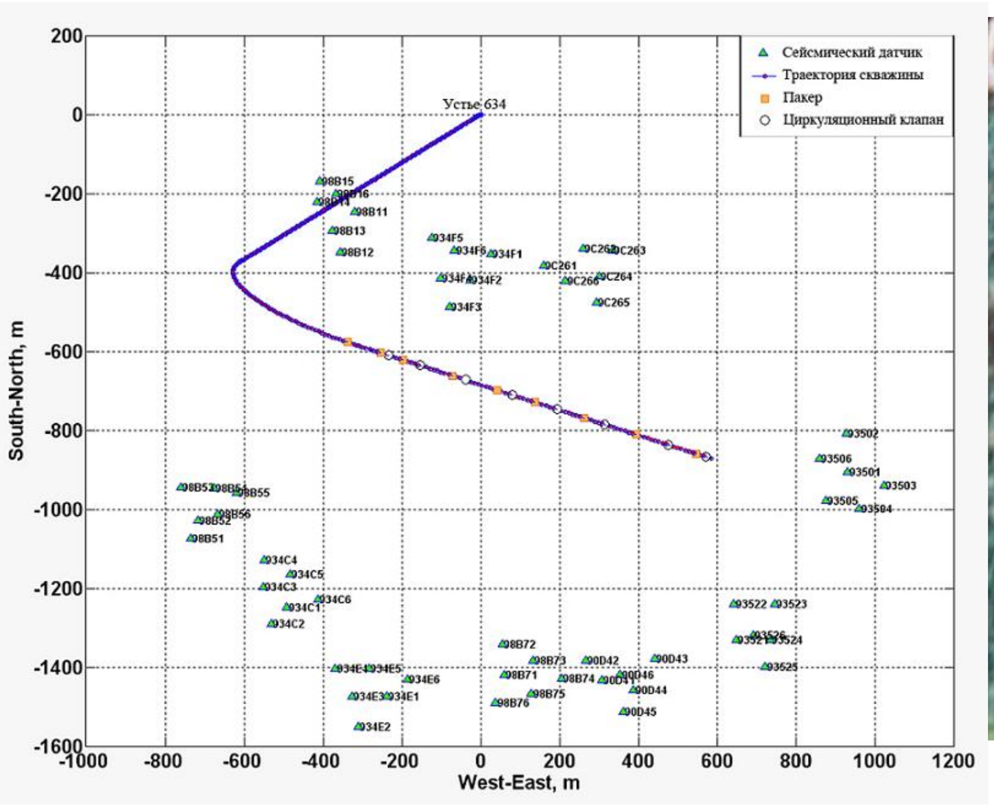

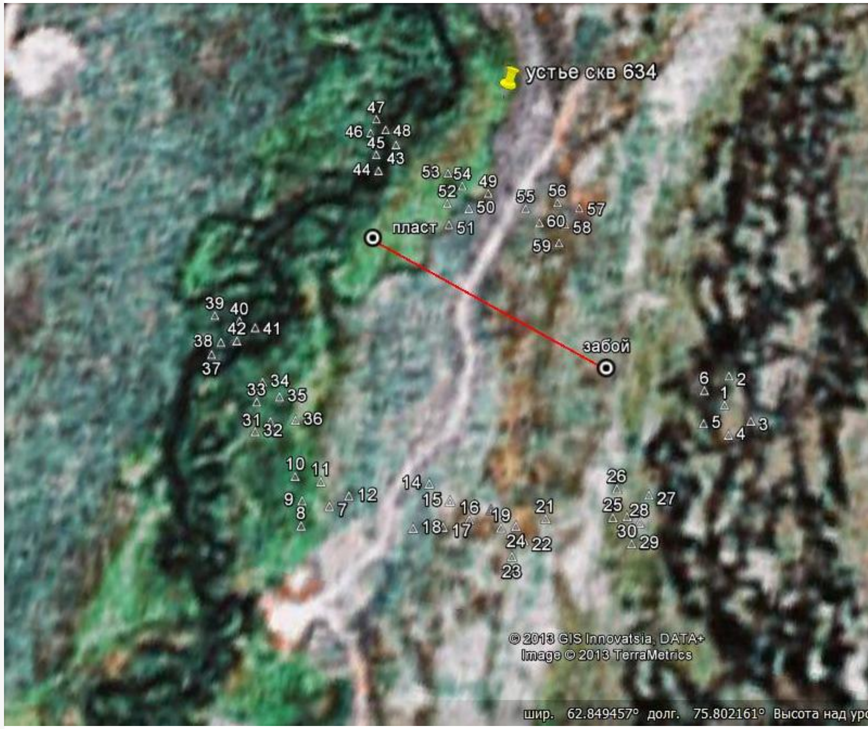

Layout of surface sensors.

Oilfield Vientoskoe, cluster well #11, well #634G, 2013, Ugra

Case study #5: Multistage Fracturing. A summary of the results of monitoring of hydraulic fracturing in 7 ports.

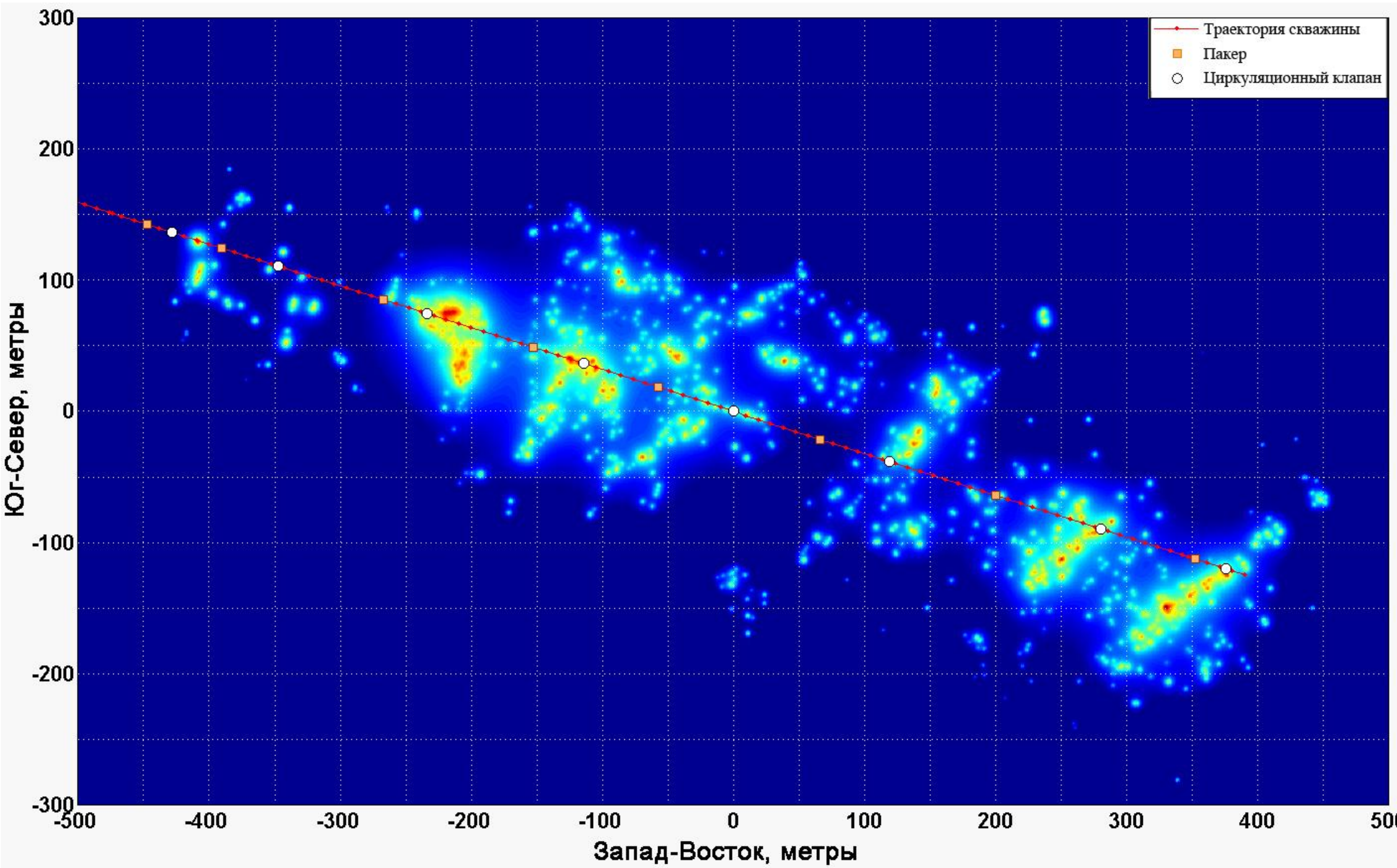

Oilfield Vientoskoe, cluster well #11, well #634G, 2013, Ugra

Case study #5: Multistage Fracturing. The results of monitoring of hydraulic fracturing in the 1st port.

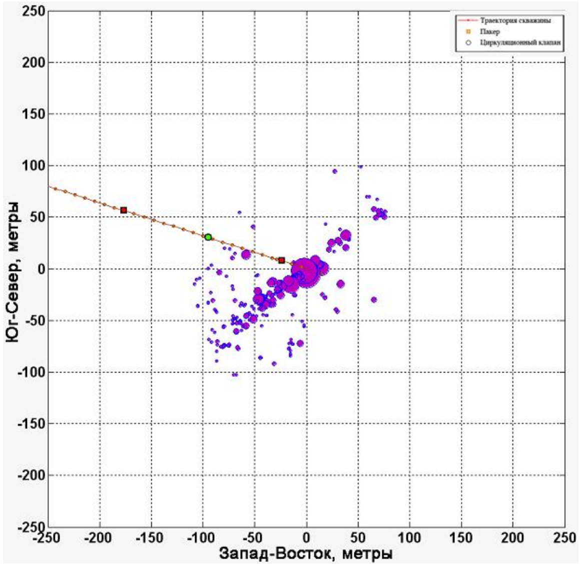

a)

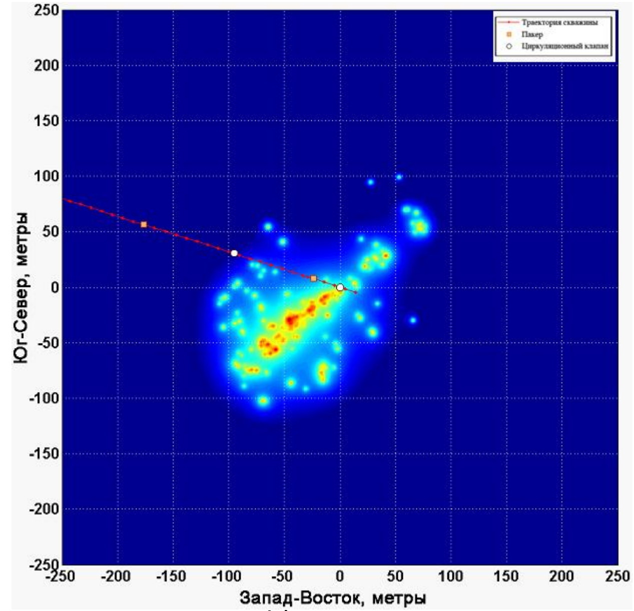

b)

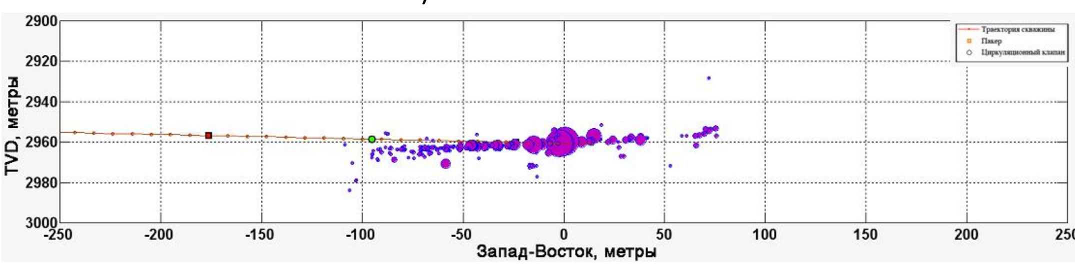

c)

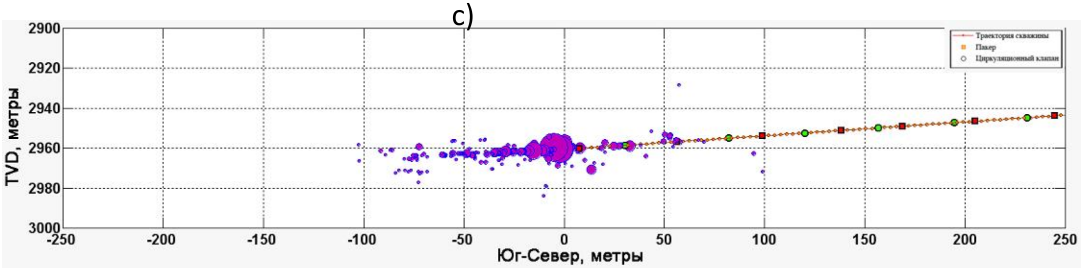

d)

The density of distribution of the sources of seismic emission projection on the horizontal plane of - a) b) and vertical c) and d)

Oilfield Vientoskoe, cluster well #11, well #634G, 2013, Ugra

Case study #5: Multistage Fracturing. Video.

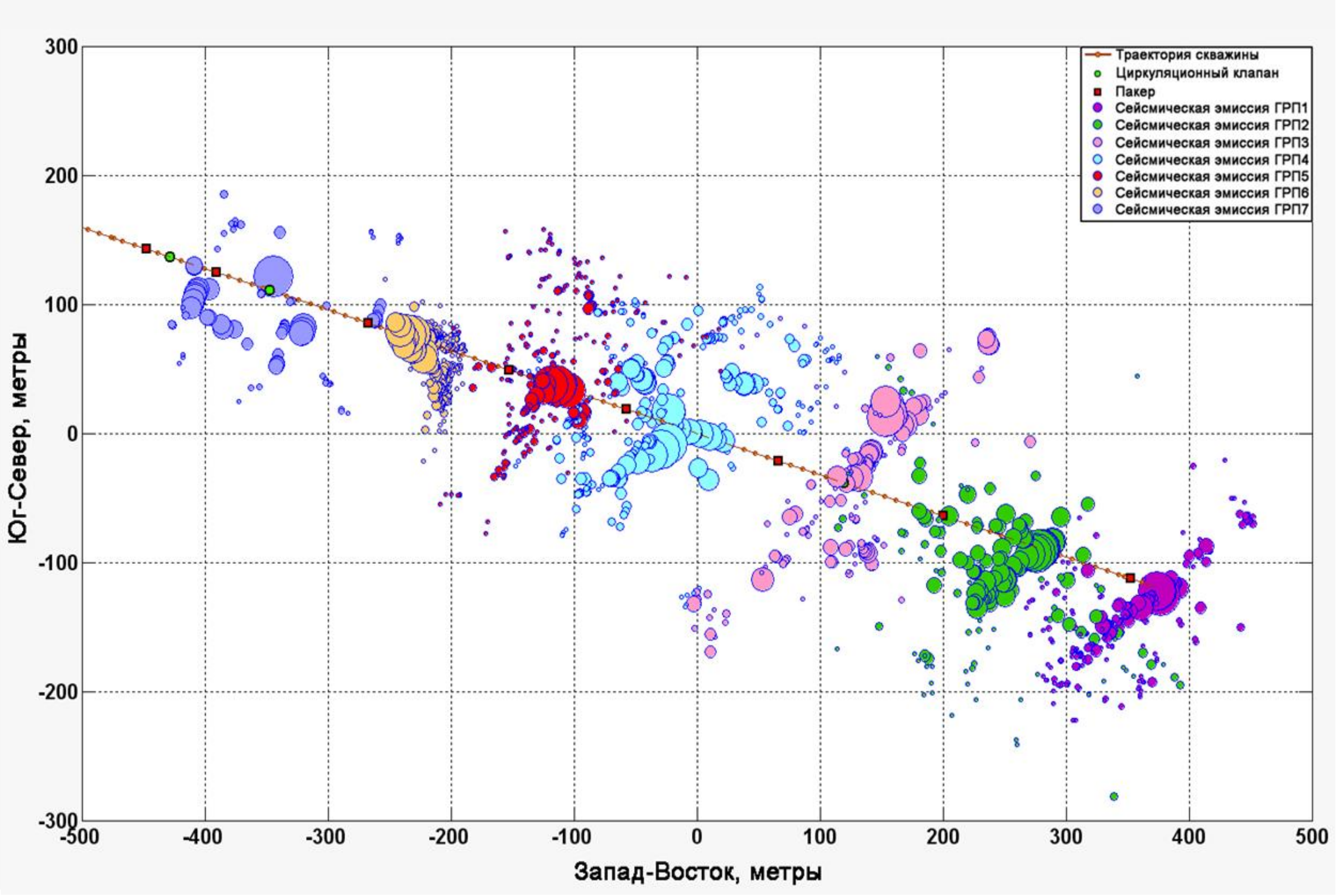

Oilfield Vientoskoe, cluster well #11, well #634G, 2013, Ugra

Case study #6: Waterflooding. Monitoring displacement front during fluid injection in the layer.

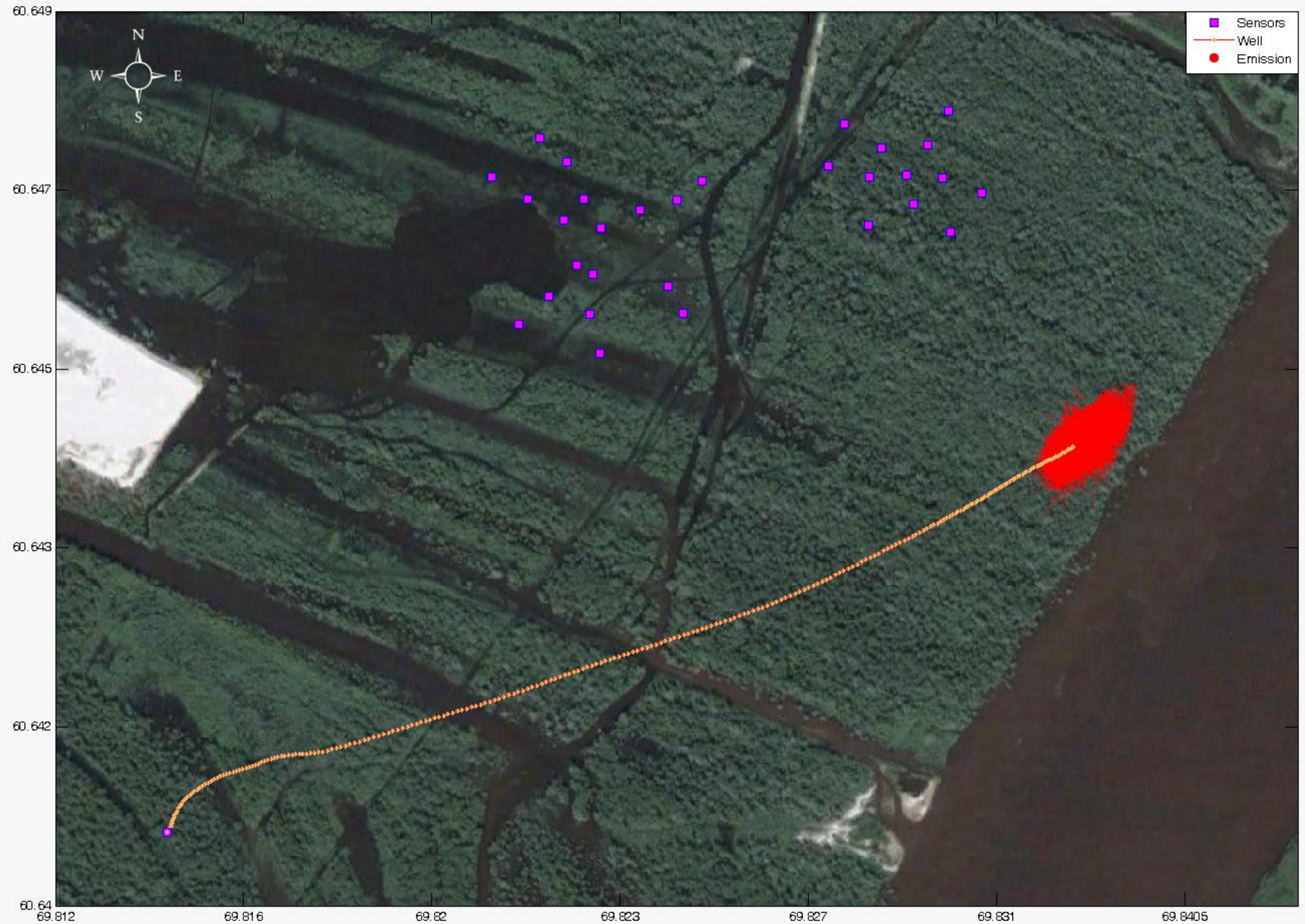

Space image of Priobskoe oilfield. Projection of well № 16502, sources of seismic emission and sensors on the day surface. Depth 2403. Ugra, 2010.

Case study #6: Waterflooding. Distribution of flooding, in accordance with the extension of the zone of seismic emission. Step - 100 hours.

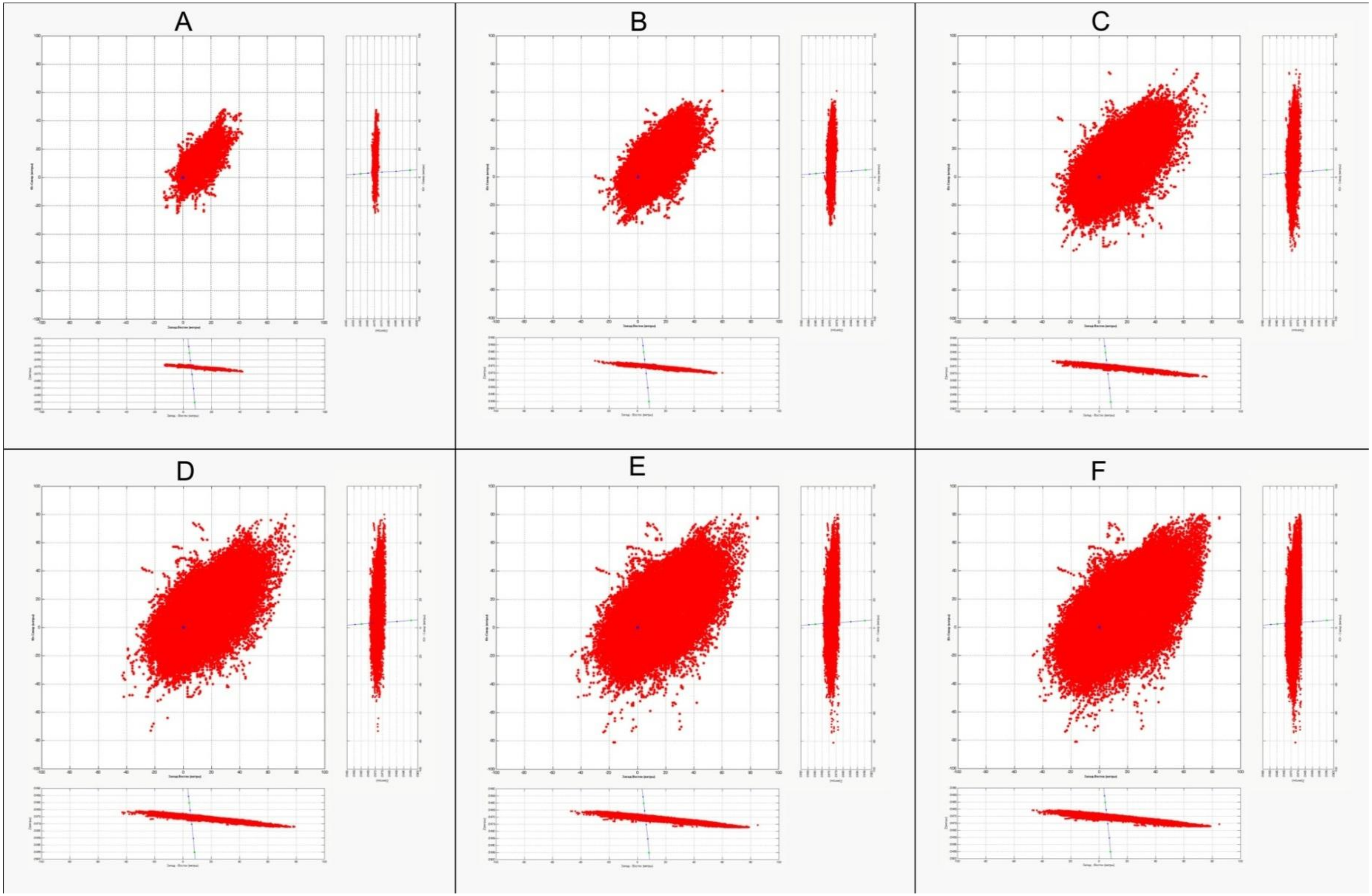

Top view (center), east view (right) and north view (bottom) of the microseismic cloud (A) 100 hr, (B) 200 hr, (C) 300 hr, (D) 400 hr, (E) 500 hr, (F) 600 hr after the start of the injection

Case study #7: Estimation of drainage area of deposits . The layout of surface sensors and oil wells . Time data collection – 30 days.

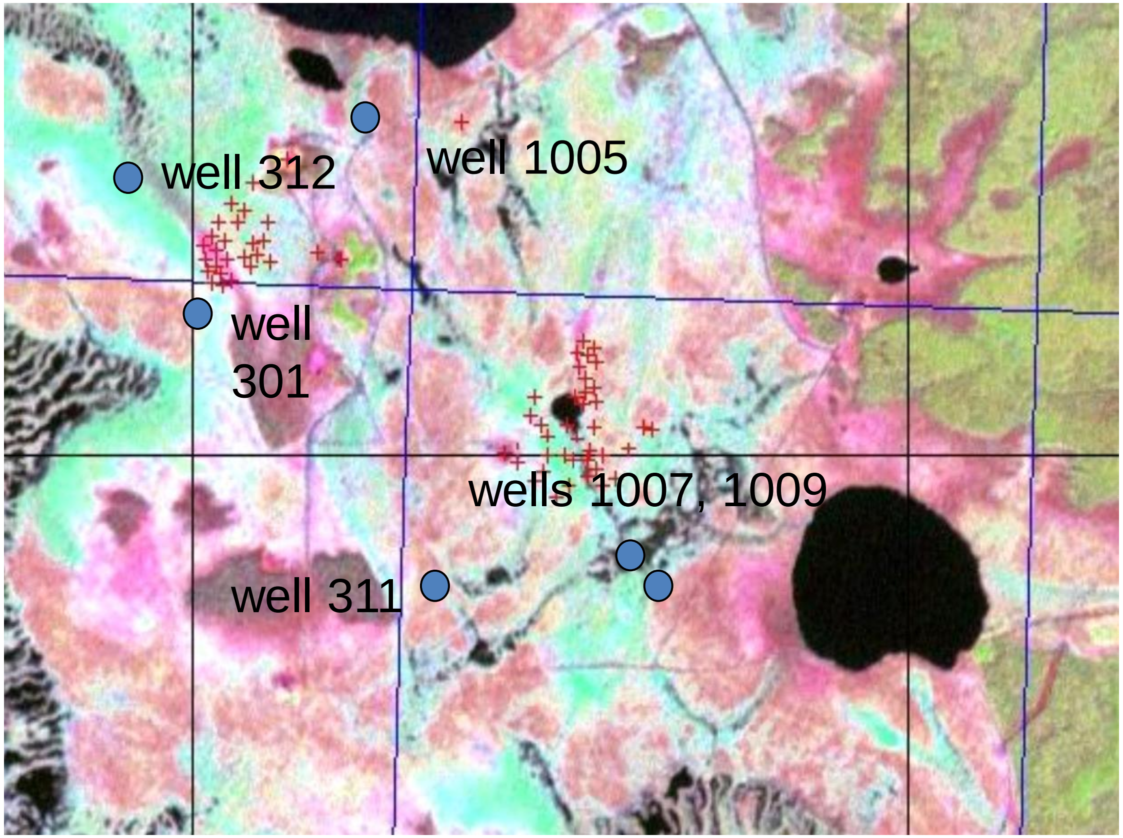

Geometry of the surface receiver array, wells. Deposit Lebyazhye. The depth is 2680 meters. Red cross – sensors. The period of monitoring is 30 days. 2006, Ugra.

Case study #7: Estimation of drainage area of deposits . Results of microseismic monitoring at the depth 2680 meters. Time data collection – 30 days.

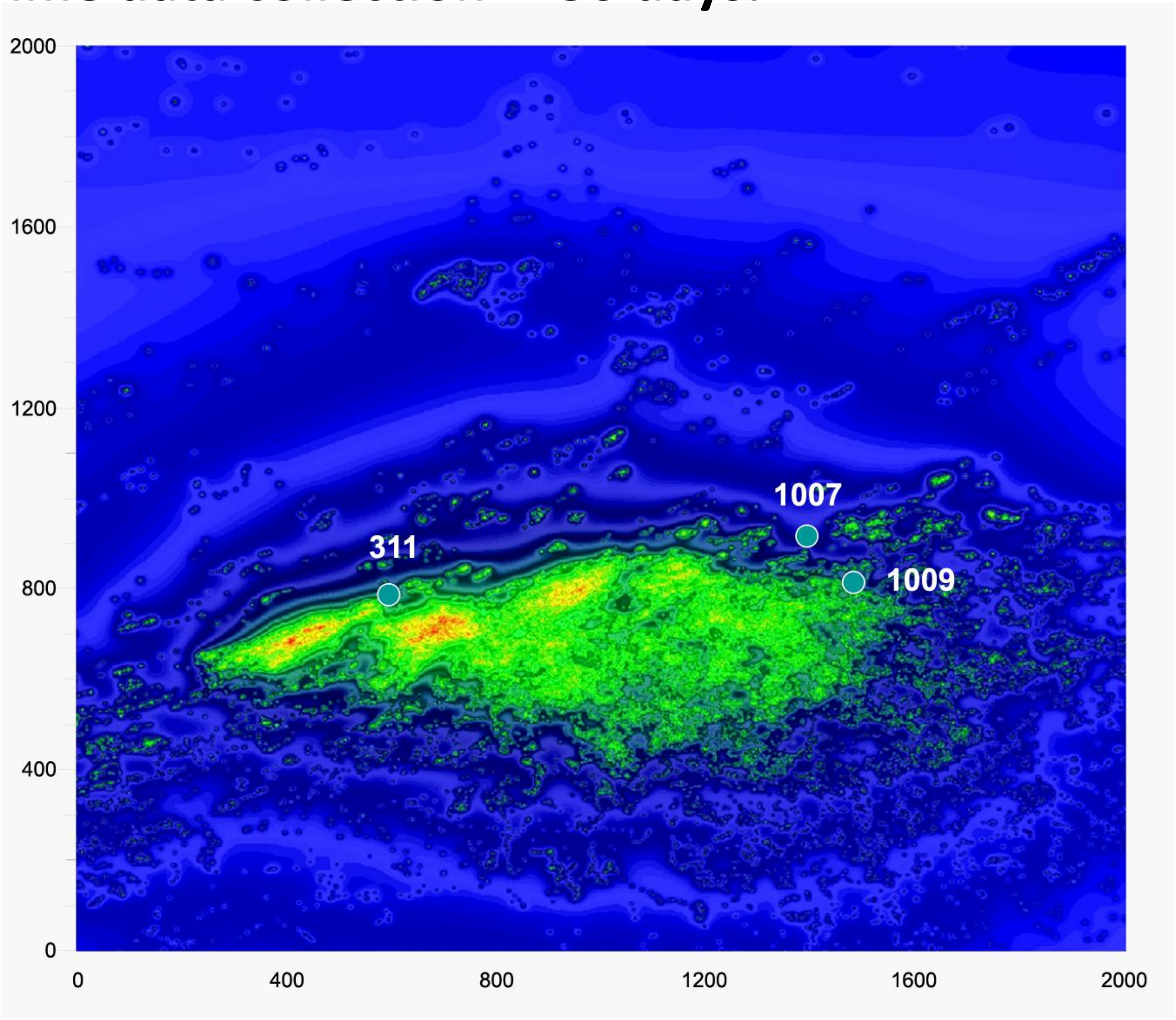

Oilfield Lebyazhye, 2006, Ugra

Case study #8: Microseismic monitoring of hydraulic fracturing and full passive monitoring (green color). Video.

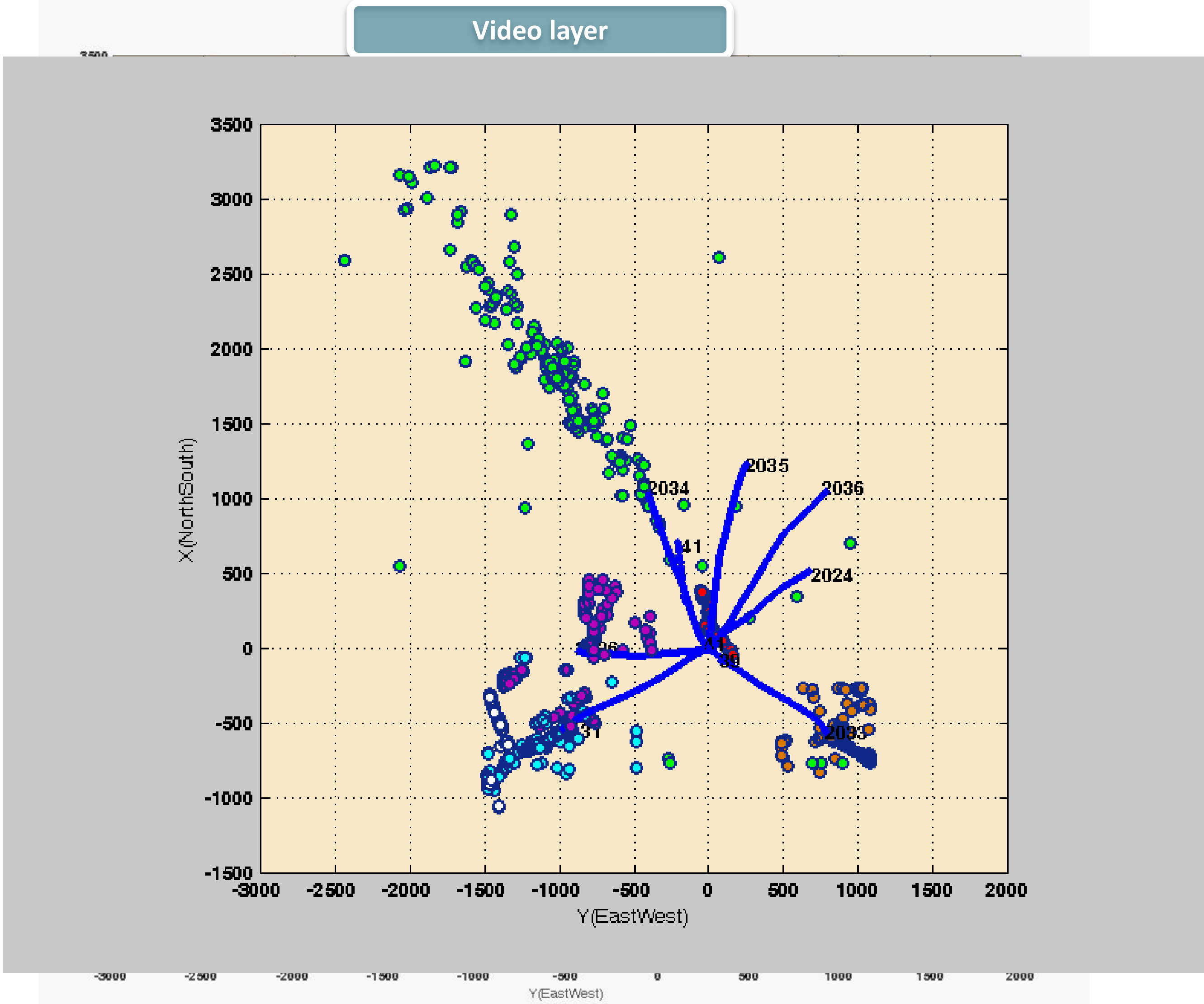

Well cluster #1. Galianovskay oilfield, UGRA, 2007. Tight oil (Bashenovsky suite)

Case study #9: Estimation of port productivity after multistage hydraulic fracturing

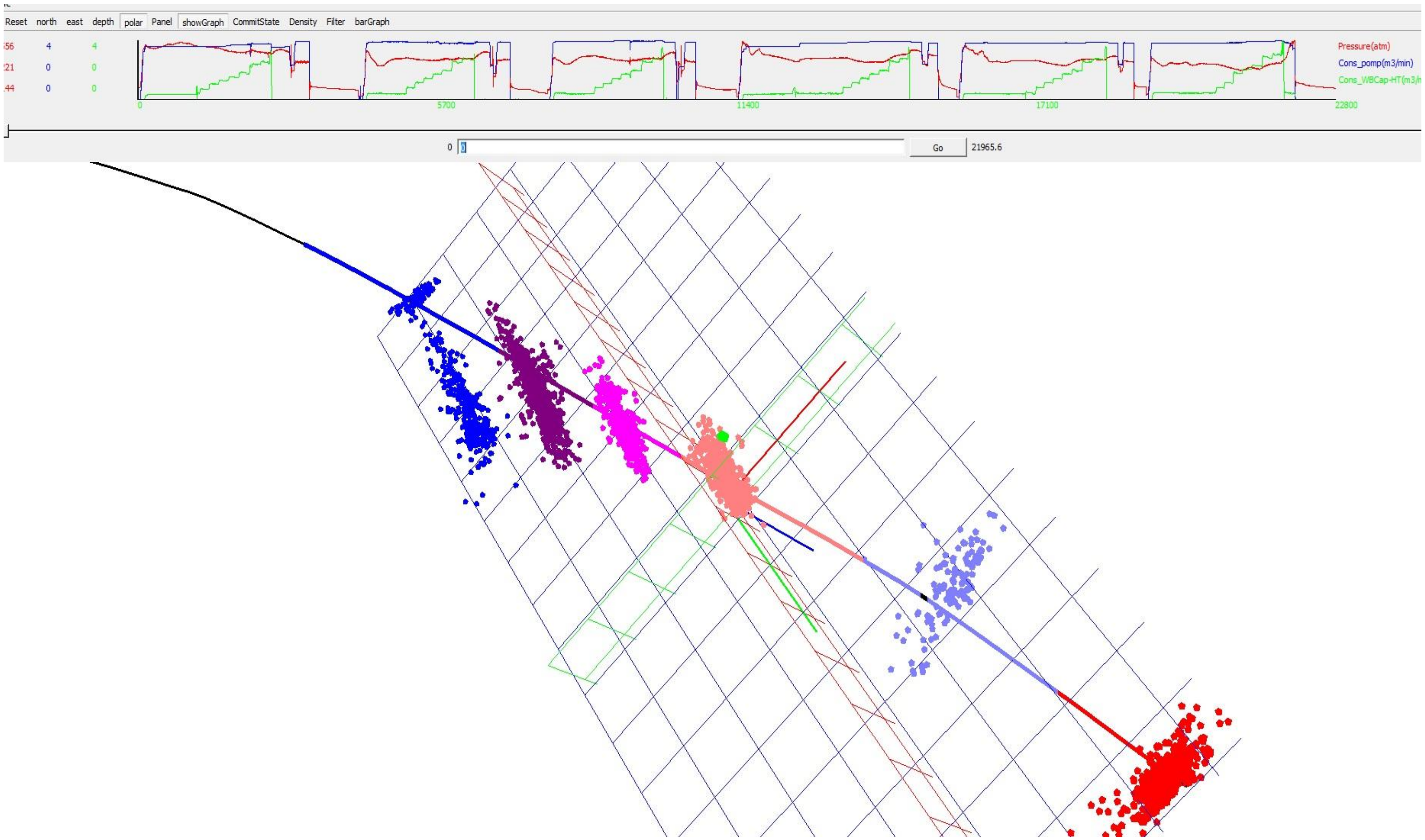

3D image of microseismic monitoring the multistage fracturing. Well 100G. Grid step 50m. Oilfield Srednenazimskay. Depth – 2700 m. West Siberia, 2013

Case study #9: Estimation of ports productivity after multistage hydraulic fracturing

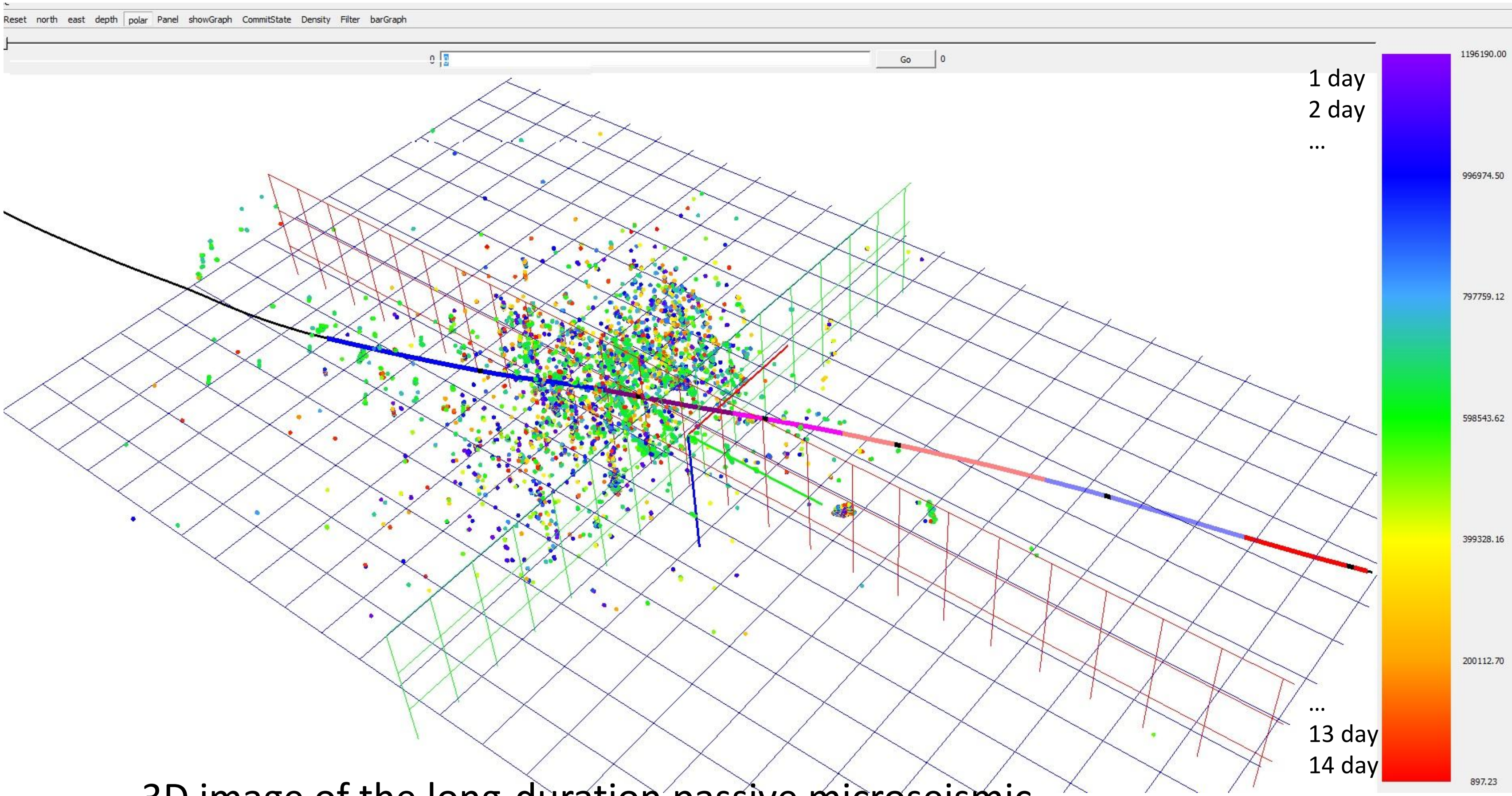

3D image of the long-duration passive microseismic monitoring after multistage fracturing. Grid step 50m. Well 100G. Oilfield Srednenazimskay. West Siberia, 2013

Case study #9: Estimation of port productivity after multistage hydraulic fracturing

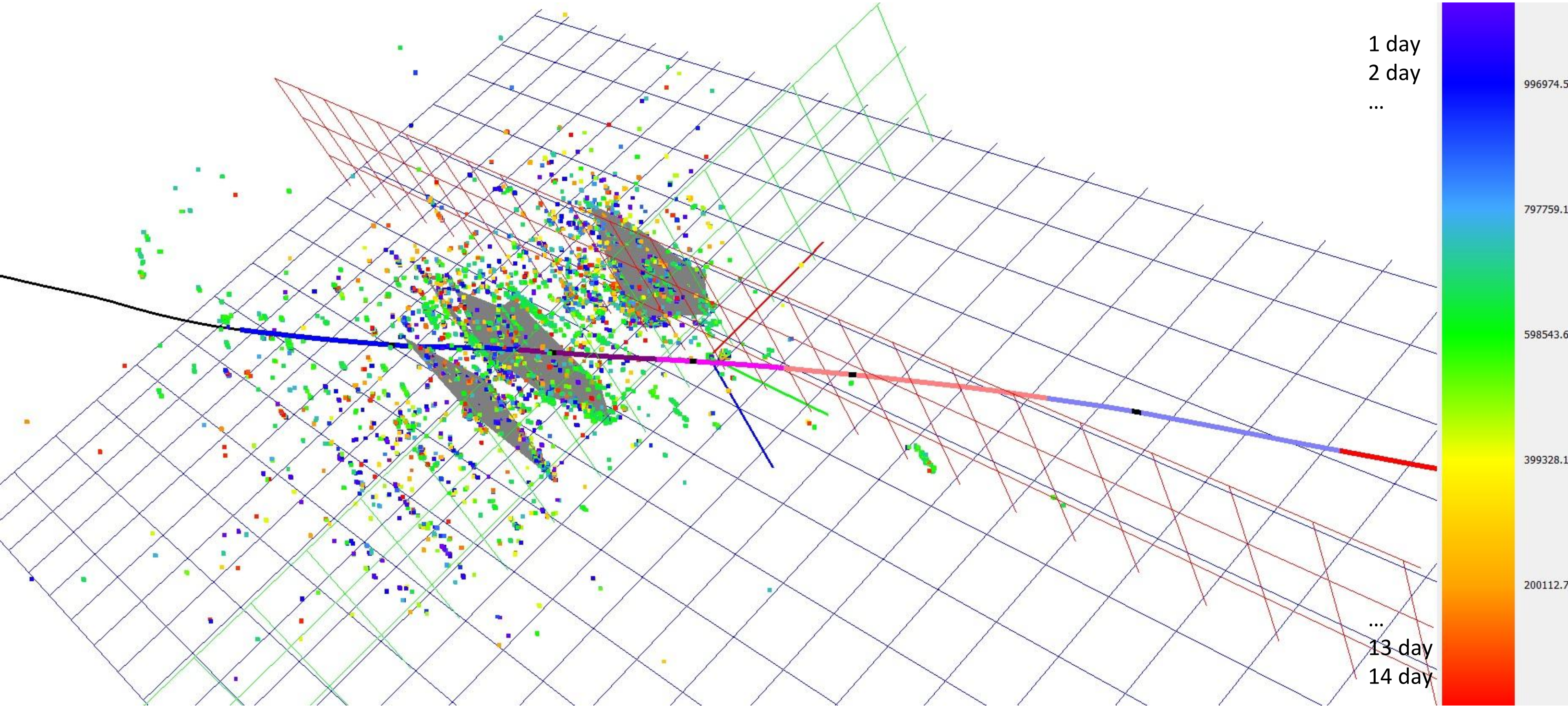

3D image of the long-duration passive microseismic monitoring after multistage fracturing with fault-block structure mapping. Grid step 50m. Well 100G. Oilfield Srednenazimskay. West Siberia, 2013

Case study #9: Estimation of port productivity after multistage hydraulic fracturing

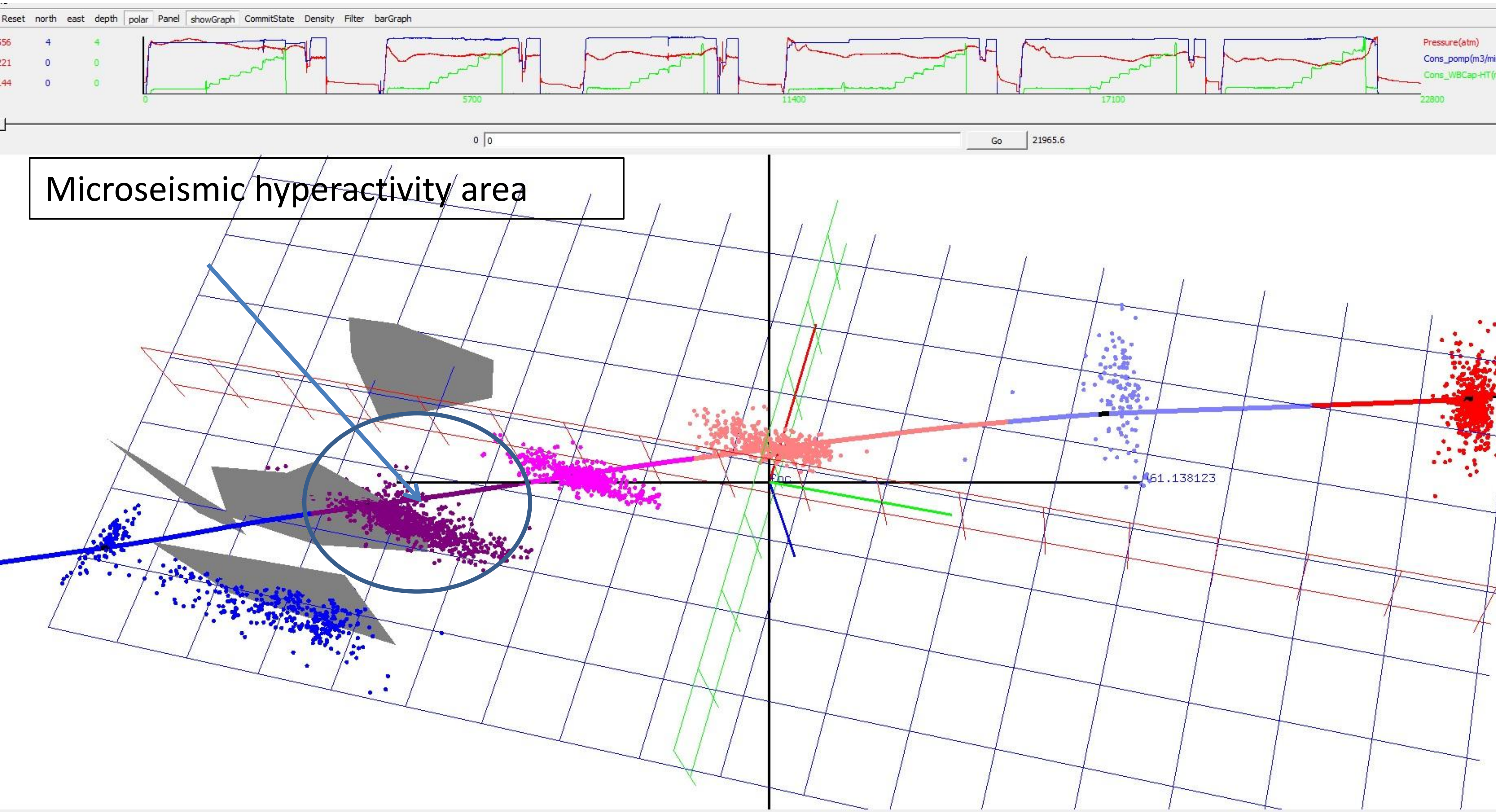

3D image of microseismic monitoring of multistage fracturing with fault-block structure mapping. Well 100G. Grid step 50m. Oilfield Srednenazimskay. West Siberia, 2013

Case study #9: Estimation of port productivity after multistage hydraulic fracturing

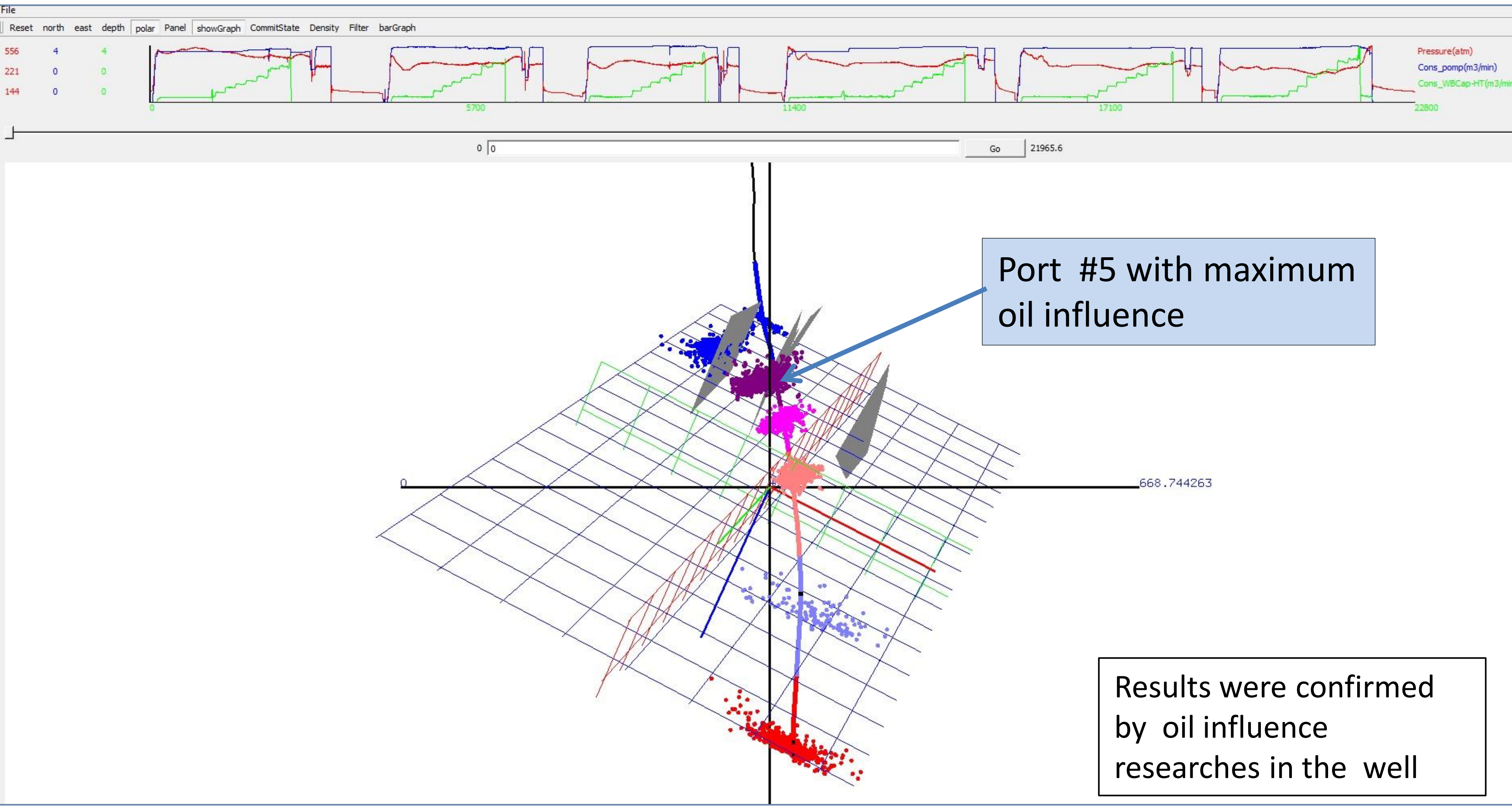

3D image of microseismic monitoring of multistage fracturing with fault-block structure mapping. Well 100G, 70 ton/day. Grid step 50m. Oilfield Srednenazimskay. West Siberia, 2013

Case study #10 Identification of the fault-block structure near a bottom-hole. Two weeks of data collection per well.

Layout of wells - points for surface microseismic monitoring.
Wells #3,5 - with oil pumping unit. Well #30 – without.
Kazakhstan, 2012

Case study #10: 3D view of microseismic events near bottom-hole.

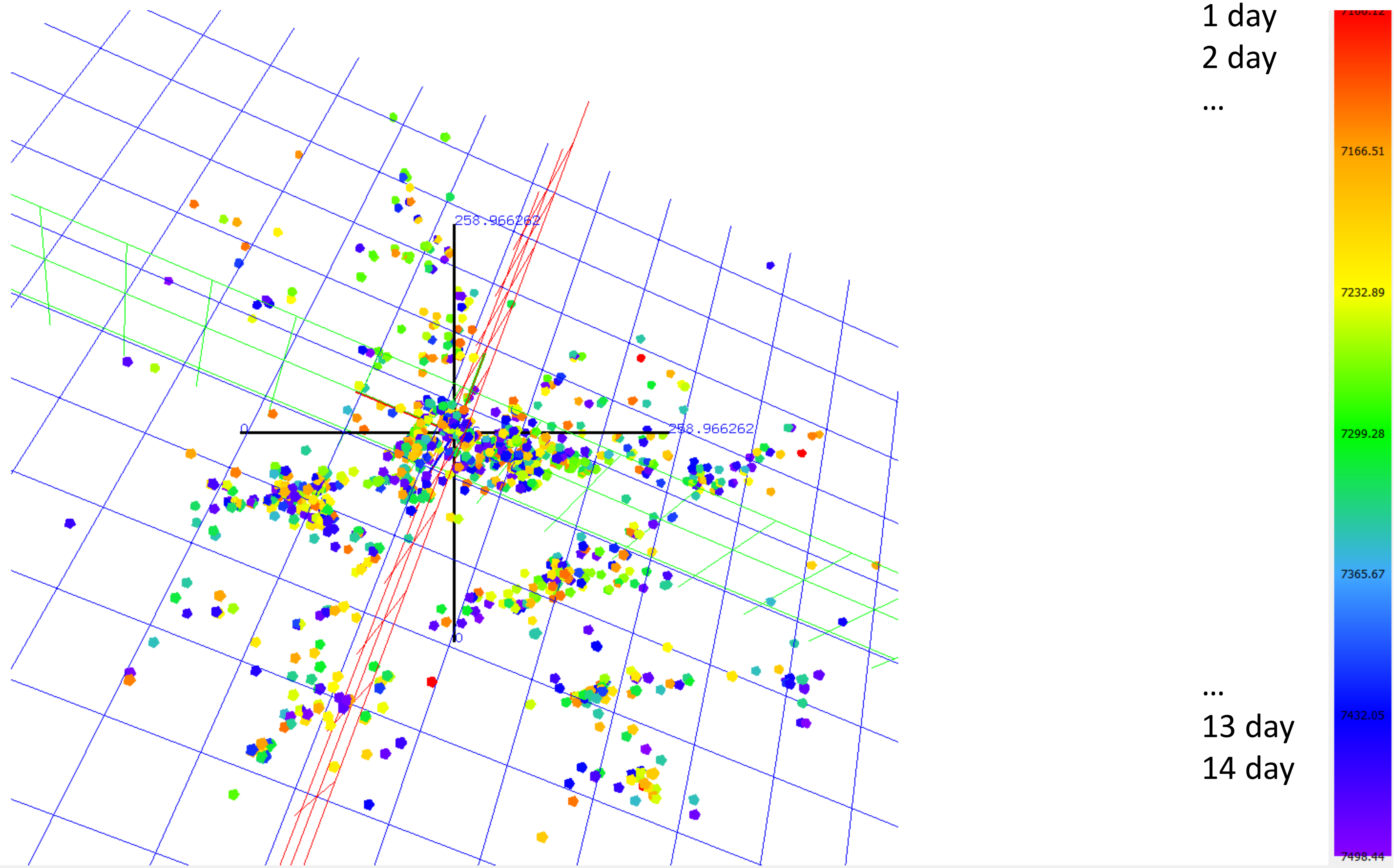

Grid step -50 m

Oilfield Atambay-Sertube, well #5, Kazakhstan, 2012

Case study #10: 3D view of microseismic events near bottom-hole.

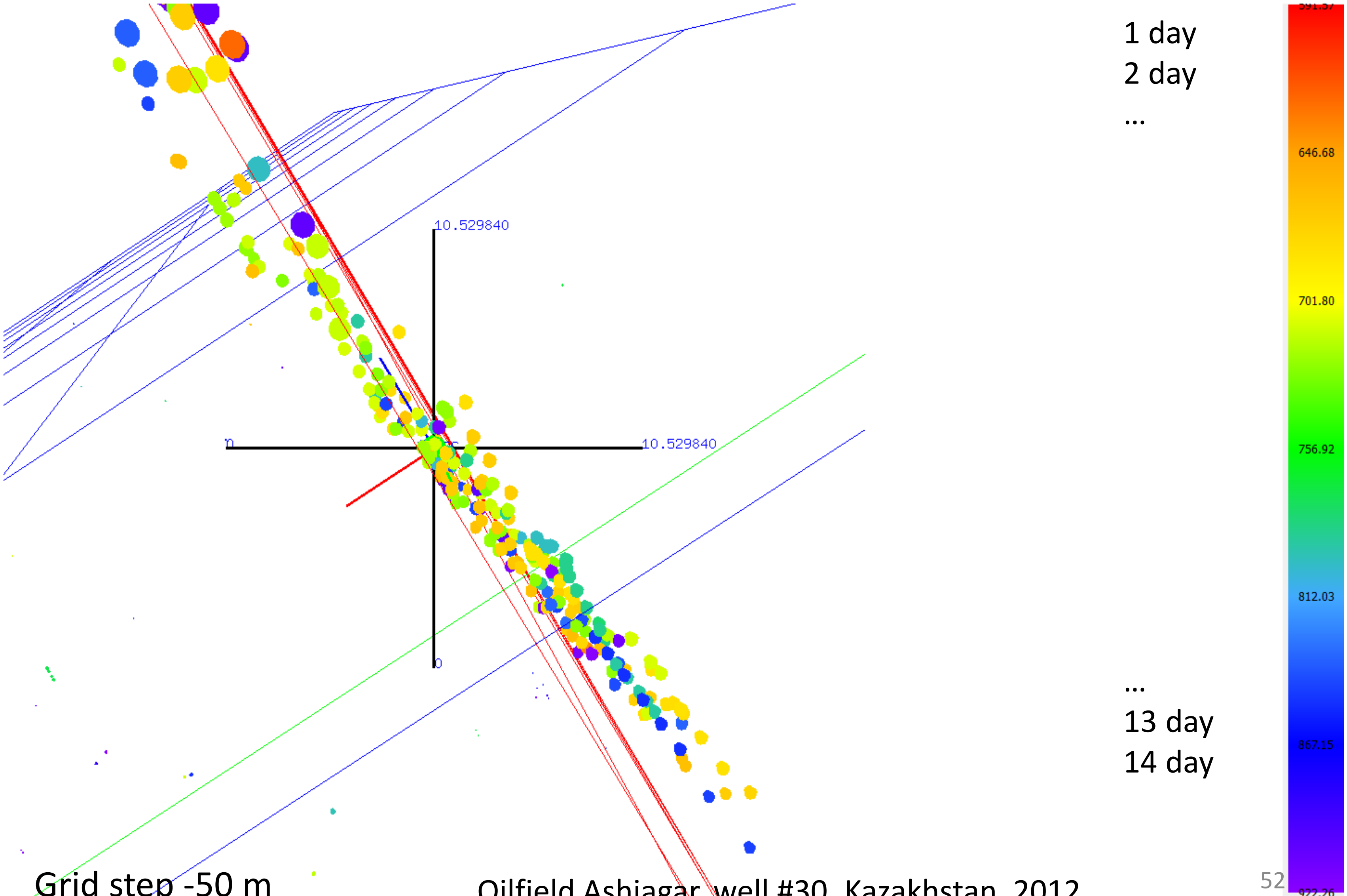

Grid step -50 m

Oilfield Ashiagar, well #30, Kazakhstan, 2012

Case study #10: 3D view of microseismic events near bottom-hole.

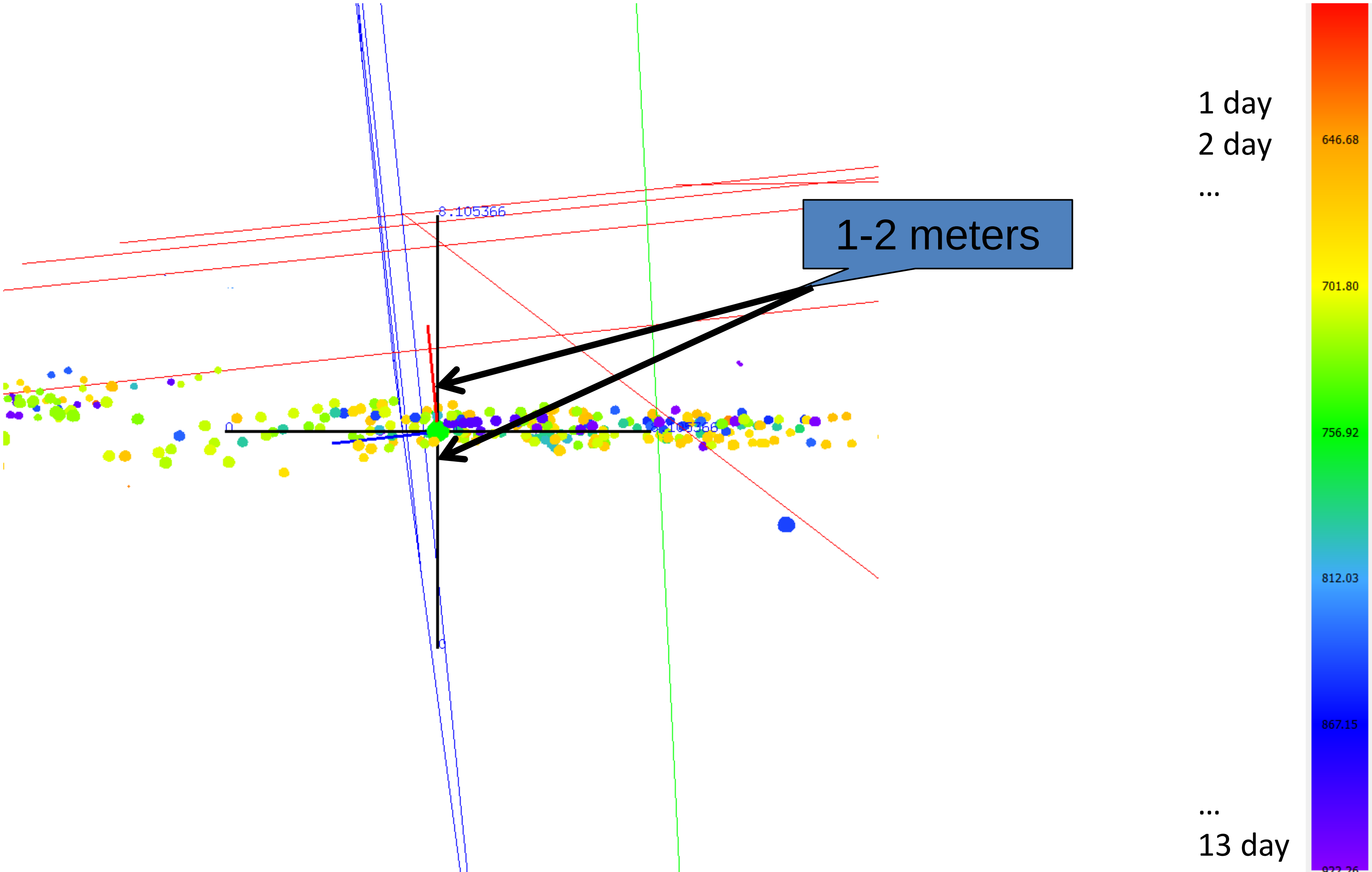

Grid step -50 m

Oilfield Ashiagar, well #30, Kazakhstan, 2012

Case study #10: 3D view of microseismic events near bottom-hole. Design of fault planes with IHS Kingdom package. Video.

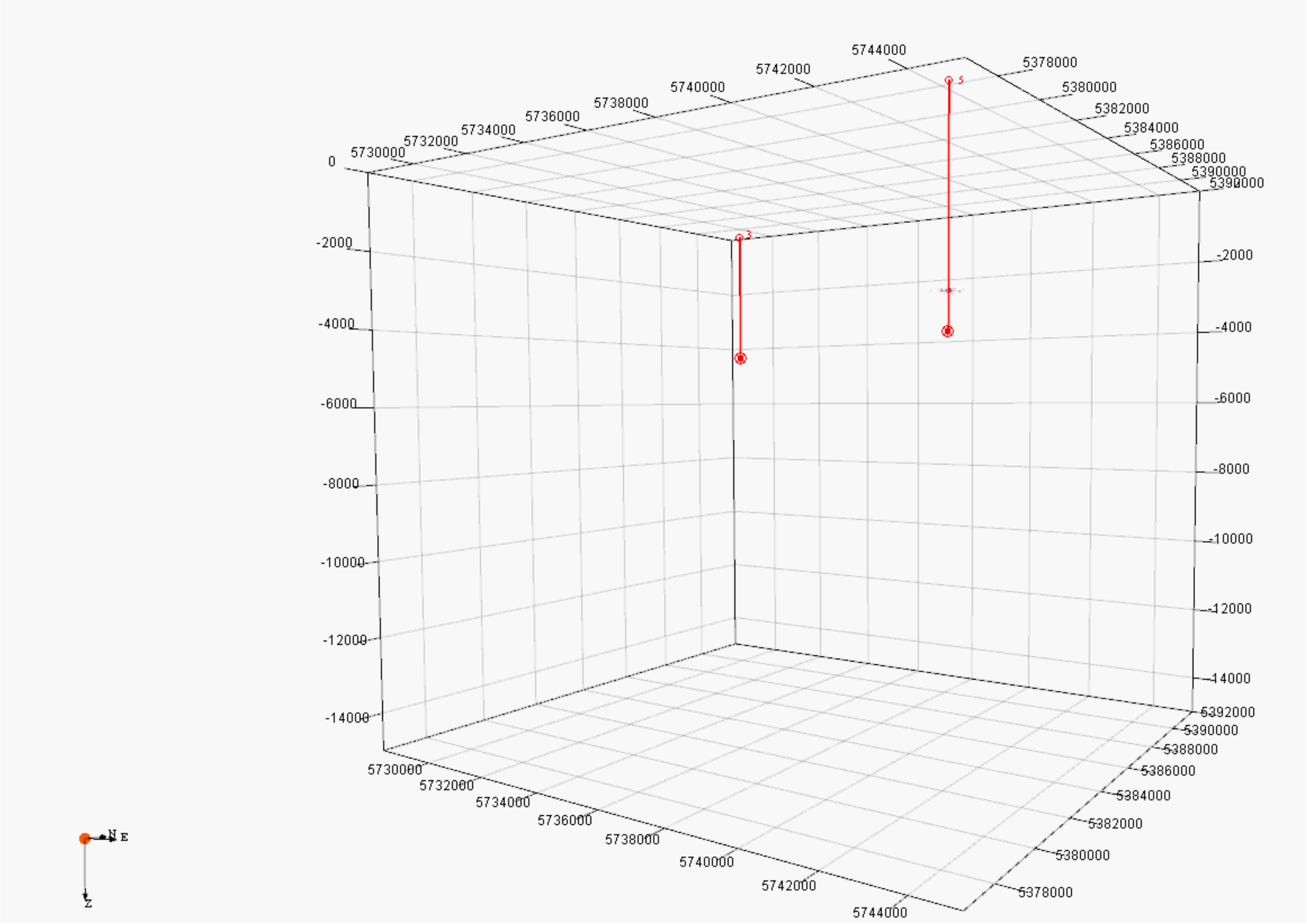

Oilfield Atambay-Sertube, well #5, Kazakhstan, 2012

Case study #10: 3D view of microseismic events near bottom-hole. Planes of faults were designed with IHS Kingdom package

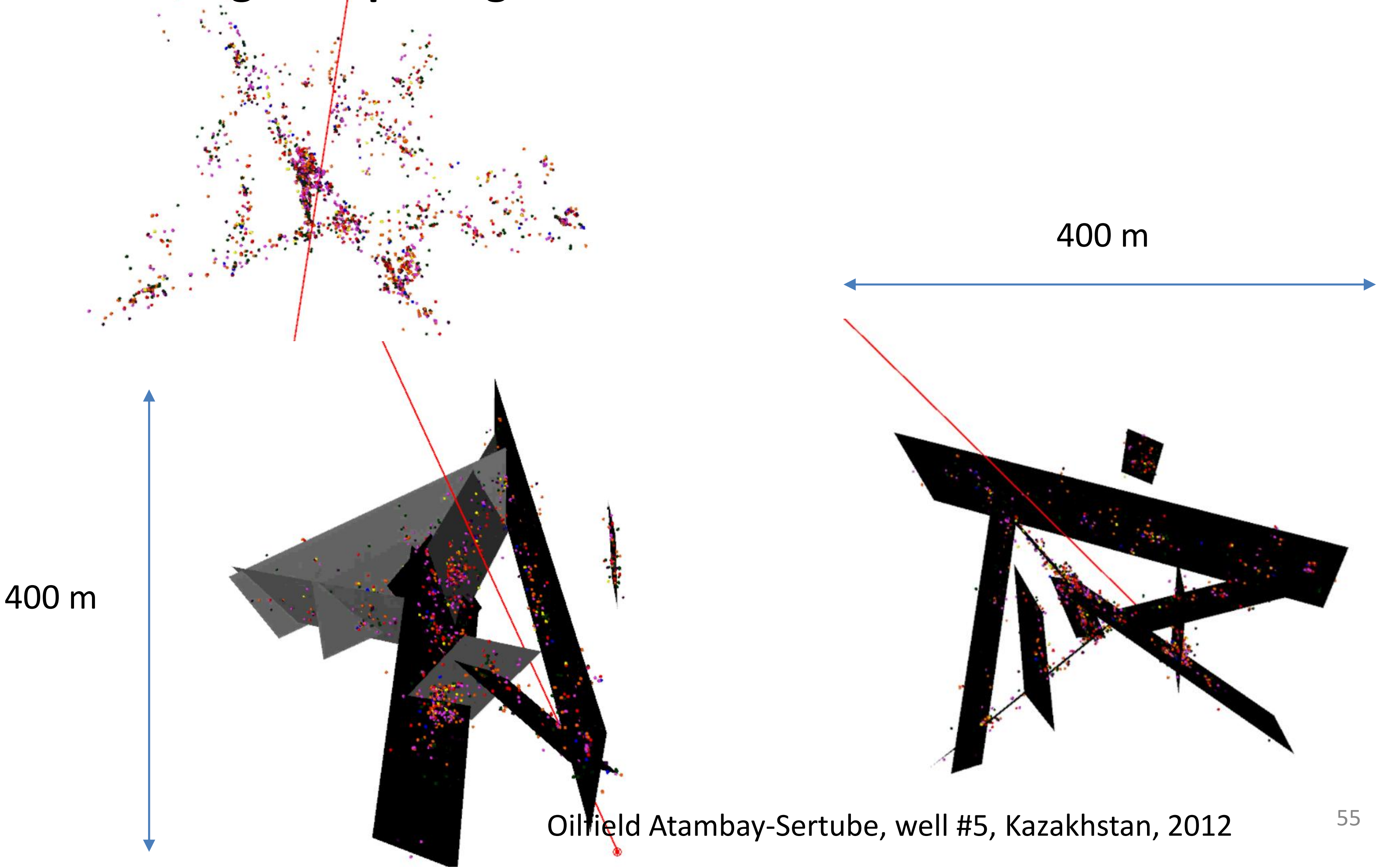

Oilfield Atambay-Sertube, well #5, Kazakhstan, 2012

Case study #10: 3D view of microseismic events near bottom-hole. Video.

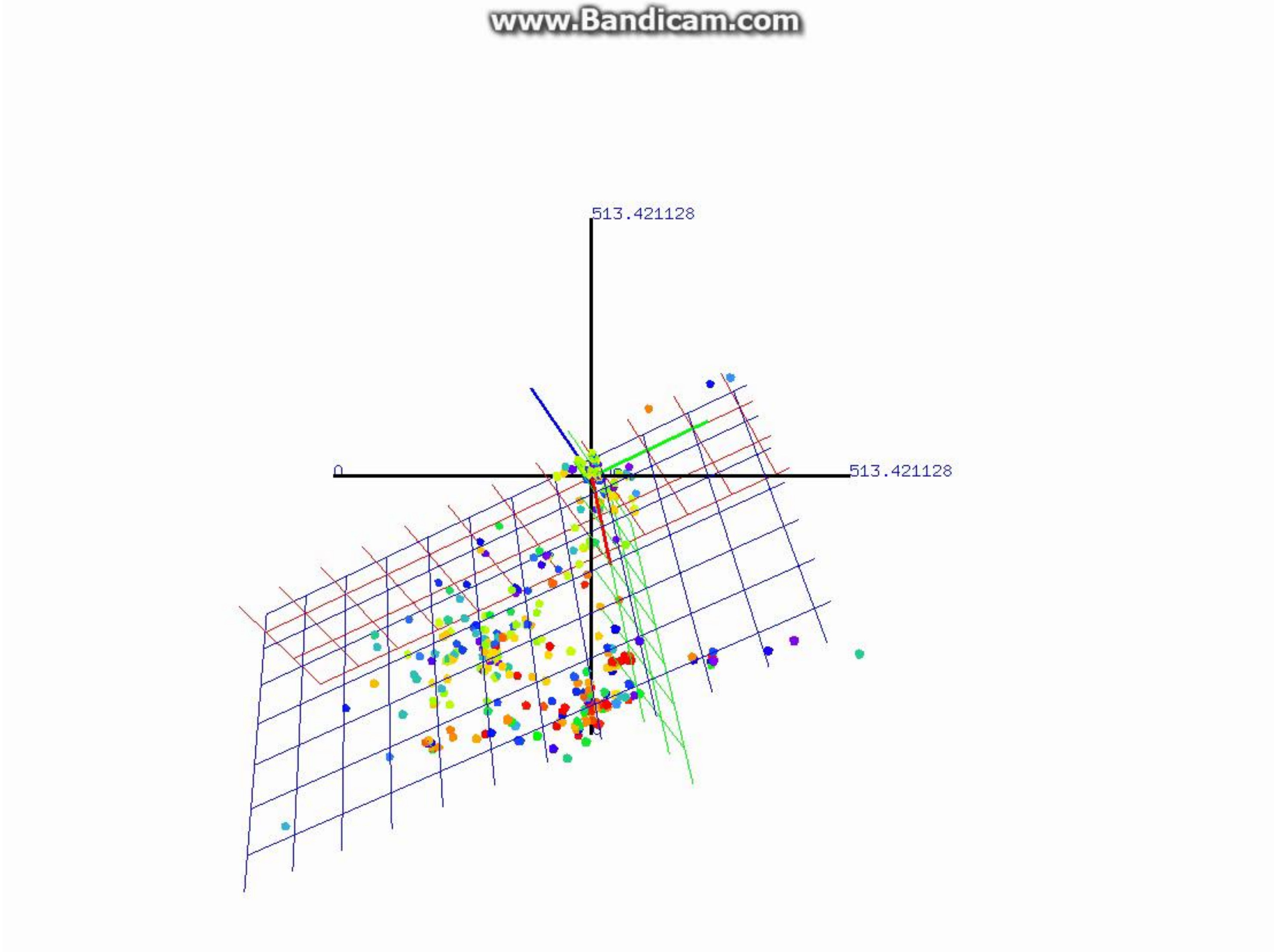

Grid step -50 m

Oilfield Ashiagar, well #30, Kazakhstan, 2012

13 day
14 day

Case study #11
Complex interpretation of pre-existing fracture (CSP- booth #3343, www.csp-amt.com) and results of MicroseismicCSP long-duration microseismic monitoring

Case studies #11: Geometry of the surface receiver array, wells.

Well #16 Well #9

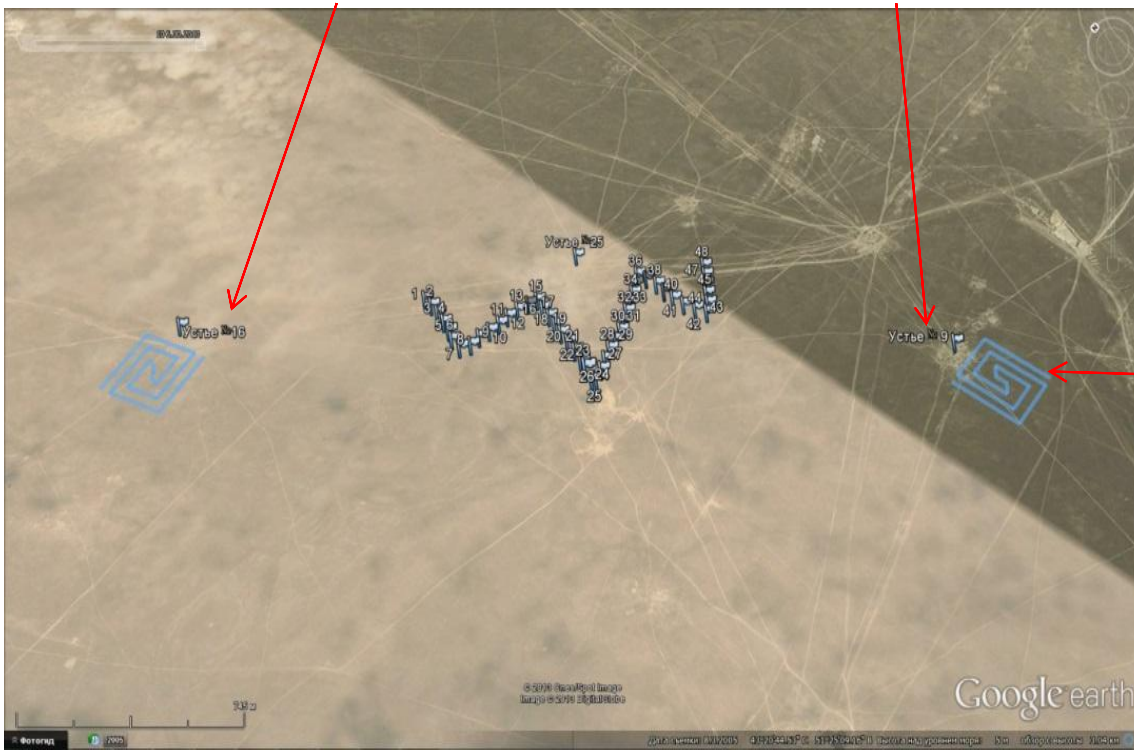

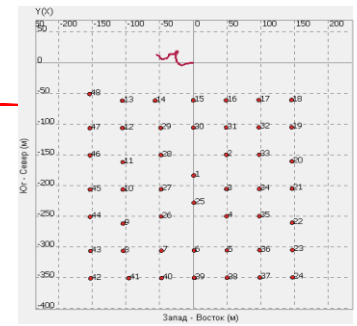

Oilfield Oimasha. Wells #9, 16, 25.
Two week registration per well. Kazakhstan, 2013. Array 300x300 m.

Case study #11: 3D view of microseismic events near bottom-hole, well #9. Oilfield block structure mapping. Two week registration.

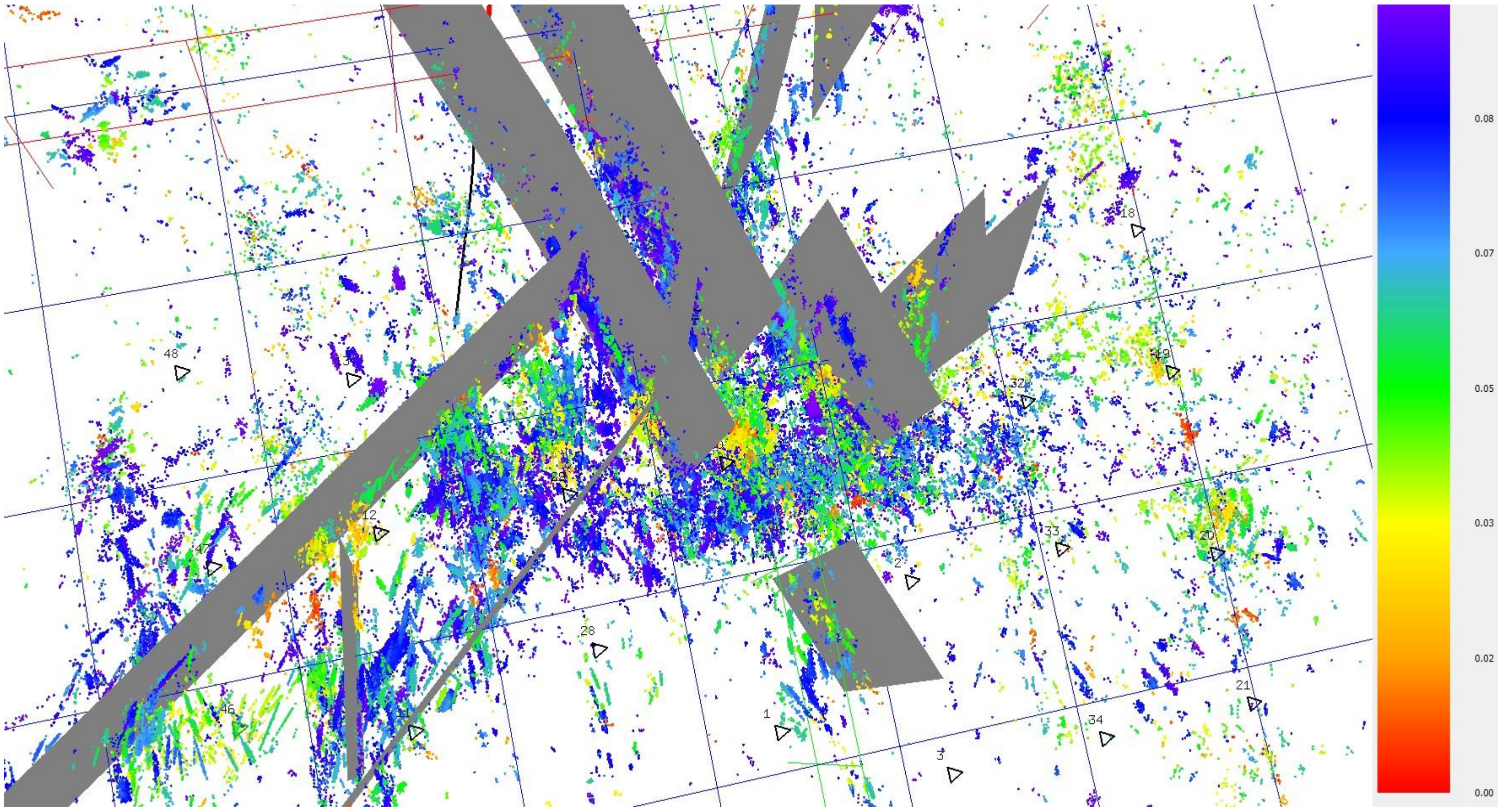

Grid step -50 m

Oilfield Oimasha, well #9 with oil pumping unit. Kazakhstan, 2013

Case study #11: Microseismic event distribution with 3D visualization of seismic moment tensor on principal stress axes. Well #9.

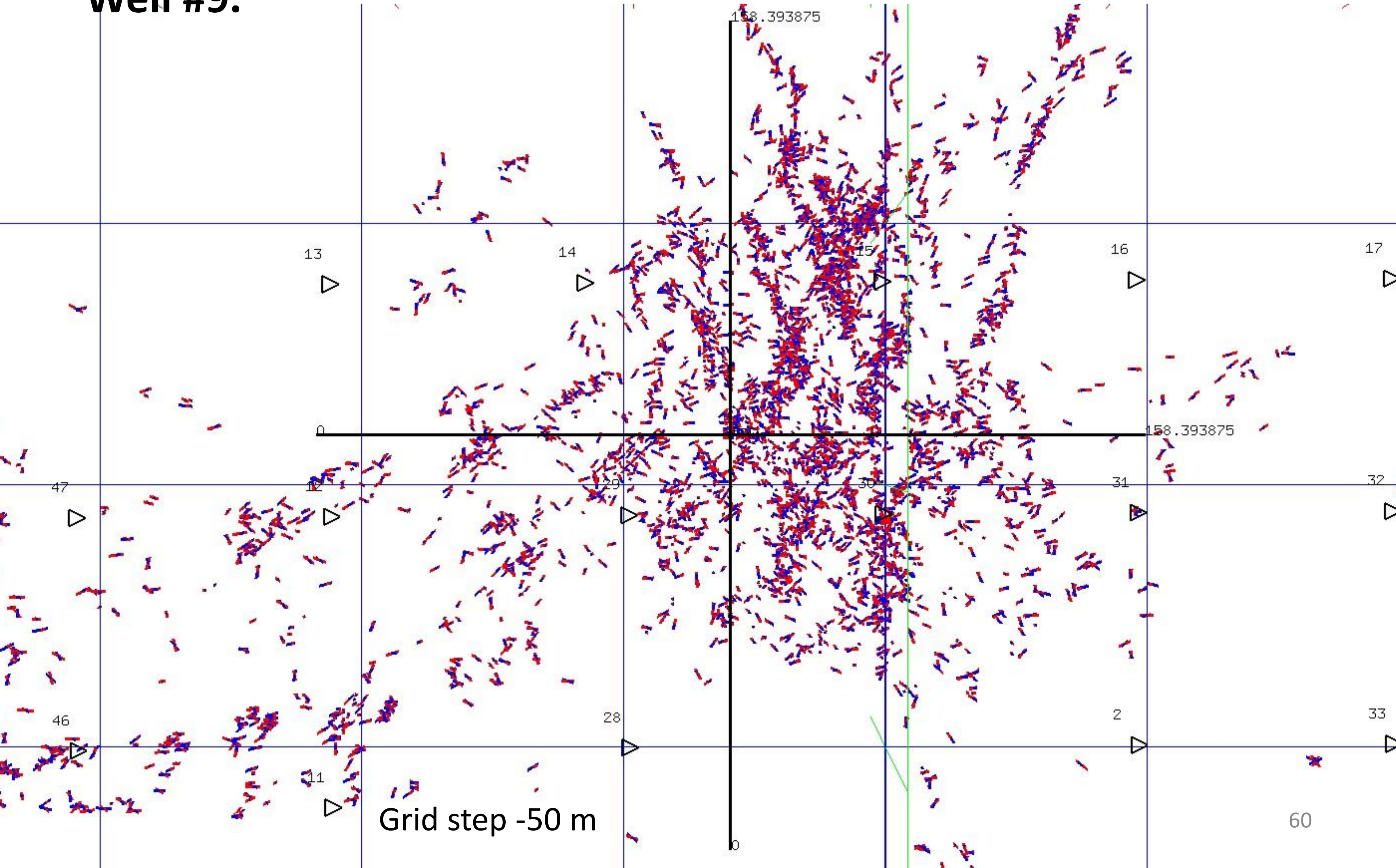

Grid step -50 m

Case study #11: CSP –maps of pre-existing fracture
(CSP- booth #3343, www.csp-amt.com)

Well #9

Well #16

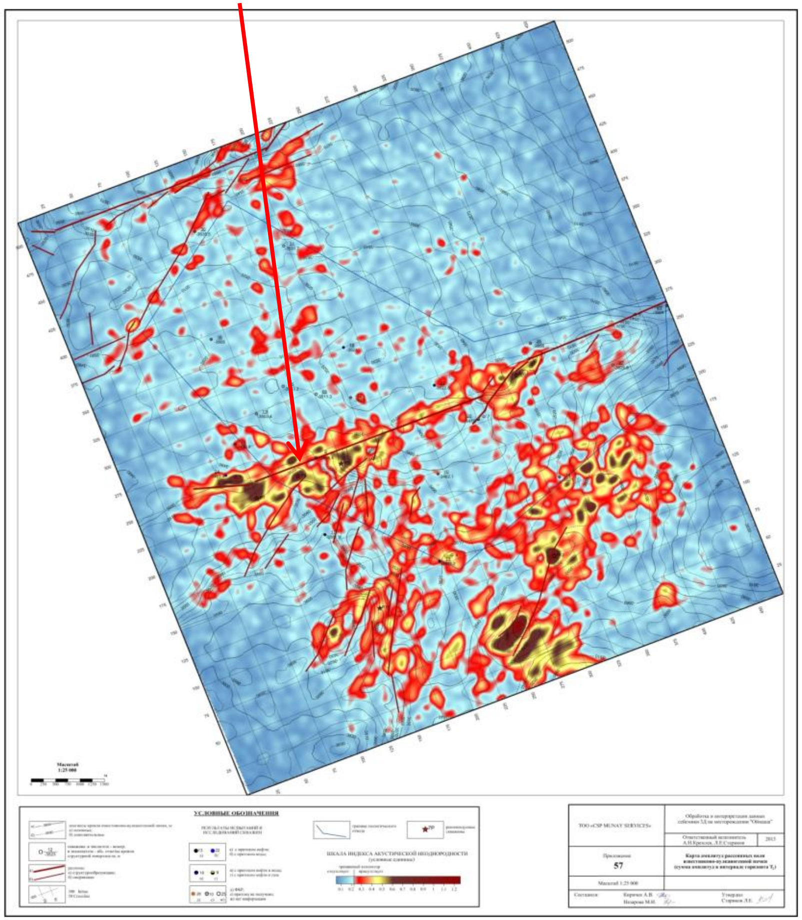

Triassic sediments

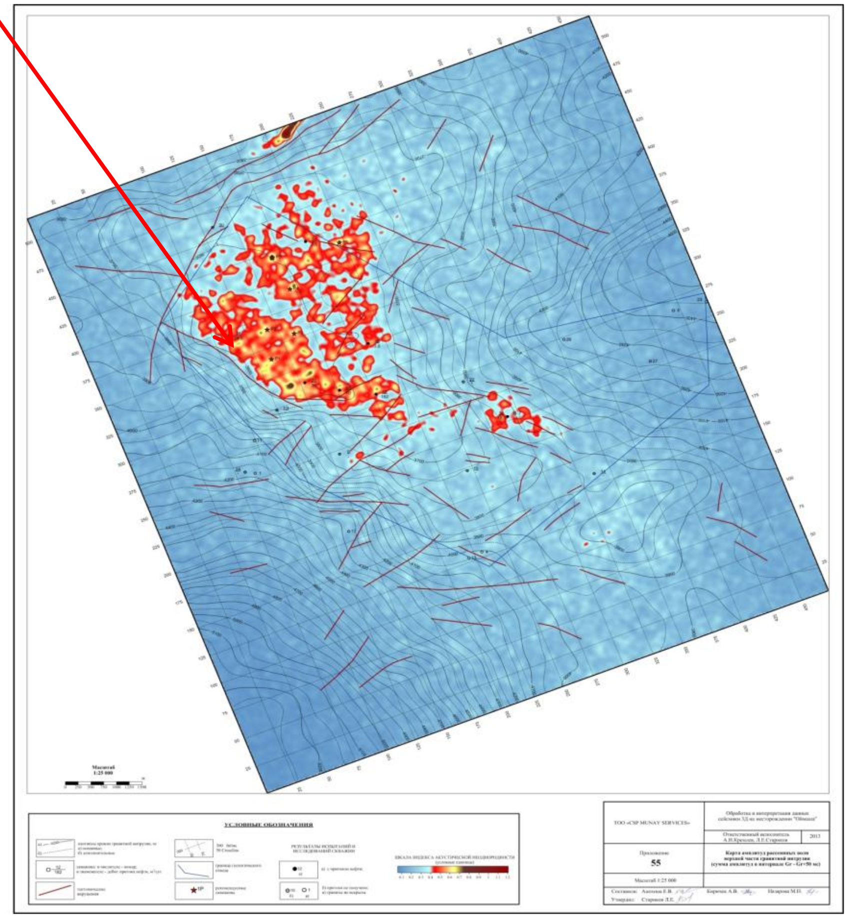

Granite intrusion

Case study #11: Time section of CSP-diffractor cube (pre-existing fracture) & results of long-duration passive microseismic monitoring.

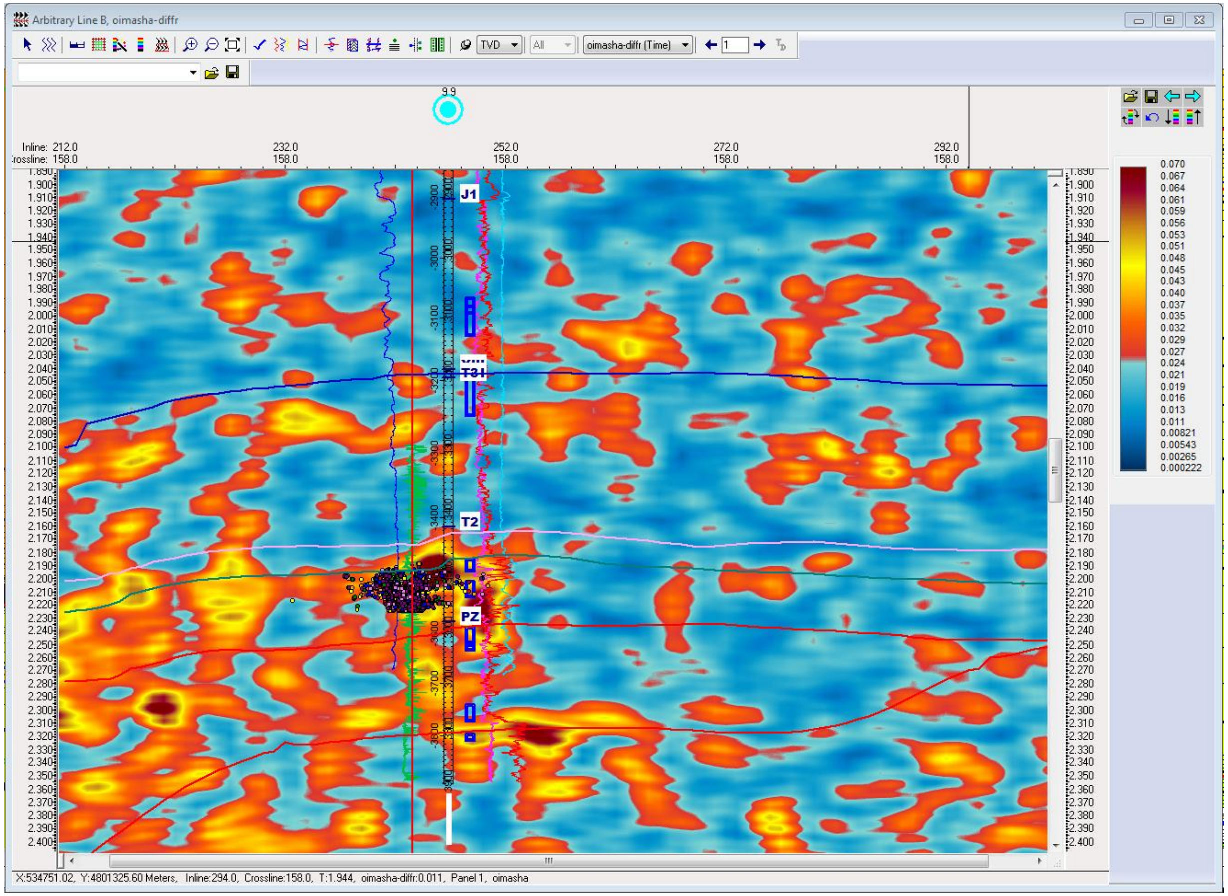

Oilfield Oimasha. Wells #9, 2013, Kazakhstan. Oil inflow 150 m3 per day

Case study #11: 3D view of results of long-duration passive microseismic monitoring with top of Paleozoic

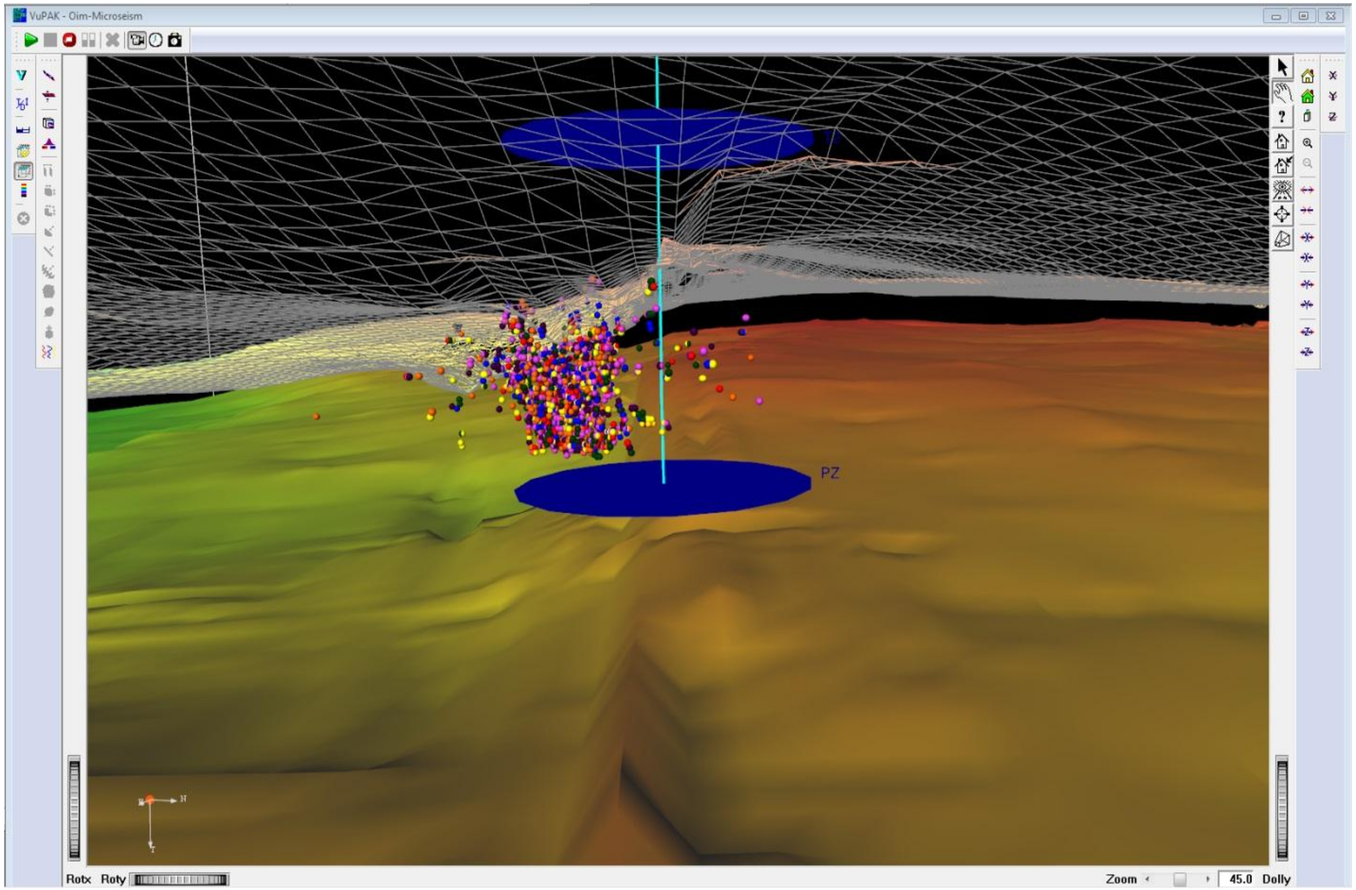

Oilfield Oimasha. Wells #9, 2013, Kazakhstan. Oil inflow 150 m3 per day

Case study #11: Projection of a cloud of microseismic events to an isochronous surface granite intrusion

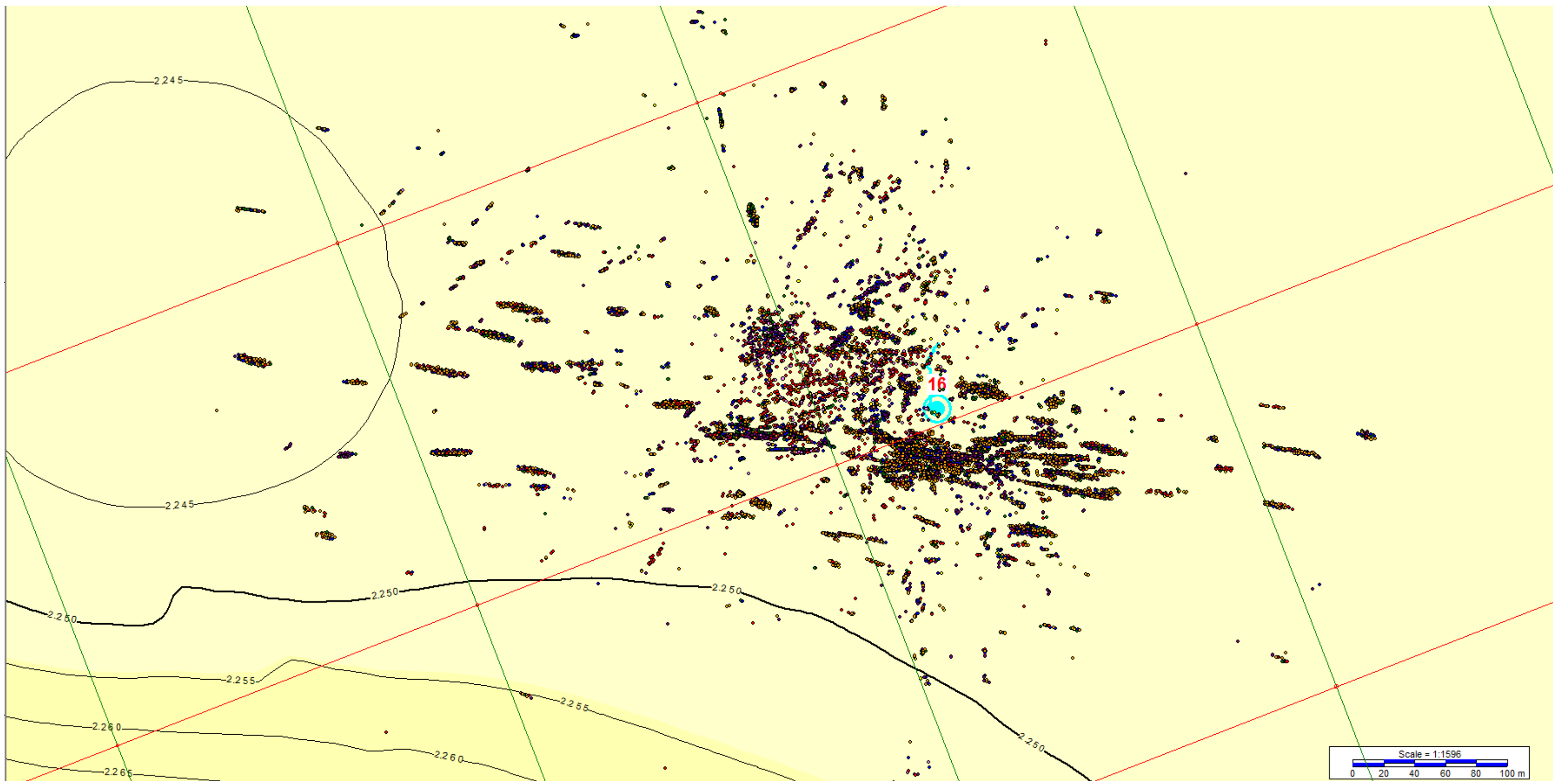

Oilfield Oimasha. Wells #16, 2013, Kazakhstan. Oil inflow 102 m3 per day

Case study #11: 3D view of results microseismic events, CSP-diffractor cube and cube of microseismic stresses

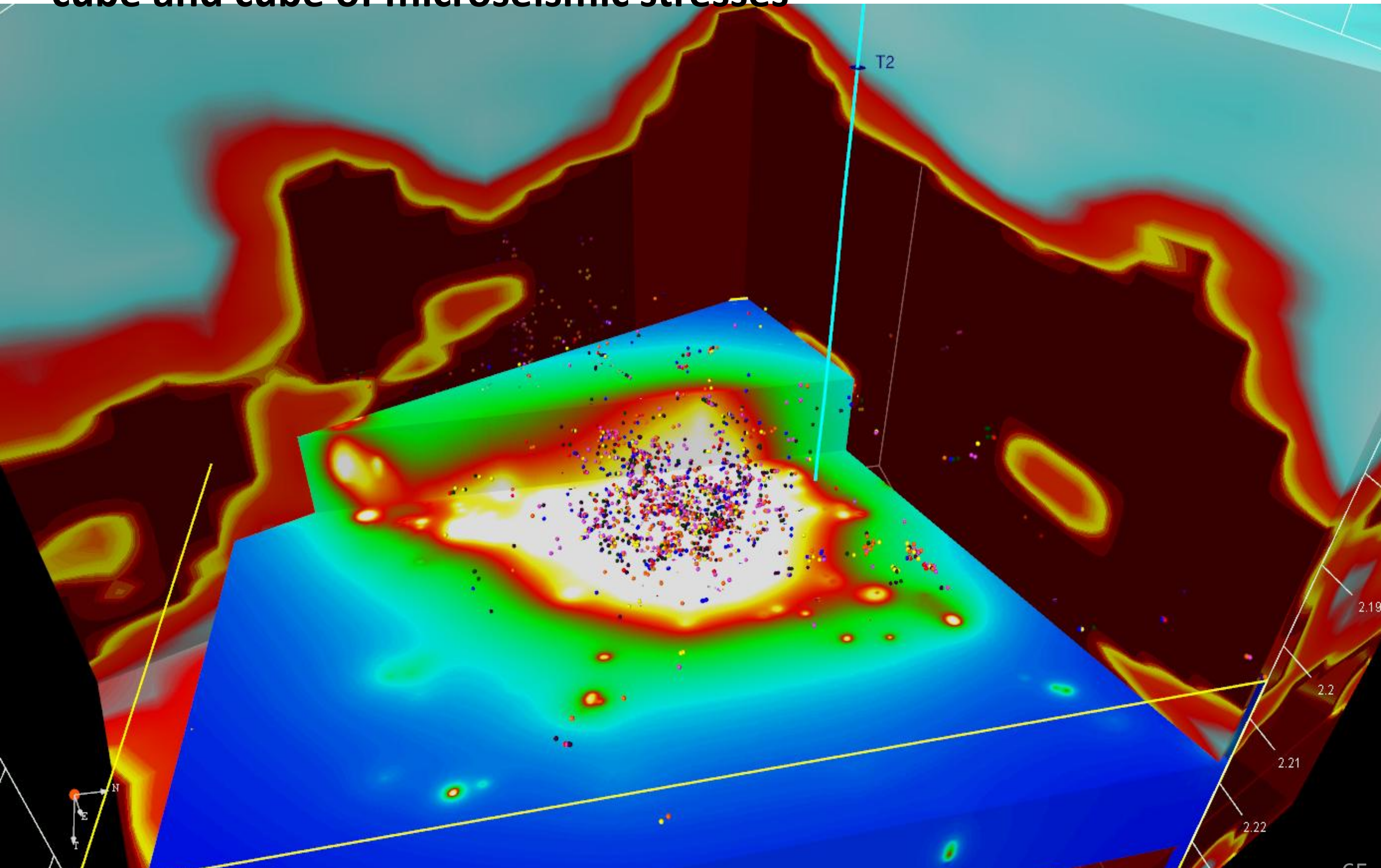

Oilfield Oimasha. Wells #9, 2013, Kazakhstan. Oil inflow 150 m3 per day

Case study #11: 3D view of CSP-diffractor cube and cube of microseismic stresses

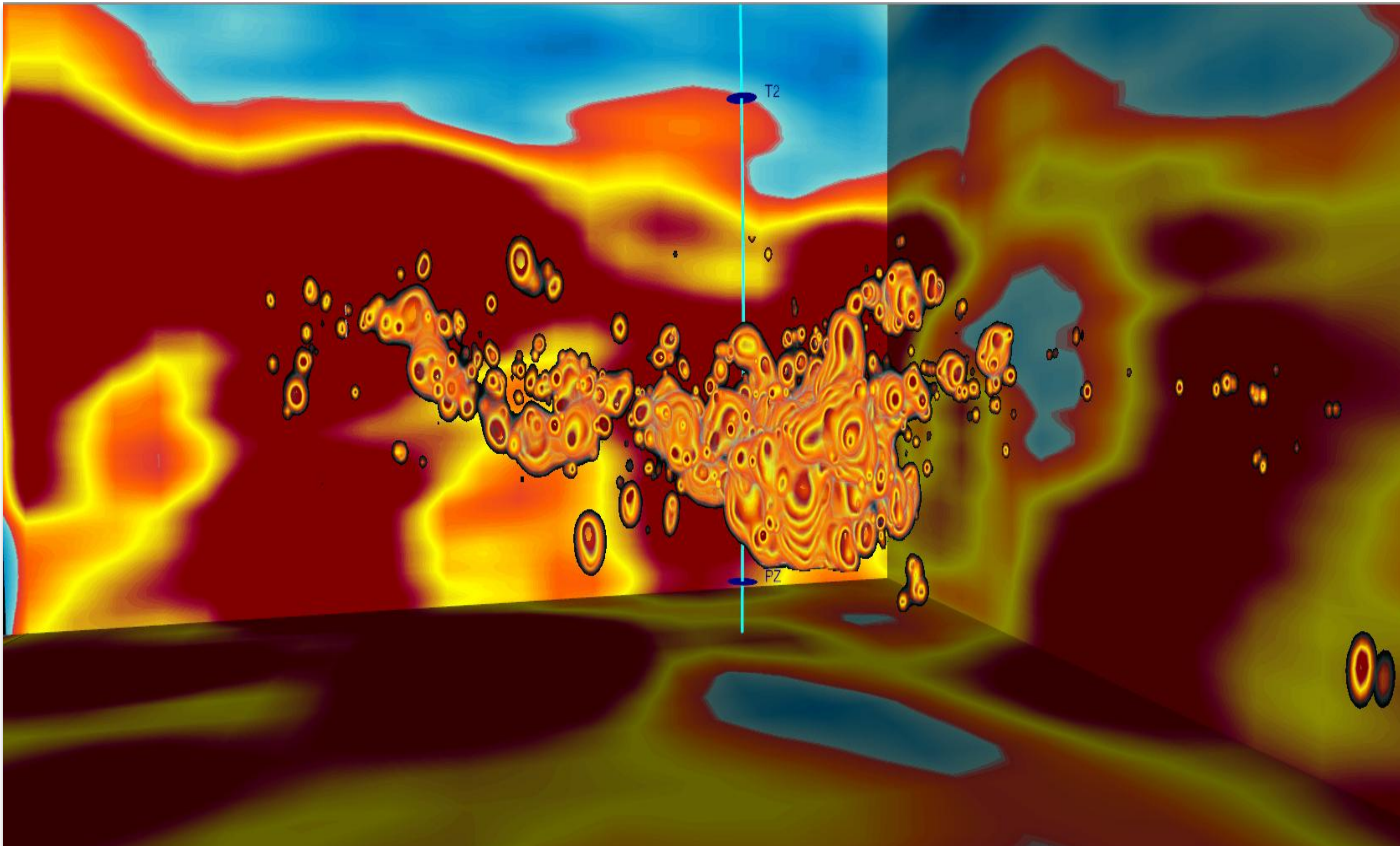

Oilfield Oimasha. Wells #9, 2013, Kazakhstan. Oil inflow 150 m3 per day

Case study #11: 3D view of results microseismic events

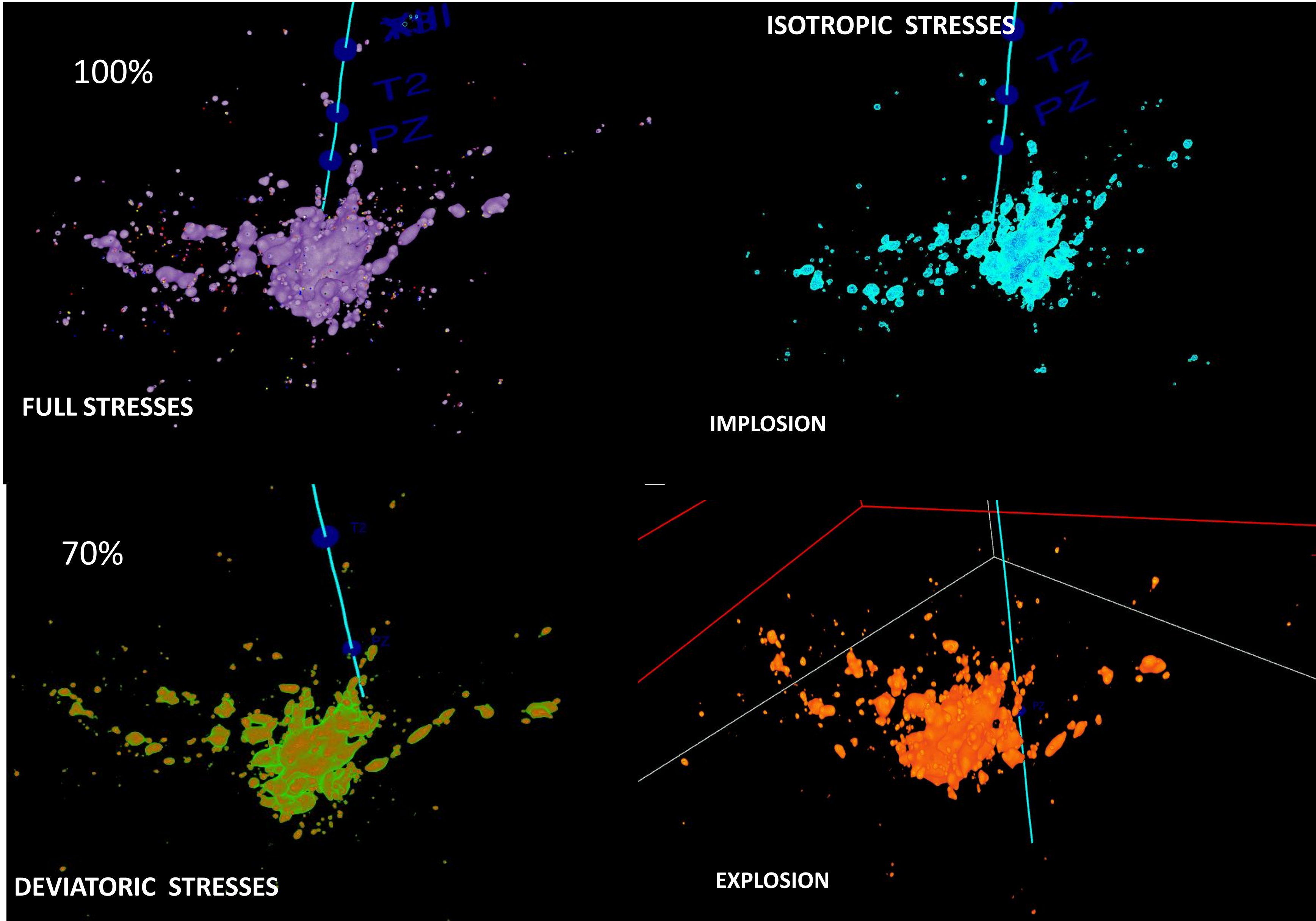

Oilfield Oimasha. Wells #9, 2013, Kazakhstan. Oil inflow 150 m3 per day

Case study #11: 3D view of CSP-diffractor cube and cube of microseismic stresses near the structural surfaces of middle Triassic and roof productive horizon T2

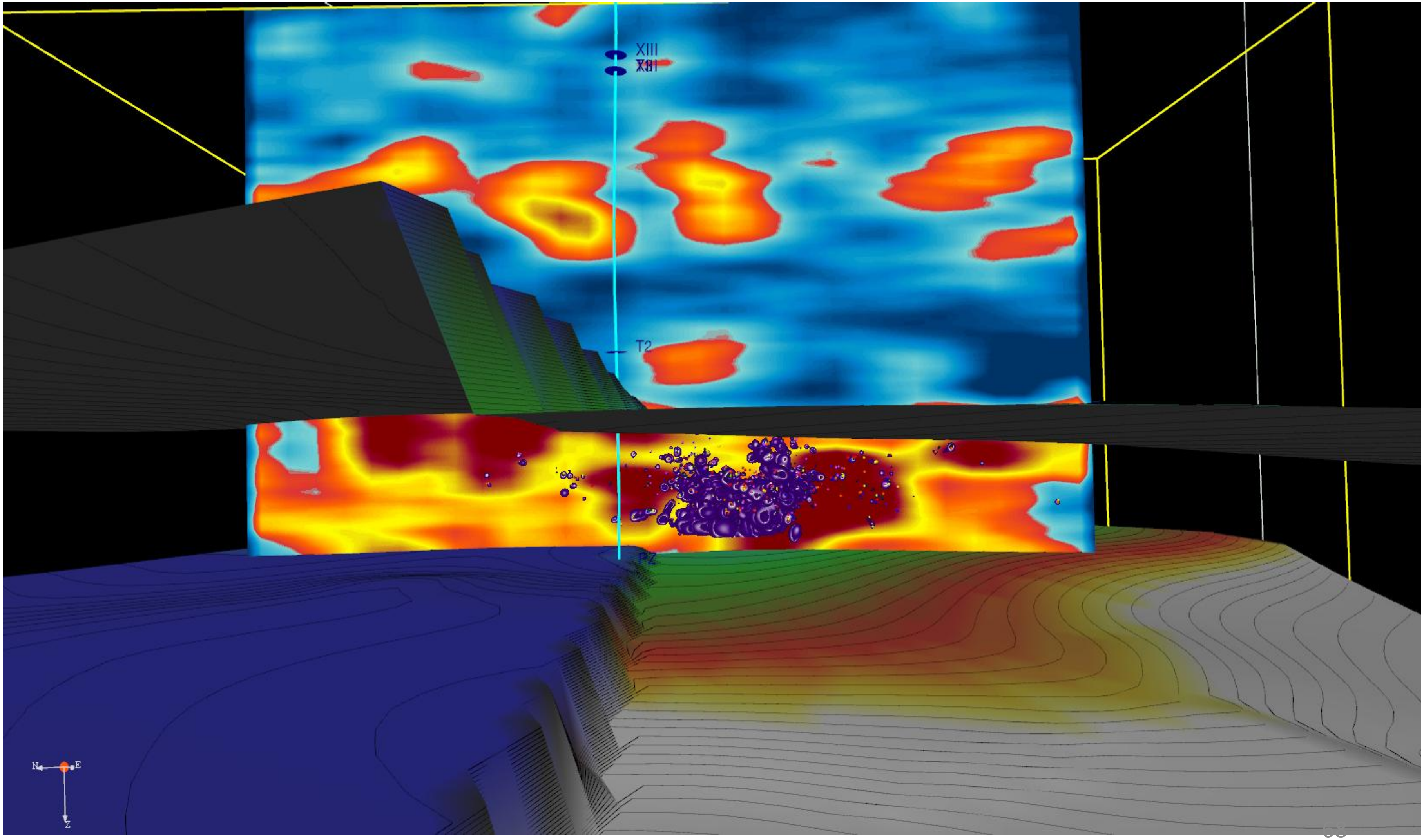

Oilfield Oimasha. Wells #9, 2013, Kazakhstan. Oil inflow 150 m3 per day

Conclusions

- MicroseismicCSP Small Surface Microseismic Monitoring Technology for oilfield development control is presented.
- The Technology is based on the SMTIP method and Small Surface Microseismic Acquisition System. Algorithms for data processing are based on the mathematical theory of inverse problems and the utilization of supercomputer calculations.
- A distinctive feature of the new technology is high mobility, compactness and universality.
- Technology is intended not only for fracturing control but also: for estimation of port productivity after multistage hydraulic fracturing, for long-duration passive monitoring of fluid injection, for hydrocarbon drainage area estimation and for oilfield block structure mapping.
- Complex interpretation of pre-existing fracturing (CSP) and results of MicroseismicCSP long-duration microseismic monitoring has a good perspective for oilfield development.

Thank you for your attention!

Email: egn@Kantiana.ru